Aalto-yliopisto
Insinööritieteiden
korkeakoulu

Lasse Kudsk Rasmussen

Dynamic Properties of Crushed Concrete used in Pavement Structures

Master's thesis for the degree of Master of Science in Technology submitted for inspection.

Espoo, 25.05.2020
Supervisor: Professor Wojciech Solowski
Advisor: Kirsi Koivisto

Aalto-yliopisto
Insinööritieteiden
korkeakoulu

Aalto-yliopisto, PL 11000, 00076 AALTO
www.aalto.fi

Diplomityön tiivistelmä

Author Lasse Kudsk Rasmussen		
Title of thesis Dynamic Properties of Crushed Concrete used in Pavement Structures		
Master programme Geoengineering		**Code** ENG23
Thesis supervisor Wojciech Solowski		
Thesis advisor Kirsi Koivisto		
Date 25.05.2020	**Number of pages** 110	**Language** English

Abstract

To reduce the environmental impact of transport in expanding cities, mass transport is an effective solution but it needs large amounts of good-quality aggregate. Recycled crushed concrete from demolition sites has the potential of substituting some of the conventionally used materials in railway construction due to its high strength and stiffness. However, knowledge about the dynamic properties of crushed concrete is very limited both in Finland and internationally. This limits the possibilities of assessing the groundborne vibrations, and hence there is a risk that the vibration levels become too large. Given the need for sustainable solutions and the large potential of crushed concrete, the dynamic properties of crushed concrete are studied and compared with conventionally used materials through a finite element simulation. In this thesis, an extensive literature review is conducted on railway dynamics and dynamic and small-strain properties of materials. The railway dynamics are studied through empirical models and conventional engineering dynamics. Based on the information found from the literature review, the small-strain stiffness affects significantly both damping, resonance frequency, and displacements related to the dynamic loading from railways. However, the existing empirical models are simplified to an extend where these properties are not included. Existing methods for estimating the small-strain stiffness and dynamic properties are also studied in the literature review, where the properties are estimated by several different methods. A resulting outcome of the literature review is an estimation of the behaviour of crushed concrete exposed to dynamic loading, where a small-strain shear modulus is found using a method by (He, et al., 2018) to be around 350 MPa at pressure of 400 kPa.

The crushed concrete is tested by resonant column and bender element test to determine the small-strain properties of the material. The small-strain stiffness found from laboratory tests is 656 MPa at 300 kPa, which is around 30% larger than the estimated value. However, by analysing the measured values with the estimated values, a correction of the assumed void ratio and particle density yield a good fit. The conventionally used materials and the crushed concrete is compared through finite element simulations. The comparison shows no significant difference in the vibration dispersion and propagation resulting from the different materials. The velocities transmitted to the surrounding material are damped nearly equally fast for the compared materials. There is a small difference to the stronger ballast material and similar results between the subgrade and crushed concrete. The surrounding material seem to have a strong effect on the vibration propagation, which calls for an extended study on the geometry's influence on the wave propagation.

Keywords Recycled concrete (RCA), Small-strain stiffness, damping, Railway induced vibrations, wave propagation, bender element, resonant column, dynamic properties

Acknowledgements

Firstly, I would like to thank Ramboll for arranging this interesting, educational, and practically useful subject. Also, I wish to show my gratitude to the financiers for their economical support to the project, it has enabled a deeper understanding of the subject in the form of laboratory test results and personal financing. Financiers are city of Helsinki, city of Vantaa, city of Turku, city of Tampere, Finnish Transport Infrastructure Agency, Rudus Oy and Ramboll Finland Oy

I would like to pay my special regards to Kirsi Koivisto and Juha Forsman from Ramboll, who throughout the project have provided me with test results, theses and knowledge about the topic. Kirsi and Juha have been persistent in making things happen despite the very different circumstances caused by COVID-19. Their tenacity opened up for the opportunity of getting laboratory results, even though, for long time, it seemed impossible to get for this thesis.

To my professor, Wojciech Solowski, I would like to give my greatest gratitude for the invaluable and extraordinary assistance you have provided throughout my thesis studies. Throughout the whole process you have supported my learning and my goals for the quality and outcome of this thesis. Wojciech has among other made time available in his schedule for weekly meetings with fruitful conversations and genuine, honest and useful feedback. The broad knowledge of how to understand advanced topics and how to write a scientific paper has provided me with fundamental and crucial tools for the process of this thesis.

A special thanks also to my supervisor at Ramboll, Michael Mengelt, who has supported me in the process of writing my thesis, and who has taken time out of his calendar to look through my thesis before the final submittal.

Last but not least, a big thanks to my girlfriend who has coped with mood swings and who has given support and sparring during this process. The help during the last couple of weeks have been priceless and for that I am grateful.

Table of Contents

Notations

ζ	Damping ratio, $\frac{actual\ damping}{critical\ damping}$	-
ω_0	Angular frequency	$\frac{rad}{s}$
ω_n	Natural (resonance) frequency	$\frac{rad}{s}$
e	Void ratio	-
ρ_s	Particle density	$\frac{ton}{m^3}$
ρ	Particle shape regularity	-
C_u	Coefficient of uniformity	-
d_{50}	Average grain size	mm
ν	Poisson's ratio	-
γ_i	Unit weight	$\frac{kg}{m^3}$
$w_{\%}$	Water content	%
E	Young's Modulus	MPa
$E_m = E_{max}$	Young's small-strain modulus	MPa
$G_{max} = G_0$	Small-strain shear modulus	MPa
M_{max}	Small-strain constrained modulus	MPa
V_p	Compression wave velocity	$\frac{m}{s}$
V_s	Shear wave velocity	$\frac{m}{s}$
V_i	Velocity	$\frac{m}{s}$
L_v	Vibration velocity level	dB
t	Time	s
n	Refraction index	-
θ_r	Refraction angle	Degrees

θ_i	Incident angle	Degrees
θ_{cr}	Critical angle	Degrees
d	Distance to vibration source	m
d_0	Reference distance to vibration source	m
k_i	Spring stiffness	$\frac{kN}{m}$
m_i	Mass	kg
λ	Wave length	m
f	Frequency	Hz
#	Sieve size e.g. #16 = 16mm sieve size	mm
$D - D_0$	Material damping	%
D_{min}	Damping found at small strains	%
γ	Strain	%
VdB	Velocity decibel	$VdB\ re\ 1 \cdot 10^{-9}\frac{m}{s}$
dBA	A weighted decibel	dB re 20 μPa
A_E	Small-strain constant	-
n_E	Power coefficient	-
μ	Lamé's second parameter and shear modulus	MPa
γ_{unsat}	Unsaturated unit weight	$\frac{kN}{m^3}$
γ_{sat}	Saturated unit weight	$\frac{kN}{m^3}$
e_{init}	Initial void ratio	-
α	Rayleigh damping coefficient	-
β	Rayleigh damping coefficient	-
E_{50}^{ref}	Secant stiffness (std. drained triaxial)	kPa

E_{oed}^{ref}	Tangent stiffness (Primary oedometer)	kPa
E_{ur}^{ref}	Unloading/reloading stiffness (drained triaxial)	kPa
m	Power	-
c'_{ref}	Cohesion	kPa
φ_c	Angle of internal friction	°
$\nu_{0.7}$	Threshold shear strain at which $G_s = 0.722 \cdot G_0$	-
G_0^{ref}	Reference shear modulus at very small strains	kPa

Abbreviations

GBV	Ground-borne Vibrations
GBN	Ground-borne Noise
VTT	Technical Research Centre of Finland
USP	Under Sleeper Pads
BeM	Crushed concrete (Betonimurske)
UCT	Uni-axial Compression test
RCA	Recycled Concrete Aggregate
SEM	Scanning Electron Microscope
Railway	Collective term for structures with rails, mainly focused on urban structures (lower speed)

1 Introduction

The cities are constantly growing and the distances to travel within larger cities, combined with the traffic congestion and environmental footprint of cars, increasingly call for public transportation. Simultaneously, the law and regulations regarding sustainability, recycling and material efficiency increase to tighten, which encourage creative thinking in organizations and in building projects. There is an increasing need to analyse every building material from cradle to cradle, and this way exploring new ways to use materials. This opens up for new ways to reuse materials and consequently both decrease mining of new materials and increase the total lifetime of a material. Discovering ways to reuse materials, introduces a need for additional knowledge about the materials. In this thesis, the dynamic properties of crushed concrete are studied, for the use in urban transit systems such as tram and light rail transit lines.

The construction and demolition industry contribute with a large quantity of crushed concrete, which has a great potential of being used in railway projects. Crushed concrete is classified according to origin, strength and composition, whereafter possible uses are defined. The crushed concrete which is studied is classified as BeM II, which is from demolition sites and has a compressive strength higher than 0.8 MPa. The available quantity and a feasibility have previously been made, to find out which structural layers in railway construction crushed concrete can replace, but the dynamic properties of crushed concrete have been studied only minimally.

Previous studies on vibrations from railways through monitoring of existing railways, finite element modelling, differential equations, etc. have resulted in empirical models, which with relative ease indicate the vibration levels at the receiver, and determines whether the vibration level is acceptable or if measures should be taken to mitigate the vibrations. Vibrations from railways can severely impact nearby structures and diminish the wellbeing of individuals, which justify the importance of an extensive knowledge about the materials used in railways, especially in urban transit systems which are in close contact with buildings and people. Empirical models and the main principles of the finite element and differential equation models are studied in this thesis. Knowledge about these models and a more general theory behind vibrations propagations, establish the foundation of predicting the impact linked to using crushed concrete in the structural layers of a railway.

Dynamic methods have for long been used to determine stiffness and stratigraphy soil layers. Usually the stiffnesses found by dynamic methods were orders of magnitudes larger than the stiffnesses found by static laboratory testing. Until 1980's the difference in stiffness between static and dynamic loading was understood to be due to the difference in loading (strain rate and inertia), but static stiffness measurements at small strains resulted in the discovery of a non-linear relation between stiffness and strain, primarily to be due to a degradation of the soil skeleton. Subsequently it became apparent that the dynamic properties of materials were not due to inertia or strain rate effects, but rather that small-strain stiffness can be understood to be equal to dynamic stiffness.

In this thesis, through a series of laboratory tests and a considerable literature review, small-strain and dynamic properties of crushed concrete, BeM II, are estimated. In addition, the effect of substituting conventionally used materials with crushed concrete is studied.

2 Objective

Several light rail and tramway projects are under construction or being planned around Europe, including Raide Jokeri (Helsinki, Finland)), Tampere Tramway (Tampere, Finland), Odense Light rail (Odense, Denmark), as well as projects in Poland, France and other countries (Verdict Media Limited, 2020). Cities are expanding, while the environmental regulations require further reductions in emissions, more efficient use of natural resources, as well as improvements in waste management. Yet, expanding cities demand sustainable transportation solutions. In construction, we have to follow environmental guidelines while ensuring the structural safety for the users. Still, by introducing new ways to use and re-use materials we can greatly reduce the need for quarrying new raw materials. In particular, according to the following regulations:

- Law 646/2011 – Waste act (Finland)
- Decree 179/2012 – Government decree on waste (Finland)
- Decree 331/2013 – Government decree on landfills (Finland)
- EU directive 2008/98/EY – on waste and repealing certain Directives

related to the material efficiency and by EU directive, 70% of demolition waste (by weight) shall be recycled by 2020.

According to (Deloitte, et al., 2015) concrete waste produced in Finland 2011 was around 1.3 million tonnes, originating mainly from housing industry. Substituting crushed rock with concrete waste in one of the structural layers in railway projects can save a significant amount of rock quarrying, rock transportation, demolition waste transportation out of cities and disposal of demolition waste. However, while replacing the conventionally used materials with crushed concrete does not cause a problem to the structural integrity, the effect on the transmission of vibrations is still unknown.

The main purpose of this study is to acquire sufficient knowledge about the dynamic properties of crushed concrete, including its small strain non-linearity and wave propagations in soil. This should allow for making a reliable comparison with previously used materials. The main research questions in this study are:

1. Which methods are currently used in empirical models for ground induced vibrations caused by railway traffic?
2. How can the dynamic parameters for crushed concrete and similar granular materials be estimated reliably?
3. How can the small-strain parameters for crushed concrete and similar granular materials be estimated reliably?
4. How does the substitution of the commonly used material with crushed concrete affect the vibrations induced by tramways?
5. How do the dynamic and small-strain parameters of the structural layers affect the ground induced vibrations caused by railway traffic?
6. Which laboratory and in-situ methods can be used to predict and monitor the dynamic behaviour of crushed concrete waste in railway construction?

3 Background

The aim of the background section is to provide sufficient knowledge about dynamic material properties, dynamics related to railway structures, mitigations measures and estimation methods of vibrations, enabling a qualified hypothesis for the small-strain properties of crushed concrete and the effect of replacing conventionally used materials with crushed concrete. To fully understand the effect of substituting one material with another on the wave propagation, it is necessary to understand how vibrations propagate through soils, how waves are transmitted from one material to another and how the material properties affect these processes. Furthermore, it is necessary to learn how ground-borne noise and ground-borne vibrations differentiate from each other and to identify which frequencies are relevant in the study of dynamics of urban railway systems.

Empirical methods are used to determine vibration and noise levels caused by railway traffic and understanding the underlying theory used in achieving the models reveal the assumptions which are affected by a change of properties of structural materials. Furthermore, studying the underlying theory of the empirical models leads to a better understanding of the impact made by using different mitigation measures. Mitigation measures are used for reducing the impact of vibrations caused by the railway traffic, hence understanding where they are used and why they work. This might disclose some of the effects related to a change in material parameters.

Conventional materials used in railway construction include crushed rock or similar granular materials which are used as ballast, subballast and subgrade layers. These are some of the materials which have the potential of being substituted with similar recycled materials such as crushed concrete, and knowledge about these materials are therefore relevant. Studying the material properties of conventional materials and comparing those properties with those of crushed concrete highlights the feasibility, related to dynamics, of using crushed concrete instead of crushed rock.

Dynamic stiffness parameters have been found to be significantly larger than the static stiffness parameters of materials and have throughout the time been put in close relation to the small-strain stiffness of materials. For a long time, it was thought to be the strain rate which was the largest contributor to this difference but it has been found to not affect the initial stiffness insignificantly, which has led to the impression that the dynamic stiffness of materials and small-strain stiffness are likely to be equal to each other. Theory of small-strain stiffness is studied in this chapter as well as use of small-strain stiffness in dynamics ((Burland, 1989), (Clayton, 2011), (Menq, 2003)). A reliable determination of dynamic properties of materials, such as small-strain stiffness, damping ratio and resonance frequency, require laboratory testing. However, methods have been developed for estimating these properties based on more conventionally obtained material parameters such as Young's modulus, Coefficient of Uniformity and mean grainsize. This chapter aim to present some of the key methods for predicting dynamic properties, which have been made for materials such as sand, clay and smaller grainsize crushed concrete. Studying the applicability of crushed concrete, will reveal the potential of these theories. Estimating the small-strain parameters for crushed concrete, based on a literature review and empirical formulas, yield a possibility of comparing with results obtained from laboratory testing, which will reveal the usability of the estimation methods for this particular material.

3.1 Vibration Propagations in Soils

Vibrations caused by railway traffic are transmitted through soil in different frequencies, due to the source of the vibrations. The total signal of vibrations sent through the soil is a combination of several frequencies, and different frequencies are perceived in various ways by humans. At lower frequencies oscillations can be perceived as mechanical movement of your body whereas higher frequency oscillations are perceived as noise. Noise can be heard as a direct sound from the source or it can be a transfer of oscillations to structures near you, which will make these structures vibrate and result in noise.
There are several factors affecting the magnitude, frequency and propagation of vibrations. Some factors are related to properties of the soil, some to the alignment and quality of the track, some to the quality and nature of the vehicle etc. Mainly the mitigation measures are divided into three target groups; source, path and receiver, and there are factors affecting the vibrations at each of these groups. There are several reasons for the initial generation of oscillations. (Harris Miller Hanson Inc, 2005)

By looking at where mitigation measures can be done, it is possible to divide the sources of vibration and noise into different categories:

- Noise (Harris Miller Hanson Inc, 2005)
    - Noise from vehicle
    - Noise from wheel and rail interaction
    - Noise caused by a flow of wind around the vehicle
- Vibrations
    - Mechanical excitation from vehicle (Paul de Vos, 2017)
    - Mechanical excitation from track and wheel interaction (Paul de Vos, 2017)
    - Propagation of vibrations due to moving load (Lombaert, et al., 2015)
    - Stiffness, and/or change of stiffness, of track (Dahlberg, 2006)
    - Alignment of track (Dahlberg, 2006)

Several mitigation measures can be done to avoid mechanical noise and vibration coming from the vehicle and track-wheel interaction sources. These mitigation measures are further described in section 3.1.6. Dealing with vibrations resulting from the moving load can be more difficult and requires modification of super- and substructure, considering both the interaction between them and individual properties.

This difficulty dues to the nature of vibrations and vibrations' response to different stiffnesses and other material parameters. The propagation of this type of vibrations is described in section 3.1.2 and a detailed description of the wave's travel through different materials can be seen in section 3.1.3.

As waves travel through the different layers of a stratified medium, the soils' damping properties, shear wave velocities and natural frequencies directly affect the attenuation of the propagation of the waves, which emphasizes the importance of determining these parameters when dimensioning new railways and other structures subjected to vibrations.

3.1.1 Ground-borne vibrations

Ground-borne vibrations are defined by (Paul de Vos, 2017) as:

"Ground-borne vibration (which is the most commonly perceived kind of "vibration") is generated by the interaction between train and track (and subsoil). The vibration is transmitted through the ground and may reach the foundation of a building. The building responds to the vibration; vibration is transmitted through the building structure, and may be observed as perceivable vibration of the floor. Ground-borne vibration is associated with frequency range of roughly between 1 and 100 Hz."

There is a smooth transition between ground-borne vibration and ground-borne noise, where frequencies in a range from approximately 20 to 100 Hz can be perceived as both vibration and as noise. According to (Paul de Vos, 2017) and (Lombaert, et al., 2015), vibration is in a range of 1 to ≈100 Hz and ground-borne noise is in a range from approximately 16 Hz to 250 Hz, this is visualized in Figure 1. There are many factors affecting the audible noise e.g. the vibrations causing structural elements to vibrate and hence create noise indirectly.

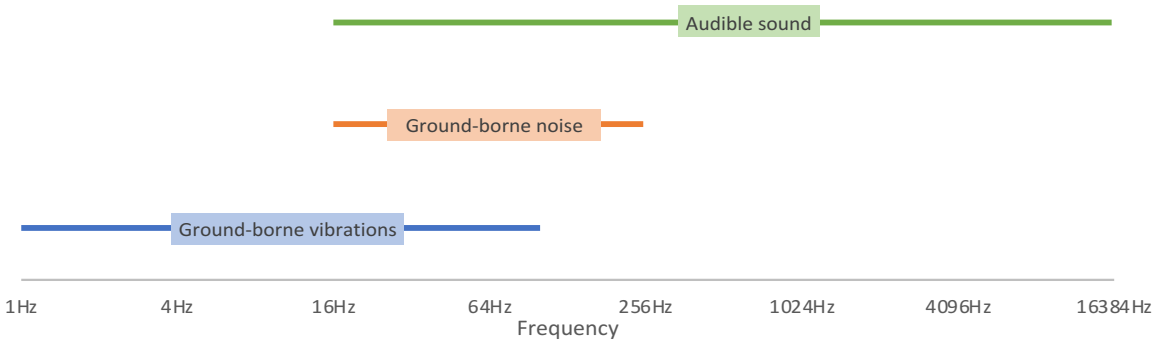

Figure 1: Frequency ranges for noise and vibrations (Paul de Vos, 2017)

Vibrations can cause material and constructions to move, which can create noise. At the same time vibrations can be at a level where they can be felt as a physical movement of the body. Noise coming from vibrations can decrease personal comfort and life quality. Likewise, physically perceived vibrations cause a discomfort due to the sometimes-associated decreased confidence in the structural safety.

Ground-borne vibrations can be destructive to nearby structures and to the track structure. If the superstructure has been designed poorly, and if the transfer of vibrations from superstructure to substructure causes resonance, deformations will become undesirably large. However, vibrations do not have to be in the range of the resonance frequency to cause damage to nearby structures. The properties of materials used in the track structure and the properties of the surrounding ground highly affect the propagation of vibrations. Damping characteristics define how the amplitudes of the vibrations are attenuated and the small-strain stiffness affects the wave velocity, resonance and deformations related to vibrations (PLAXIS, 2019). This highlights the importance of proper material knowledge and well-prepared design of the track superstructure and substructure. Identifying the material properties introduces the possibility of modelling wave propagation and vibration response on the structures, which can visualize where mitigation measures might be most effective. There

are many mitigation methods available for both ground-borne vibrations and noise, which are described in more detail in section 3.1.6..

Vibrations come from different sources, hence they are also transmitted as different frequencies, where some frequencies have a larger impact on the structures. As an example, in Figure 2, a tramline is producing an oscillation with a frequency of 0.3 Hz originating from rail irregularities and another oscillation with a frequency of 0.16 Hz coming from uneven settlements or difference in ground stiffness. The signal can be simplified to be the super-position of the two signals.

In some cases, it is worth monitoring vibrations in the ground e.g. if the vibrations induced by a train are causing significant deformation of a nearby structure. The signal which is monitored is very likely to be a combination of several signals and to find the frequency which causes the damage makes it necessary to separate the different signals from each other. The separation of different frequencies is done with the help of Fourier transformations. The Fourier transformations are widely used for signal interpretation in the field of electrical engineering, music, etc. By the help of Fourier transforms it is possible to decompose a time-domain signal into to a frequency domain spectrum. More details can be found from (3Blue1Brown, 2018).

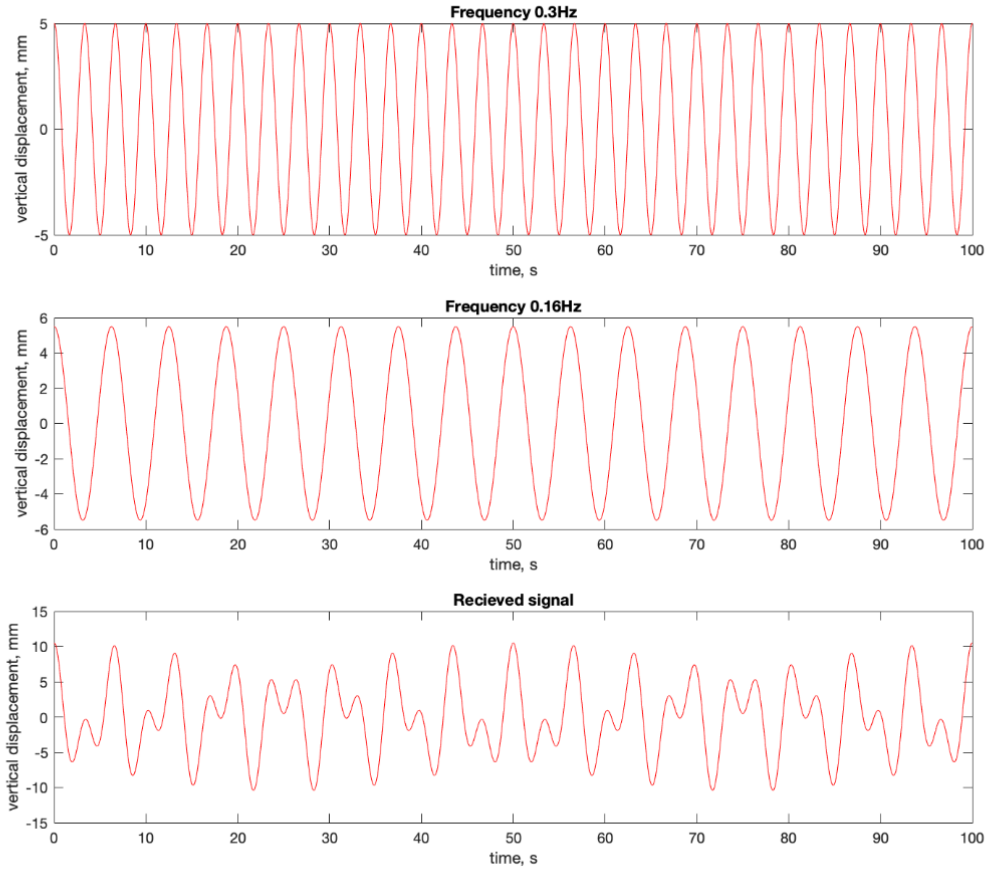

Figure 2: Oscillations from different sources

The vibration sources can be divided into three groups; vehicle vibrations, track and wheel, and moving load excitation.

Vehicle vibrations

Vehicle vibrations are typically resulting from the unsprung mass oscillating when the vehicle is in motion. The suspension system of the train and the quality also affect the vibrations transferred to the tracks. Track unevenness, wheel roundness etc. will to some extend displace the train wheel and as the train wheel is displaced the mass of the wagons will oscillate in the suspension systems at the wheels. (Paul de Vos, 2017) In addition, operating the vehicle generates vibrations due to e.g. engine oscillations, aerodynamics, wind blows, etc.

Track and wheel

Unevenness and roundness will cause an excitation of the position of the wheel and train. This excitation can result in an eccentric positioning of the point loads from the train, which finally causes excitation and oscillations of the track. Furthermore, any discontinuities in the track can cause periodical change of displacements in the track. These discontinuities can be rail joints, rail switches, difference in stiffness of the track due to sleeper stiffness, difference in superstructure or supporting ground stiffness which can be due to poorly executed construction, etc. The suspension systems quality influences the impact of these vibrations. (Paul de Vos, 2017)

Moving load excitation

When a load moves along the rails this will create a short vertical displacement of the track, which will generate a propagation of waves along the tracks. This topic is addressed further in section 3.1.2. (Lombaert, et al., 2015)

Vibration waves are generally divided into three different types:

a) Rayleigh waves; a result of the interaction between S- and P-waves at the surface
b) P-waves; primary or pressure waves
c) S-waves; secondary or shear waves

In Figure 3 the different wave types are illustrated.

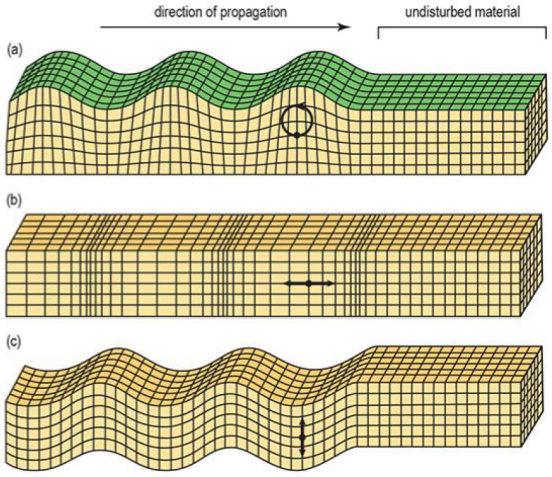

Figure 3: a) Rayleigh wave, b) Pressure wave, c) Shear wave (Paul de Vos, 2017)

S-waves are slower than P-waves and the particles in this type of waves are oscillating perpendicular to the direction of the wave hence generating a rapid shearing of the ground. The S-waves' velocities range from 30 to $500\frac{m}{s}$ compared to P-waves, which moves with velocities around 800 to $1500\frac{m}{s}$, depending on the stiffness of the soil. Different from the S-waves, the P-waves act as an expanding and contracting movement of the particles along the wave propagation direction (Paul de Vos, 2017).This difference can also be seen in the interpretation of the signals received in the bender element testing, see section 4.1.2.

At a free surface, the interaction between P- and S-waves results in Rayleigh waves, which have a more circular movement because it is a combination of shear and pressure waves. The velocity of Rayleigh waves is slightly lower than S-waves and depend more on the frequency of the oscillations. (Paul de Vos, 2017)

3.1.2 Vibrations from a dynamic moving load

Besides the vibrations that occur due to mechanical faults, oscillations are also generated by what is known as a moving point load. Each wheel on the train create a point load on the rails, and as the train is moving, any point on the rail will endure an alternating loading due to the passing wheels. In addition, as the point load is moving, the stiffness of the rail system will change and alternate the deflection of the ground. This can e.g. be due to the sleepers, which are equally distributed, increasing the stiffness of the system, hence generating oscillations.

Starting from a stationary point load e.g. a wheel load, the deflection of the ground is constant, hence there are no oscillations. As it can be seen from Figure 4, the magnitude of the deflection is constant in the time-domain.

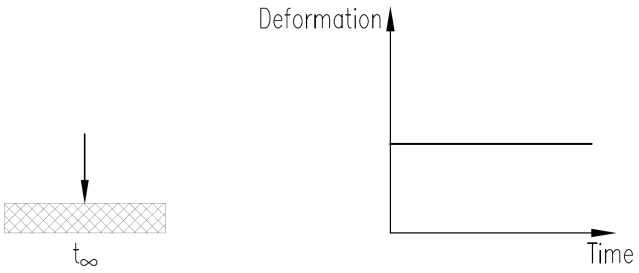

Figure 4: Deformations from constant point load

If this point load is repeatedly varying in magnitude with time, it will create oscillations. If the variation is switching at the same frequency as the underlaying soil's resonant frequency, deformations might become self-perpetuating and therefore become more destructive to the neighbouring structures. In Figure 5 the varying point load in time is illustrated. Note that a simplification to the drawing has been made, by having a linear relationship between each value of deformation. This is illustrating the mechanism of a point load creating oscillations, not representing the reality.

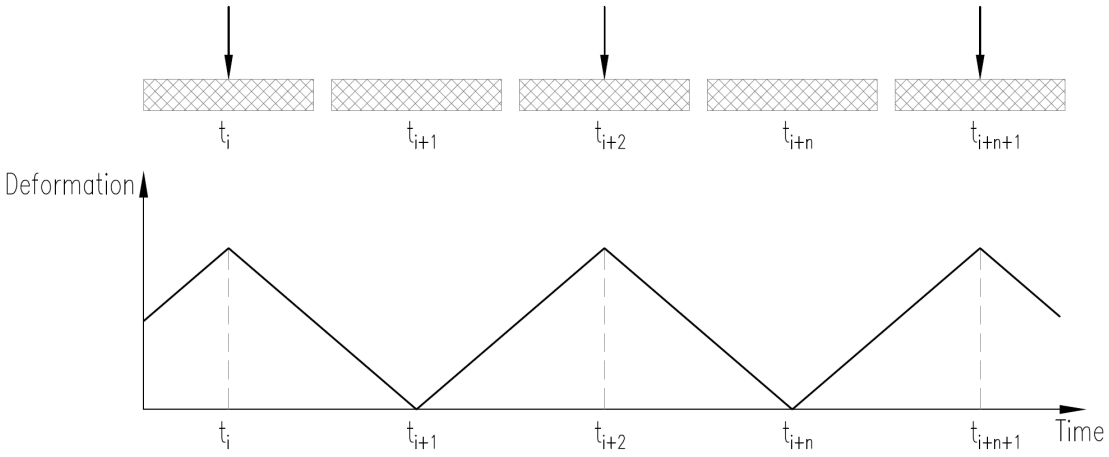

Figure 5: Varying point load

As the point load's magnitude is varying between 0-100 % with time, the strain levels will vary simultaneously. The strain level depends on the stiffness of the material, and, assuming an elastic behaviour of the material, it will undergo recoverable deformations as the load is activated. As the load deactivates the deformations recover to the initial position. Repeating the varying magnitude of the load matches the oscillation propagation coming from a train passing through. The return to the initial position depends on the damping ratio of the material which has been deformed.

In 1980's, a connection between the dynamic stiffness and the stiffness at small-strains were established. It was found that the stiffness decreases non-linearly with increasing strain and furthermore that the dynamic stiffness could very well be defined as the small-strain stiffness for soils (Clayton, 2011); hence it is relevant to know the small-strain stiffness of the materials in the railway superstructure.

A railway vehicle usually comprises of several wagons, each with two or more rows of wheels. The wheels are transferring the load from the wagon down to the rails and the rails transfer the load on to the soil, usually passing the superstructure before entering the ground. As each point load is passing by any point on the rails, the magnitude of the load at that given point will be changing in time, hence creating oscillations. Furthermore, the sleepers under the rails add some stiffness to the system, which will alter the magnitude of the strain response to the moving load, due to the changing stiffness. This variation is also a source of vibrations in the ground and is necessary to account for when modelling the vibrations in a railway structure. (Lombaert, et al., 2015)

A vehicle driving at the same velocity as the wave velocity of the underlaying material will create an amplifying situation, where the attenuation of the material is at its lowest and therefore this might cause exaggerated wave propagation in the oscillating ground. The use of good construction materials in the track structure can decrease the transmission of S- and P-waves to the underlying ground materials due to the damping properties of the materials. However, some oscillations are usually transmitted to the ground and it is important to know how those materials transmit the oscillations. Table 1 presents values of wave velocities for

soils in three different categories. These values can be used for comparison with the results obtained in this thesis, hence categorizing the crushed concrete according to wave velocity.

Table 1: Indicative values of wave velocities (Lombaert, et al., 2015)

SOIL TYPE	SHEAR WAVE VELOCITY, V_s	DILATIONAL WAVE VELOCITY, V_p
Peat (soft soil)	$50\frac{m}{s}$	$357\frac{m}{s}$
Medium stiff soil	$150\frac{m}{s}$	$300\frac{m}{s}$
Stiff soil	$400\frac{m}{s}$	$800\frac{m}{s}$

The same applies to the resonance frequency of the ground. The frequency generated by e.g. passing the sleepers, might match the natural resonance frequency of the ground and again the attenuation is decreasing exponentially as the ratio between the induced frequency and the resonance frequency approaches 1. (Paul de Vos, 2017) In the end this can affect nearby structures and the bearing structure itself. A train moving at $200\ km/h$, which is equivalent of roughly $55.5\frac{m}{s}$ has a higher risk of initiating a wave propagation in the ground if the ground is e.g. peat, than if the ground would be a stiffer material. This is due to the train moving at speeds closer to the natural wave velocity of the ground.

When designing the bearing structure of a new railway it is important to know how the waves travel through materials and how the materials, which the railway structure comprises of, behave.

3.1.3 Transmission of waves through different media

A wave transmitted through different media will change direction according to Snell's law;

$$\frac{V_{i+1}}{sin(\theta_r)} = \frac{V_i}{sin(\theta_i)} \qquad \textit{Eq. 1}$$

Or rewritten to accommodate the refraction index (see more in (Giancoli, 2016))

$$n_{i+1} \cdot sin(\theta_r) = n_i \cdot sin(\theta_i) \qquad \textit{Eq. 2}$$

Where
$n = refraction\ index$
$\theta_r = refraction\ angle$
$\theta_i = incident\ angle$
$V = velocity$

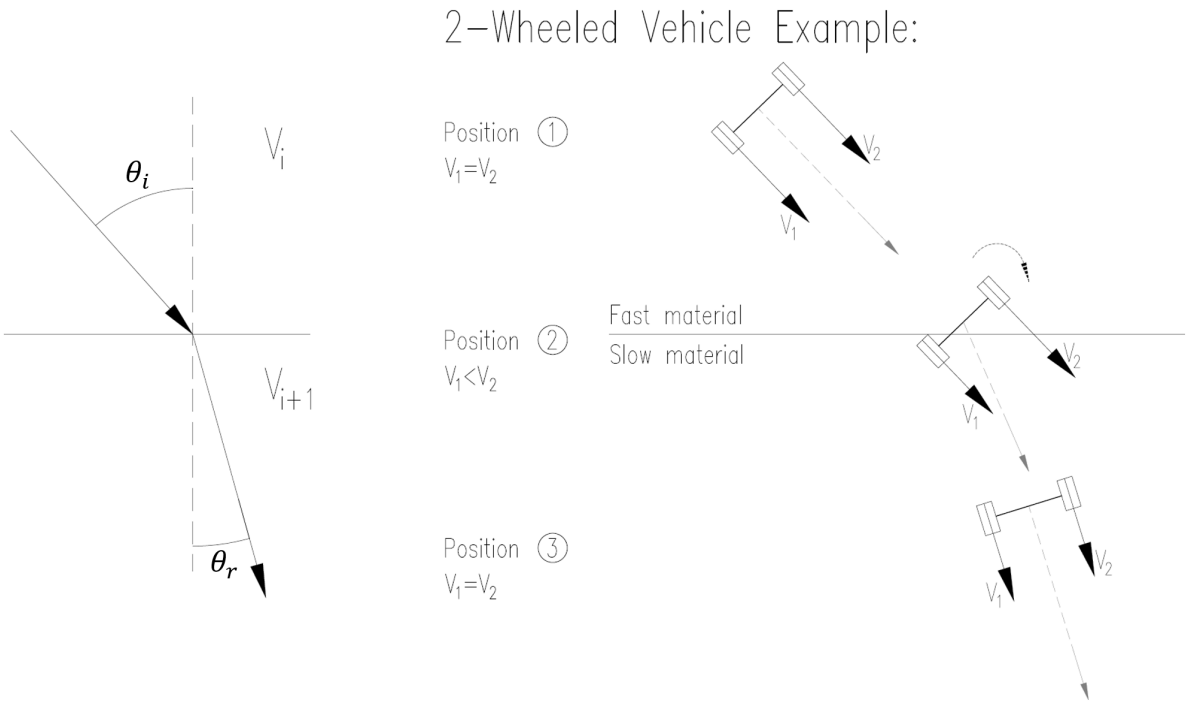

Figure 6: Inter-media wave transmission - Snell's Law (Khan, 2013)

Let's consider two connected bodies travelling with the same velocity on a fast material in an angle of θ_i at a continuous speed. As the body with velocity V_1 reach a slower material it will immediately loose speed while the other body continues at the same speed. This will cause a rotation of the entire system which will stop once both bodies are at the same material with same speed. At that point the initial angle of incident will have changed.

When a wave coming from vibration approaches the boundary between two materials it will change direction as well. An angle can be defined for each material, where the incident angle is at such a degree that it will cause total internal reflection, meaning that the wave will be repelled at the surface and sent back into the material it came from in a new angle. For soils this angle, the critical angle θ_{cr}, varies with the stiffness, porosity and other parameters of the soil. Furthermore, the stiffness affects the angle of refraction and the speed at which the wave will travel in the new material. The speed, frequency, wavelength etc. at which oscillations can travel in a soil material depend on the stiffness, the small strain stiffness, the density and several other parameters.

The resonant frequency and damping parameters are related to the dynamic properties of each material and have a direct influence on the wave propagation in materials. Furthermore, small strain parameters are related to these and have in addition to previously mentioned also an impact on the wave propagation from railway traffic in soil. See section 3.5 for further about small-strain properties.

Attenuation of the wave propagation in the soil has a clear connection to the relation between resonance frequency and the frequency which the soil is subjected to. Damping affect the magnification of the displacements, when the applied frequency is approximating the resonance frequency. When the applied frequency is below the resonant frequency there exists

only a small amount of amplification or damping of the waves. As soon as the frequency exceeds the resonant frequency the attenuation increases rapidly (Paul de Vos, 2017).

3.1.4 Ground-borne noise

Ground-borne noise is defined by (Paul de Vos, 2017) as:

"Ground-borne railway noise is defined in (Technical Committee ISO/TC 108, 2005) *as "noise generated inside a building by ground-borne vibration generated from the pass-by of a vehicle on rail". It applies to both heavy and light rail. Ground-borne noise excludes direct air-borne noise. Note that ground-borne noise is sometimes referred to as re-radiated noise, structure-borne noise and solid-borne noise (according to ISO 148437). Ground-borne noise is the term used in the report. Its frequency is roughly between 20 and 250 Hz."*

Ground-borne noise arises from the soil carrying vibrations to solid material. This could be from ground to foundation of a house and from the foundation to inside the house where the vibrations would make solid materials in the structure move and that way create noise. The other type of noise, which results from railroad traffic is the direct air-borne noise, which is not addressed in this thesis. Figure 7 is an illustration of how the vibrations travel through the ground and result in vibrational noise in the structures.

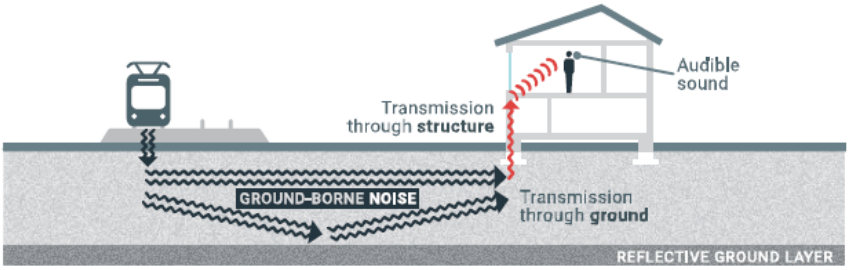

Figure 7: Ground-borne Noise (Paul de Vos, 2017)

3.1.5 Empirical models

There are many empirical models on assessing the vibration propagation from railways both dealing with noise and vibration spectrum. Below are listed a few of them:

- Method by the Swiss Federal Railways (SBB).
- Methods by Madshus et al., based on measurements in Norway and Sweden.
- Hood et al. developed under the Channel Tunnel Rail Link in United Kingdom
- Method by the Federal Railroad Administration (FRA), U.S. department of transportation
- Method by the Federal Transit Administration (FTA), U.S. department of transportation

The method by the Federal Transit Administration concerns mainly lower speed rail traffic where the Federal Railroad Administration report is based on railway traffic at higher speeds. Both methods have the same approach in assessing vibrations. The models used in Finland also use the same approach to vibrations, hence these models are in focus in this section.

The General Vibration Assessment is divided into three parts; screening, general assessment and detailed analysis. The model's aim is to detect structures which are inside critical distance or of critical category when subjected to vibrations produced by railway traffic. When

these structures have been found it is possible to use mitigation methods to reduce the impact to an acceptable level.

The screening process limits the amount of structures which will be included in the general assessment and finally the detailed analysis. The screening process includes two parts, where initially the structure is categorized and that way the threshold of vibrations is defined at the same time. Next, the distance to the vibration source is compared with the screening distances. If the distance from the structure is below the screening distance, the structure will be evaluated according to the general assessment. If the structure is further away it will not be assessed further in the General Vibration Assessment.

A structure, which is near by a planned railway has to be categorised in category 1, 2 or 3 or in the special building's category. The categories are defined in (Hanson, et al., 2006) report for the Federal Transit Administration on transit noise and vibration assessment as:

*"**Vibration Category 1** - High Sensitivity: Included in Category 1 are buildings where vibration would interfere with operations within the building, including levels that may be well below those associated with human annoyance. Concert halls and other special-use facilities are covered separately in Table 8-2. Typical land uses covered by Category 1 are: vibration-sensitive research and manufacturing, hospitals with vibration-sensitive equipment, and university research operations. The degree of sensitivity to vibration will depend on the specific equipment that will be affected by the vibration. Equipment such as electron microscopes and high resolution lithographic equipment can be very sensitive to vibration, and even normal optical microscopes will sometimes be difficult to use when vibration is well below the human annoyance level. Manufacturing of computer chips is an example of a vibration-sensitive process.*
The vibration limits for Vibration Category 1 are based on acceptable vibration for moderately vibration-sensitive equipment such as optical microscopes and electron microscopes with vibration isolation systems. Defining limits for equipment that is even more sensitive requires a detailed review of the specific equipment involved. This type of review is usually performed during the Detailed Analysis associated with the final design phase and not as part of the environmental impact assessment. Mitigation of transit vibration that affects sensitive equipment typically involves modification of the equipment mounting system or relocation of the equipment rather than applying vibration control measures to the transit project.
Note that this category does not include most computer installations or telephone switching equipment. Although the owners of this type of equipment often are very concerned about the potential of ground-borne vibration interrupting smooth operation of their equipment, it is rare for computer or other electronic equipment to be particularly sensitive to vibration. Most such equipment is designed to operate in typical building environments where the equipment may experience occasional shock from bumping and continuous background vibration caused by other equipment.

***Vibration Category 2** - Residential: This category covers all residential land uses and any buildings where people sleep, such as hotels and hospitals. No differentiation is made between different types of residential areas. This is primarily because ground-borne vibration and noise are experienced indoors and building occupants have practically no means to reduce their exposure. Even in a noisy urban area, the bedrooms often will be quiet in buildings that have effective noise insulation and tightly closed windows. Moreover, street traffic often abates at night when transit continues to operate. Hence, an occupant of a bedroom in a noisy urban area is likely to be just as exposed to ground-borne noise and vibration as someone in a quiet suburban area. The criteria apply to the transit-generated ground-borne vibration and noise whether the source is subway or surface running trains.*

***Vibration Category 3** - Institutional: Vibration Category 3 includes schools, churches, other institutions, and quiet offices that do not have vibration-sensitive equipment, but still have the potential for activity interference. Although it is generally appropriate to include office buildings in this category, it is not appropriate to include all buildings that have any office space. For example, most industrial buildings have office space, but it is not intended that buildings primarily for industrial use be included in this category."*

Besides from these categories, there are special buildings such as concert halls, studios, theatres, etc. These need to be analysed individually and have their own impact criteria. Each category has a criterium for when the impact is too large and mitigation measures will have to be used This also depends on the frequency of events i.e. how often the excitation occurs. These criterium levels can be seen from Table 2.

Table 2: Ground-borne vibration (GBV) and ground-borne noise (GBN) impact criteria for general assessment (Hanson, et al., 2006)

Land use category	**GBV Impact Levels** (VdB re $1 \cdot 10^{-9} \frac{m}{s}$)			**GBN Impact Levels** (dB re 20 μPa)		
	Frequent events[1]	**Occasional events[2]**	**Infrequent Events[3]**	**Frequent events[1]**	**Occasional events[2]**	**Infrequent Events[3]**
Category 1: Buildings where vibration would interfere with interior operations.	93 VdB[4]	93 VdB[4]	93 VdB[4]	N/A[4]	N/A[4]	N/A[4]
Category 2: Residences and buildings where people normally sleep.	100 VdB	103 VdB	108 VdB	35 dBA	38 dBA	43 dBA
Category 3: Institutional land uses with primarily daytime use.	103 VdB	106 VdB	111 VdB	40 dBA	43 dBA	48 dBA

1. " Frequent events" is defined as more than 70 vibration events of the same source per day. Most rapid transit projects fall into this category.
2. "Occasional events" is defined as between 30 and 70 vibration events of the same source per day. Most commuter trunk lines have that many operations.
3. "Infrequent events" is defined as fewer than 30 vibrations events of the same kind per day. This category includes most commuter rail branch lines.
4. This criterion is based on levels that are acceptable for most moderately sensitive equipment such as optical microscopes. Vibration-sensitive manufacturing or research will require detailed evaluation to define the acceptable vibration levels. Ensuring lower vibration levels in a building often requires special design of the HVAC systems and stiffened floors.
5. Vibration-sensitive equipment is generally not sensitive to ground-borne noise.

When the building has been categorized the need for further assessment can be found from the distance to the vibration source. The following table presents threshold values, where distances above the indicated values does not need to be analysed in the General Vibration Assessment.

Table 3: Screening distances for vibration assessment (Hanson, et al., 2006)

Type of project	**Critical Distance for Land Use Categories[1] Distance from Wight-of-Way or Property Line[2]**		
	Category 1	**Category 2**	**Category 3**
Conventional commuter train	185 m	65 m	40 m
Rail rapid transit	185 m	65 m	40 m
Light rail transit	140 m	50 m	35 m
Intermediate capacity transit	65 m	35 m	20 m
Bus projects (if not previously screened out)	35 m	20 m	-

1. The land-use categories are the 3 categories defined in the report by (Hanson, et al., 2006). Some vibration-sensitive land uses are not included in these categories. Examples are: concert halls and TV studios which, for the screening procedure, should be evaluated as Category 1; and theatres and auditoriums which should be evaluated as Category 2.
2. Distances are converted distances from feet to meter and rounded up, if exact values are needed these can be found from the original report made by (Hanson, et al., 2006).

The screening process reveals which structures need to be assessed in the General Vibration Assessment. In addition, the categories and different limit values which for each category define whether a detailed vibration assessment in necessary.

The general vibration assessment is based on a baseline principle, where a baseline vibration level for a building is defined based on the distance to the vibration source. After defining the baseline vibration level, tabulated reduction or addition values can be determined based on the present condition at the specific site. The baseline graph which is used in the method for urban transit systems is based on measurements made in North American transit systems and summarized in the Federal Transit Administration report, (Hanson, et al., 2006). For the higher speed trains, measurements have been made in various places around Europe including France, Italy, Sweden and more. (Harris Miller Hanson Inc, 2005).
The baseline vibration level can be found from Figure 8:

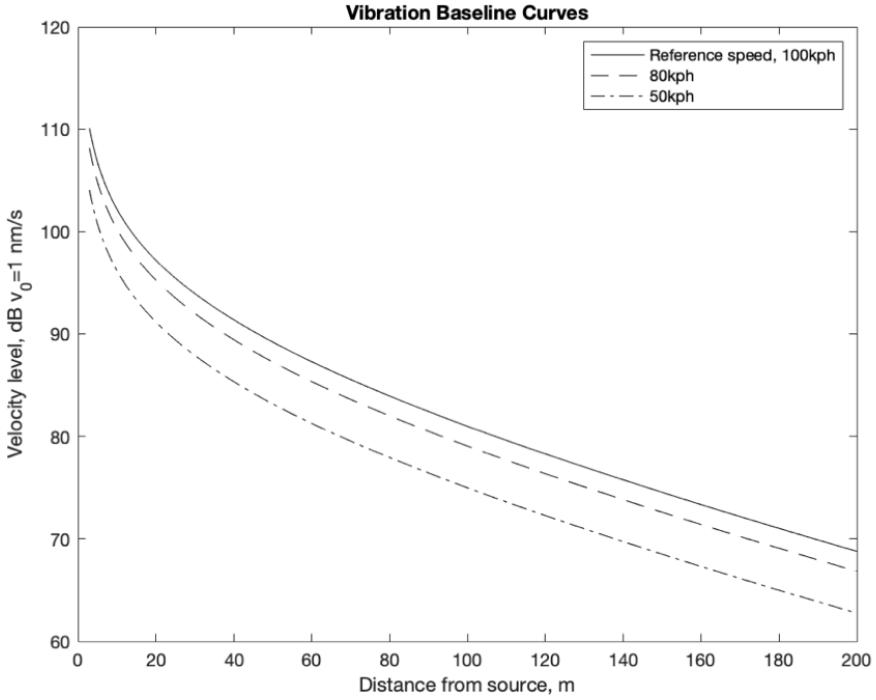

Figure 8: Generalized ground surface vibration curves (Talja & Saarinen, 2009)

Baseline curves are found in the Finnish guidelines made by VTT (Talja & Saarinen, 2009). The baseline defined by VTT is based on a speed of 100 km/h, which in Figure 8 is illustrated as the reference speed. As the train speed in the city centres rarely reach 100 km/h the baseline levels have been adjusted according to methods described in the Federal Transit Administration report. (Hanson, et al., 2006) The formula given for the baseline level (100 km/h) is given below:

$$L_v = A - B \cdot log10\left(\frac{d}{d_0}\right) - C \cdot \left(\frac{d}{d_0}\right) \quad \textit{Eq. 3}$$

Where
$A = 103\ dB$
$B = 14\ dB$
$C = 0.8\ dB$
$d_0 = 10\ m$
$d = distance\ from\ the\ source, m$
$L_v = Vibration\ velocity\ level, VdB$

The curves were adjusted according to the reference speed and this can be done further if other speed levels are needed. Using the following relation:

$$adjustment(dB) = 20 \cdot log10\left(\frac{speed}{speed_{ref}}\right) \quad \textit{Eq. 4}$$

As soon as the baseline level of vibration has been found it should be adjusted according to site specific measures. The nature and magnitude of the adjustments can be found from Appendix 1: Adjustment Factors for Generalized Predictions of Ground-Borne Vibration and Noise.

The factors affecting the vibration propagation in this model are divided into three categories; source, path and receiver. The Source factors are mainly related to the quality of the suspension systems, the track conditions and the state of the rails/wheels. The path is considering reflective soil layers such as bedrock, the coupling to the building and the ground conditions. The receiver is covering factors related to the actual building.

Note that the ground condition factors are significantly simplified and do not accommodate variations in soil properties beyond not-propagating soil and efficiently propagating soil.

The purpose of the general vibration assessment is to get an indication of the vibration levels at the receiver, enabling an evaluation according to the defined impact criteria. If the impact criteria are exceeded, mitigation measures must be used. In some cases, the screening process or the general vibration assessment yields that a building should be evaluated according to the detailed vibration assessment. In the detailed vibration assessment, the issue with e.g. the ground conditions is significantly decreased due to the amount of testing required in-situ in this assessment. The detailed assessment comprises of three different steps; surveying existing vibration, predicting future vibration and vibration impact, and developing mitigation measures.

The surveying of the existing vibrations is decreasing the amount of uncertainty to the ground conditions by measuring the actual conditions.

3.1.5.1 Modelling of Vibration Propagation Through Soil

The empirical models seek to simplify the assessment of ground-borne vibrations while using parameters found from real data to improve the reliability of the results. Modelling the ground behaviour with numerical models is a more complicated approach to predict the ground vibrations. The more complex approach enables results which response with a higher

compliance to the reality of each individual site. It is possible to define parameters for each element in the track structure and the surrounding ground and generate a coupled system, which naturally also is a simplification of the reality, that produces simulations of the system's response to different cyclic loads. This gives a deeper understanding of which elements and parameters influence the vibration propagation most and therefore the possibility of improving the system where it is most effective.

A system widely used in predicting the vibration propagation in the ground is shown in Figure 9. The system is one of many similar systems analysed by other researchers ((Auersch, 2005), (Jones, et al., 2004), (Sheng, et al., 2003), (Lei, 2015), etc.). In a spring system, the load is transferred to the rail which is supported by springs, which could be e.g. rail pads. The rail is assumed to act as a Euler beam with the stiffness $k_{rail} = EI$ and the mass m_{rail}. The supporting springs have a stiffness, k_1, and are connected both to the rail beam and the sleepers or concrete slab, which similarly with the rail is modelled as a beam, with mass and stiffness. (Jones, et al., 2004)

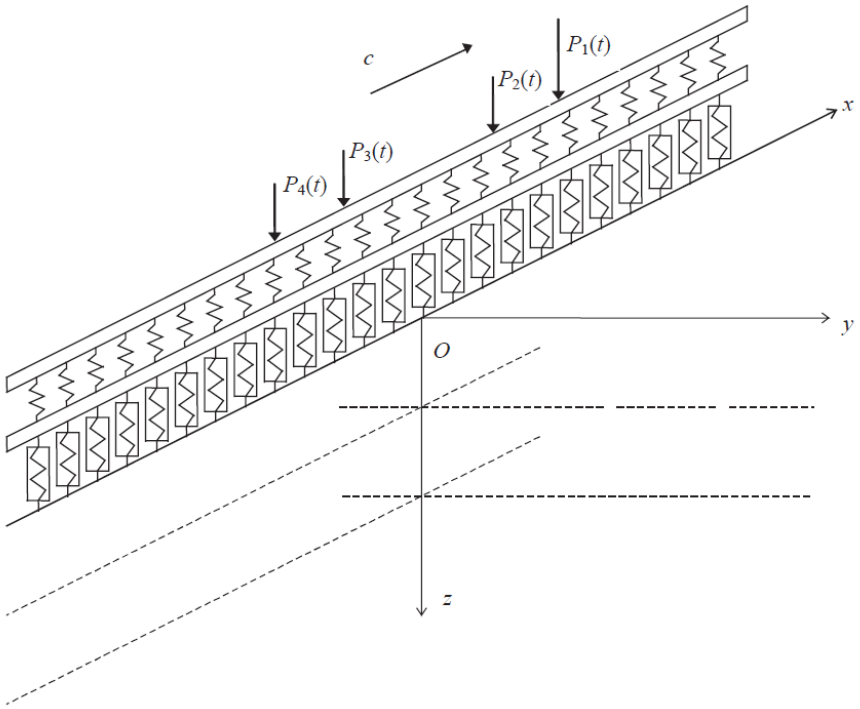

Figure 9: Dynamic system of track structure (Jones, et al., 2004)

The concrete slab or sleepers are typically placed on either a ballast material or the subgrade. The subgrade and/or ballast material is modelled as a viscoelastic material, which deforms elastically and has the stiffness k_{soil}. The subgrade and/or ballast has a viscous damping effect on the track system, which depends, among others, on the resonant frequency of the material and the frequency of the cyclic load that the material is exposed to. When the frequency the material is exposed to approximates the resonant frequency, the damping becomes infinitesimally small as shown in Figure 10. As;

$\frac{\omega_0}{\omega_n} < 1$ there is only little damping and amplification

$\frac{\omega_0}{\omega_n} > 1$ the damping is significant and there is no amplification

$\frac{\omega_0}{\omega_n} = 1$ the amplification is at its maximum and there is close to zero damping (Paul de Vos, 2017)

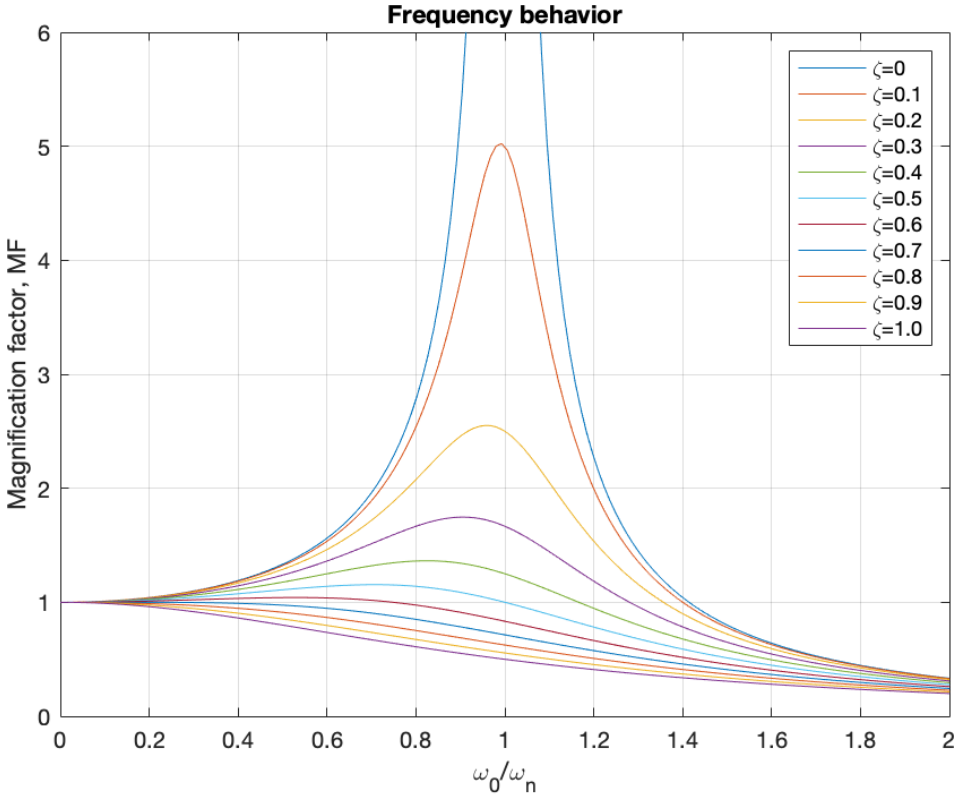

Figure 10: Frequency behaviour at different damping factors (Hibbeler & Beng Yap, 2013)

When modelling the behaviour of the whole track system this tendency is also observed and the influence on the whole system can be analysed. When modelling a system of e.g. springs it is possible to analyse the dispersion of the vibrations and that way indicate how far the waves travel and at what magnitude. (Jones, et al., 2004)

3.1.6 Mitigation Methods

Noise and vibrations from railway traffic can have a significant impact on our wellbeing and the impact increases the closer to a railway we live. To reduce the impact, different mitigation methods have been developed gradually along with the railway becoming an increasingly normal part of the urban areas. The mitigation methods described in this thesis are divided into two groups; Mitigation methods for vibrations and mitigation methods for noise. There is a clear difference in the way the two groups affect the surroundings. Noise is mostly affecting the wellbeing of individuals nearby, whereas the vibrations can have a larger structural impact and cause a feeling of structural instability. Vibrations impacting the structural surroundings can in worse cases have an influence on the buildings and other structures, and in other cases it can impact the accuracy of highly sensitive laboratory equipment.

Mitigation methods are continuously developed and improved. Widely used mitigation methods are shown, but not limited to, those in Table 4.The mitigation measures are divided into three groups; The source, the path and the receiver.

Table 4:Mitigation methods and estimated impact (Paul de Vos, 2017)

	Mitigation method	Method for Noise	Method for Vibration
Source	*Improving wheel roundness*	2-12 dB	2-12 dB
	Reduction of unsprung mass	2-12 dB	2-12 dB
	Track alignment & defects in track and substructure[1]	0-10 dB	0-10 dB
	Specially made vibration-resistant rail fasteners	0-13 dB[2]	0-13 dB
	Rail fixed and suspended in a concrete slab	2.5dB	2.5dB
	Under sleeper mats	2-20 dB[3]	
	Under ballast mats	6-14 dB	0-3 dB
	Un-ballasted slab-track with vibration and noise reducing connection systems.	0-6 dB	Limited
	Floating slab track[4]	20-26 dB	14-20 dB
	Column stabilization	-	X[5]
Path	*The mitigation idea in the path is to install a construction which due to its stiffness and density obstruct the wave propagation beyond the point of the construction significantly. This can be a trench, wall, elevation or drop in height etc.*[6]	X	X
Receiver	*Elastic shield around foundation of building*	2-6 dB	
	Piling – increase of soil stiffness	-	<50%
	Resilient bearing of building (The buildings foundation is placed on a system of elastomeric material and steel springs)[7]	20-26 dB	20-26 dB
	Additional stiffening of wooden floors with e.g. extra beams	Negative effect	2-6 dB

The impact noted in columns three and four are indicative values, and hence are not scientifically proved. There are generally many factors affecting the propagation of vibrations and development of noise from railways. As a rule of thumb, it is important to make sure that the condition of the track and underlaying supporting structure is acceptable and likewise ensuring that the condition of the train corresponds to the standards.

[1] Note that it clearly depends on the state of the railway structure prior to the improvement
[2] Impact is highest on the noise, and lower for the vibrations
[3] Depends on the properties of the fastening systems and the quality of the mats. There is a risk that the installation of under sleeper mats can increase the air-borne noise levels
[4] A very costly method, usually used in tunnels
[5] Increasing stiffness of soft layers decrease the wave propagation in those layers. No actual estimates available, but structures in Sweden has shown possible reduction in ground-borne vibrations up to 45%
[6] Impact must be evaluated separately in each case.
[7] Also used in bridge structures as supports/bearings

3.2 Urban Railway Systems

The railways nowadays have several functions and are constantly under development. Railways are natural to be used for transportation at higher speeds and longer distances because it saves money, emissions, time etc. These higher-speed railway systems are under development, and issues are appearing regarding the propagation of vibrations in the ground and the increasingly higher risk of the doppler effect impacting the nearby structures in a more severe manner than previously with trains going around 180-250 km/h.

Due to the increasing awareness of the environmental issues present in the society today and their development, the demand for transportation systems reducing ordinary car traffic in the city centres is increasing. Systems which reduce emissions and enable people to travel together and which are reliable regarding time schedules, are increasingly being introduced in modern cities. Simultaneously the larger cities are growing, and the suburban areas are moving further away from the city centres. Many of the larger cities are facing these issues and are trying to solve it by building light rail systems, limiting access for fossil-fuel driven cars to the centre etc. As an example, the three largest cities in Denmark are either planning, building or expanding their light rail systems and several new light rail systems are coming in Finland's largest cities.

In Figure 11 the two sketches illustrate two widely used principles when building railways. One significant difference in the systems is where they are used and how the load is transferred from the rail to the ground. Usually the lower structure is used in the city centres, because the rail is integrated in the road by the concrete slab, which allows cars to pass easily over the track. The upper structure is commonly used outside the urban area, because it does not act well with other types of transportation. In this structure the load is transferred to sleepers with a fixed spacing, which periodically change the stiffness of the support system. The distance between the sleepers highly affects the vibrations transmitted to the ground due to the effect of the changing stiffness. In the slab supported track structure the transmitted frequencies due to changing stiffness of the support system are significantly reduced; hence the vibrations and noise are reduced, which also increases the suitability of the system for urban use. In addition, the slab supported system distributes the load more equally to the underlying ground, which decreases the stress induced on the ground. More about sleeper related vibrations is found from section 3.2.1.

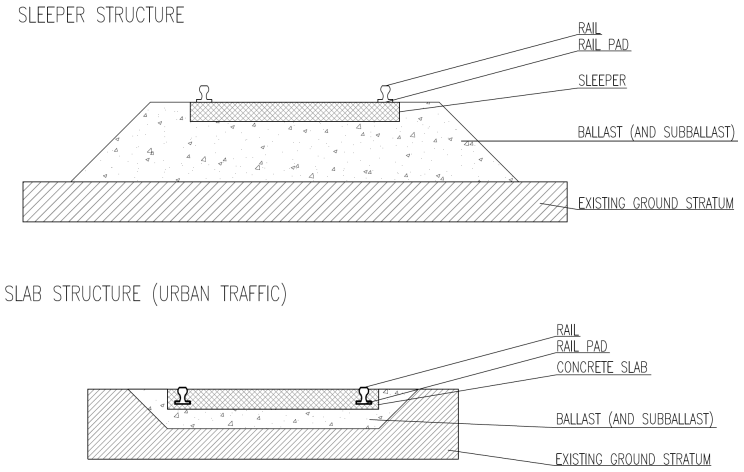

Figure 11: Railway systems sketch (Linden, et al., 2019) and (Dahlberg, 2006)

Note that Figure 11, only depicts an illustration of an example of the components in an urban and non-urban railway system. In the following the functions of the different parts are described briefly. In both systems shown in Figure 11 the concrete slab or the concrete sleeper is installed in a granular material, which usually is a ballast material of crushed rock that is used in the sleeper structure but for the slab structure this is not always the case.

The rails are creating the path for the train to travel and allow relatively stiff transmission of loads, which means that they are distributed over a larger area. The rails' hardness also increases the durability of the track. If the rails are not made from good material, there is a much higher risk of the rail getting significantly more irregularities, which leads to higher amount of vibrations. The rails are in many urban cases installed with rail pads under them. These rail pads can be of two different types, where one is soft and the other one is made stiffer, which increases the transmission effect of the load. The softer rail pads usually have a significantly higher damping ratio and a lower resonance frequency. By using rail pads, there is a possibility to adjust their properties of these according to the critical frequencies. The rail pad acts as a sort of filter which, depending on the properties, attenuates some frequencies so fast that they do not impact the underlaying structures significantly. E.g. a soft rail pad with a very low resonance frequency will have extremely high damping at the higher frequencies. The use of under sleeper pads (USP) has also been tested and it has been shown that they are mostly effective in the frequency range which lies below 250 Hz. (Johansson, et al., 2008)

The rail pads are located under the rails and are in contact with either the sleeper or the concrete slab. The rails are attached to the sleepers or concrete slab in such a way that the stability of the rails is as high as possible and according to standards, this allows full transmission of forces from the rails to the sleeper/slab.

The sleeper and slab's role is to create contact between ground and rail, to transfer horizontal (e.g. breaking force) loads, to transfer vertical loads and while accommodating these features, generating a stable and installation friendly base for the rails. The sleeper/slab structure is used to ease the levelling and alignment of the rails. One of the most significant sources to vibrations both in the physically noticeable and in the noisy spectrum is the quality of the track's alignment. (Harris Miller Hanson Inc, 2005) In a sleeper structure the sleepers are surrounded by ballast material. The ballast is usually made of relatively large grainsize crushed rock material and helps distributing the loads over a larger area. Furthermore, the damping properties of the ballast layer support the attenuation of the vibrations, this way decreasing the vibrations transferred to the surrounding ground. The ballast layer is usually followed by a subballast layer, which is a separating layer between the subgrade and the ballast layer, preventing the two layers to blend.

The subgrade is beneath the subballast layer and is often made by levelling the original ground depending on the properties of the original ground. (Dahlberg, 2006) Sometimes the subgrade is just the existing ground levelled in the wanted way, other times it is made by applying new material and levelling it to the desired level. The subgrade is very important for the overall structural safety of the track construction. (Li & Selig, 1995) These 3 layers are all further described in section 3.3.1. Finally, the structure reaches the ground stratum where the loads are carried, and vibrations are transmitted to the structures nearby.

The slab structure does not necessarily have the ballast layer but can also be built directly on the subgrade. The slab is providing support the whole way under the rails, hence giving a better stability to the rails. The continuous support also enables a better alignment, which, as previously mentioned, results in a longer lifetime and a decrease in vibrations. (Dahlberg, 2006)

3.2.1 Frequency domain in urban railways

The frequency domain refers to the range of frequencies which are relevant for design. It is important for modelling and estimation of vibrations to know which frequencies the track system will be exposed to. In this particular context, the frequency range for urban railways is studied to achieve information about the frequency domain of which the crushed concrete will be exposed to. For the estimation of the frequencies it is assumed that the urban transit systems are moving with speeds of interest from 20 km/h to 100 km/h (Vuchic, 2007). For categorising the frequencies as vibrations, noise or audible sound see Figure 1. The excitation frequencies are found according to the following expression (Dahlberg, 2006):

$$f = \frac{v}{\lambda} \qquad \textit{Eq. 5}$$

Where v is the velocity, λ is the wavelength and f the frequency. The main excitations may occur due to wheel/rail irregularities (wavelength, $\lambda = 0{,}03 - 0{,}3m$), uneven settlements (wavelength, $\lambda = 0 - 100m$), sleeper distance (wavelength assumed equal to distance, $\lambda = 0{,}6m$) and, as described in more detail in section 3.1.2, the moving point load. Using the wavelengths and speeds for both the urban rail traffic and the regional (not-high-speed trains) traffic, the frequencies related to these two categories are obtained. (Dahlberg, 2006)

Figure 12 shows the relation between the speed, the wavelength and the frequency, and this way it is clear to see that an increase in speed increases the frequency and a decrease in the distance between irregularities increases the frequency. The frequencies obtained from the irregularities for the urban traffic range from around 20 Hz to around 740 Hz.

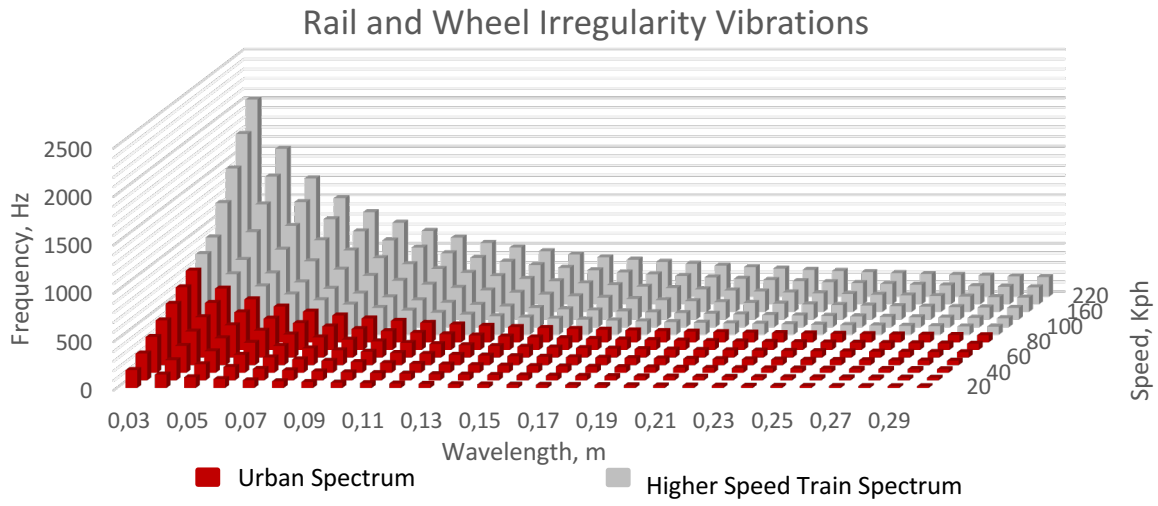

Figure 12: Rail and wheel irregularity frequencies

Uneven settlements result from differences in the deflection of the track due to different support stiffnesses. The wavelengths of the uneven settlements are generally ranging from small to very large, $\lambda < 1 \rightarrow 100 < \lambda$. The large range of wavelength is due to the source of the uneven settlements, which can be caused from a change in the support stiffness. The change in support stiffness can be due to a change in ground conditions, insufficient compaction of the track structure, insufficient compaction between sleepers etc

Usually the differences in stiffness in the track structure can be avoided by increasing the construction quality and construction quality control. It is natural that over large distances the uneven settlements can be difficult to avoid due to the natural inhomogeneity of soil (Dahlberg, 2006). The frequencies coming from uneven settlements are seen in Figure 13, and are low in comparison to the other sources of vibration due to the long wavelength. The frequency domain from the uneven settlements are found to vary from around $0.1\ Hz$ to around $2.5\ Hz$.

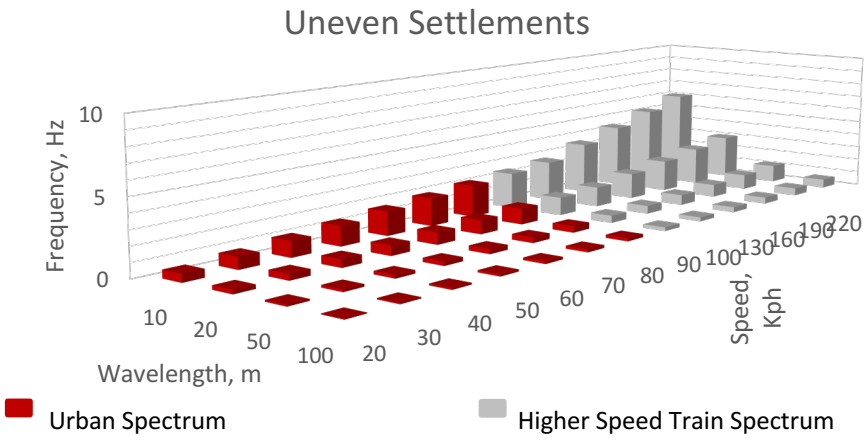

Figure 13: Uneven settlements frequencies

The usual distance between sleepers are around $0.6\ m$ (Bonnett, 1996), hence a wavelength of $0.6\ m$ is assumed in obtaining the frequency range for the sleeper vibrations. The frequencies therefore depend only on the speed of the train and is found to vary from around $10\ Hz$ to around $100\ Hz$, see Figure 14.

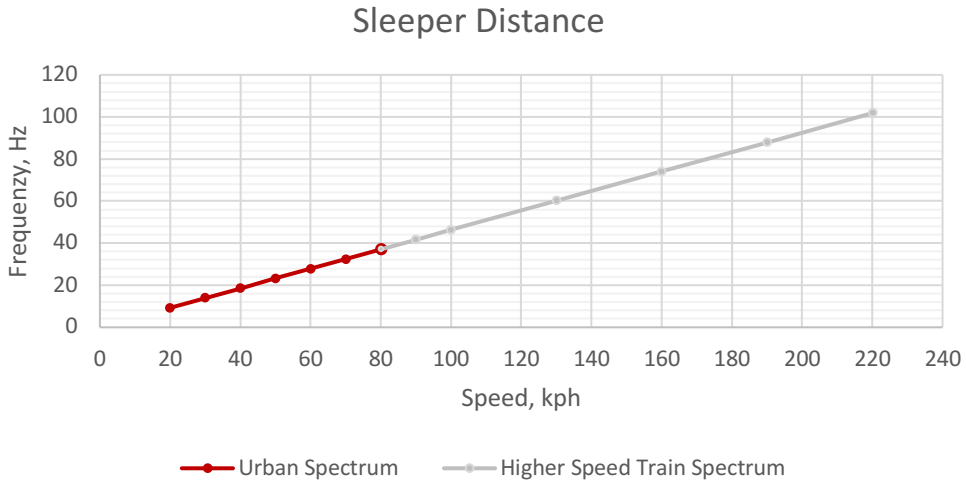

Figure 14: Sleeper distance frequencies

3.3 Conventionally Used Materials

The conventional railways are built up as shown in Figure 11, and are using stone material to form the ballast and subballast layers. As described in section 3.2 there are several ways to build up railway superstructures depending on the purpose, ground properties, alignment, etc. The quality of the superstructure is of great importance for the overall stiffness and lifetime of the railway track, and can greatly affect the deterioration of the rails, vibrations to neighbouring structures, stability and much more. Replacing one of the materials in the superstructure with a new material requires extensive knowledge about the new material to lower the economical, safety and durability risk. This section aims to briefly address the main purposes, uses and properties of the ballast, subballast and subgrade layers.

The load transfer path from conventional railways is usually from the wheel → rail → railpad → sleeper → ballast → subballast → subgrade. The railpad can either be soft or stiff, where the soft railpad isolates the high frequencies from the trainload and the stiffer railpad transfers the load more directly and rigidly to the sleeper. The sleeper is usually submerged into the ballast, hence supported on all sides, transferring the all loads directly to the ballast layer.

Usually the ballast layer consists of highly compacted crushed rock or stone material. The ballast layer should be as stiff as possible to distribute the point loads from the train to as large an area as possible. When the loads are transferred from the sleepers to the ballast, the ballast distributes the load onto a larger area so that the stresses are reduced.

When the load has travelled through the ballast layer it arrives at the subballast layer, which is a finer grained material that connects the ballast layer with the subgrade. The use of a subballast layer is to avoid direct contact between the ballast layer and the subgrade, so that there is no risk of mixing the two layers. At the same time the subballast works as a frost protection layer and is packed relatively hard to perform as a load distributing layer. (Dahlberg, 2006)

The subgrade can have different functions depending on the railway type. In a conventional regional railway built up with sleepers, the subgrade would serve as a levelling of the structure above. In this case it would most likely be made by levelling the existing ground. The slab structure is often used for the urban transit systems, where there is significantly less space to build on. There is usually a thinner layer of granular material between the original ground and the slab, which depending on the quality of the original ground and the purpose of the railway, is made of a ballast material or a finer granular material. The idea is to level the ground and give an attenuating effect before the vibrations are transferred to the ground. (Dahlberg, 2006)

3.3.1 Ballast, Subballast and Subgrade Material

The ballast material comprises of material with larger grain sizes than the subballast material. Normally good quality rock or stone material is used for the ballast material, this could be limestone, granite, crushed stone or gravel, where the granite is usually considered as the best option (Bonnett, 1996).

The ballast layer has two main purposes, which are to drain water away and to receive and distribute the load to a larger area. The preferred material is uniformly graded and angularly

shaped and because of the contact between the sleeper/slab and the ballast the grain size should not be too large. Too large grain sizes will reduce the contact area between the sleeper/slab and the ballast and aggravate the distribution of the loads. At the same time the ballast layer should have proper drainage properties and should therefore not have too small particle sizes which by time might become increasingly impermeably due to grease, dust etc. filling up the voids. Thus, the preferred grainsize interval for the ballast layer is from 28mm – 50mm (Bonnett, 1996).

The subballast layer should perform both as a frost protection layer and a drainage layer leading the water away from the superstructure. Subballast material is usually finer grained than the ballast, often sand or gravel. Besides the frost protection and drainage qualities of the subballast layer, it also acts as a filter between ballast and subgrade (Dahlberg, 2006).

As the purpose of the subgrade layer varies according to the type of railway, the properties of the material also vary from levelled original ground to well stabilized material. In the urban railway systems where the slab structure is supported by the subgrade, the subgrade material should be of a material which can be compacted to a stiff supporting layer. The subgrade should accommodate most of the features from the ballast layers in case the concrete slab is placed directly on the subgrade. In countries like Finland where the bedrock is relatively close to the ground surface it is important that the vibrations coming from the railway are attenuated significantly before reaching the bedrock. Due to the very low damping in the very stiff bedrock, vibrations travel at high speeds and can clearly be felt in the nearby structures. Hence, the quality of the subgrade used in these situations is very important (Dahlberg, 2006). In Table 5 dynamic parameters from different sources on different materials are listed.

Table 5: Dynamic properties from literature review

Material	Density	S-wave velocity	P-wave velocity	Damping, $\frac{c}{c_c}$	Poisson ratio	Spring stiffness	Small strain modulus, Emax	Reference
Unit:	*kg/m3*	*m/s*	*m/s*	*%*	*-*	*MN/m*	*MPa*	
Ballast	2000	150-300	600	2	-	-	-	(Faure, et al., 2015)
	1600	250	-	-	0.2	-	-	(Verbraken, et al., 2015)
	-	270	-	30	-	-	-	(Zhang, et al., 2020)
	-	244	-	20	-	-	-	
	-	345	-	20	-	-	-	
	-	-	-	9-44	-	-	245-690*	
	-	-	-	160**	-	120	-	
	-	-	-	225**	-	170	-	

Ballast	2000	270	-	5	0.33	-	-	(Auersch, 2005)
	-	-	-	-	-	-	315*	(Jones, et al., 2000)
Subgrade	1700	200	-	-	-	-	-	(Lombaert, et al., 2015)
	2000	200	400	2.5	-	-	-	(Coulier, et al., 2015)
	-	200	400	2	-	-	-	(Faure, et al., 2015)
	1500	-	-	10	0.4	-	60*	(Jones, et al., 2000)
Crushed concrete	-	150-450	300-750		0.26-0.37	-	200-500	(He. & Senetakis, 2016)
*) Not mentioned as Small-strain modulus, but used in vibration modelling **) Not a ratio, but actual damping with unit of *kN/m*								

3.4 Crushed Concrete

Concrete waste is a useful waste product from demolition plants and concrete production industry. Depending on the origin, cleanliness and compression strength, the concrete waste can be classified into four different classes, which define how the concrete waste can be reused (Dettenborn, et al., 2015). The limiting factor for the use of the crushed concrete waste varies from project to project, however the limiting factor for infrastructure projects would be the strength and chemical composition.

The crushed concrete material has a great potential to be used in road construction, railways and many other areas where granular material is needed. In each case there might be different limiting factors defining which crushed concrete class has to be used. For railway systems the crushed concrete is not yet used for its full potential (Linden, et al., 2019).

By defining the dynamic parameters of the crushed concrete material, expectantly this will stimulate the incentive to start using the crushed concrete to a higher extend in the railway industry where a large portion of granular material is used. The concrete classes are seen from Table 6, where the concrete is classified by origin, and in Table 7, where it is classified based on material parameters and composition[8].

Table 6: Concrete class from origin (Anttila, 2020)

Concrete class	Material description and origin
BeM I	Impurity free concrete waste from e.g. concrete element industry
BeM II	Concrete waste from e.g. demolition sites
BeM III	Concrete waste from demolition sites or similar, where the reinforcement content is uncertain
BeM IV	Concrete waste from demolition sites or similar, where the reinforcement content is uncertain

[8] Note that not all categories are included in the table and that these requirements are requirements from Finland and can therefore not be generalised to the rest of the world.

Table 7: Concrete class from composition and parameters (Anttila, 2020)

Class	Compressive strength [MPa]	Young's Modulus, E_2[5] [MPa][1]	Max. brick content [%-weight]	Max. percentage other materials[2] [%-weight]	Floating materials[3] $\left[\frac{cm^3}{kg}\right]$
BeM I	≥ 1,2[6]	700[4]	10	1	5
BeM II	≥ 0,8[6]	500[4]	10	1	10
BeM III	-	280[4]	10	1	10
BeM IV	-	Varies	30	1	-

1) BeM I and BeM II reach the Young's modulus shown after 1-3 months, and BeM III reach their Young's modulus after 0-1 month. This is considering favourable conditions and layers constructed according to standard instructions. In other cases, moduli might be different and/or take longer to obtain.
2) Metals, wood, plastics, rubbers, etc.
3) Foams, mineral wool, etc.
4) Dimensioning must take the underlaying layers bearing capacity into account.
5) This modulus is not the traditional Young's modulus, but the modulus used in road design.
6) 28 days hardened cylinder samples, diameter 100 mm and height 100 mm

The crushed concrete can come in many different grain sizes, from boulder size to fine granular material, this is depending on the purpose of the concrete material. In case the material is used as a subbase material, the maximum grainsize is 90 mm and generally 45 mm is used. Crushed concrete may be utilized with an environmental license granted by environmental authors or based on a Governmental Decree on the recovery of certain waste in earth construction, the so called "MARA-decree" (Finnish Ministry of Environment, 2017). If the utilization is based on the "MARA-decree", the maximum grainsize is 90 mm.

In Finland, the regular design and construction parameters for crushed concrete have been studied extensively since the early 1990-s, when the intensive development began to reclaim crushed concrete in construction works. However, there has been no national research into the dynamic properties of crushed concrete and only fairly moderately on an international level. These properties would be needed for proper design using crushed concrete in railway structures and for a proper estimation of the related ground-borne vibrations.

The intention by defining the dynamic parameters of the crushed concrete is to be able to use it instead of the subgrade in urban railway systems, which are slab supported and directly on top of the subgrade. Due to the purpose of the concrete, it consists mainly of material which is like well graded gravel.

According to a feasibility study made by (Linden, et al., 2019) the crushed concrete material has been found to be suitable for replacing the subbase (subgrade) and base-course materials in railway construction. For replacing the structural layers, more research is currently needed. As the dynamic perspective of the material has not yet been covered, these properties are still needed for the acceptance of the material as a substitutive material in some projects.

3.4.1 Properties

The initial characterization of crushed concrete material has been done partly for this thesis and partly for previous reports ((Linden, et al., 2019), (Vuorimies, 2002), (Anttila, 2020), (He. & Senetakis, 2016)). Furthermore, parameters have been found during the literature review. To increase the available amount of material to be used in the subgrade layers, the material which is tested is BeM II. BeM II is from demolition sites and has slightly lower requirements than BeM II, which increases the availability of the material. There are large amounts of concrete waste coming from the demolition sites and the contractors working on the demolition sites need to get rid of the material usually paying for the disposal, meaning there are both money and resources to save.

BeM II has been further divided into groups according to the grain sizes of the mix before they were cut.

- BeM II – 90: originates from concrete with grains ranging from #0-90mm
- BeM II – 150: originates from concrete with grains ranging from #0-150mm
- BeM II – 300: originates from concrete with grains ranging from #0-300mm

All three materials are from Rudus Oy from the same concrete waste batch, which means that the only difference is the grainsize distribution and the maximum grainsize. In Addition, all three materials have been cut to a maximum grain size of 31.5mm before this study. Their grain size distribution curves are shown in Figure 15.

Figure 15: BeM II, sieving results before material is cut second time.

Uni-axial compression tests made on the material were made on samples with the dimensions $100mm \cdot 100mm$ (cylinder), and tested according to PANK-9003 standards. UCT results have been found after both 7 and 28 days hardening and can be seen from Table 8.

Table 8: Uni-axial compression test results - Previous study (Anttila, 2020)

Material	7d compression strength [MPa]	28d compression strength [MPa]	Dry density (average) $\left[\frac{kg}{m^3}\right]$
BeM II- 90	1.0	1.2	1810
BeM II- 150	0.8	1.0	1793
BeM II- 300	0.7	0.9	1814

The material is modified further before creating samples for the bender element testing. The material used in the bender element testing is a mix of BeM II – 90 and BeM II – 150, which both have been cut to a maximum grain size of #16 (no grains from the #16 sieve were included in the mix) and then mixed. The grainsize distribution for the crushed concrete mix is shown Figure 16.

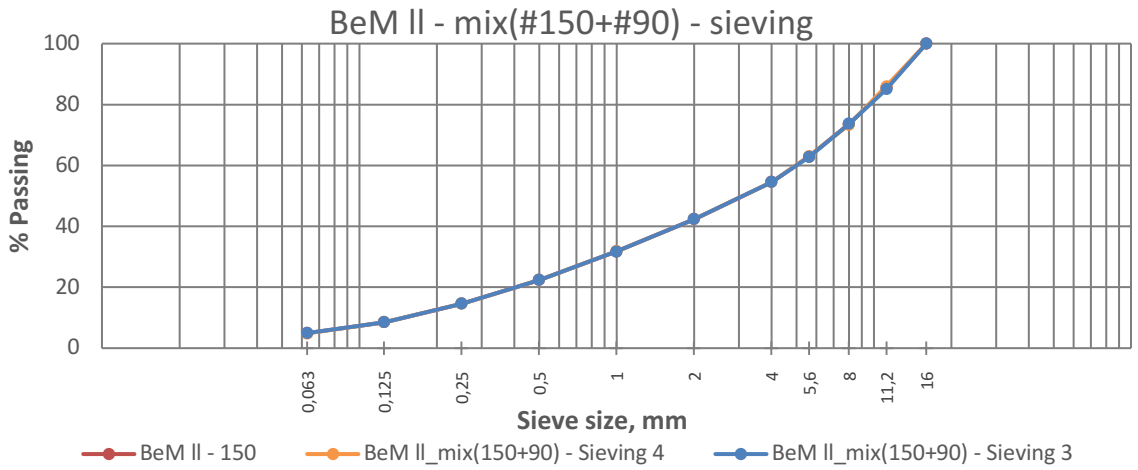

Figure 16: Sieving results from BeM II mix of #90 and #150 cut to maximum grain size #16 mm

Material parameters found from the sieving and from a literature review form the basis of the hypothesis found in section 3.7 and is collected and shown all together in Table 9.

Table 9:Crushed concrete parameters

Parameter	Unit	BeM II – Mix – Value
Dry density, γ_d	$\frac{kg}{m^3}$	1813
Particle density, ρ_s	$\frac{t}{m^3}$	2.55-2.65(1)
Angle of internal friction, φ_c	°	40(2)
Optimum water content, $w_{\%}$	%	8-12(1)
Permeability, k	$\frac{m}{s}$	$10^{-4} \rightarrow 10^{-5}$ (2)
Void ratio, e	-	0.43
Poisson's ratio, ν	-	0.26-0.37(3)
Coefficient of Uniformity, C_u	-	32.8
Average grain size, d_{50}	mm	3.25
Youngs modulus, E_i(4)	MPa	275(1)
Particle shape regularity, ρ (estimated)	-	0.4-0.6 chosen $\rho = 0.5$

1) Based on results found in (Vuorimies, 2002).
2) (Anttila, 2020)
3) (He. & Senetakis, 2016)
4) Young's modulus based on initial elastic stiffness from triaxial tests on BeM 1

The void ratio is not determined experimentally but calculated according to the predetermined particle density.

3.5 Small Strain Stiffness

The magnitude of strain has by several well-known researchers been found to significantly influence the stiffness of soils. In classic solid mechanics elastic strains relate to the fully recoverable deformations of a material and as the strain increases the amount of recoverable strain decreases. For soil it has been found that the range of strains in which the soil behaves fully elastic is actually very small (PLAXIS, 2019). It has been found that the stiffness of soils with increasing strain is decreasing non-linearly as shown in Figure 17. The loss of soil stiffness has been associated with the degradation of internal bonds such as inter-granular surface bonds and interparticle friction. Naturally, at larger strains the displacement of the soil particles increases, hence there is an increase in the degradation of the internal soil bonds.

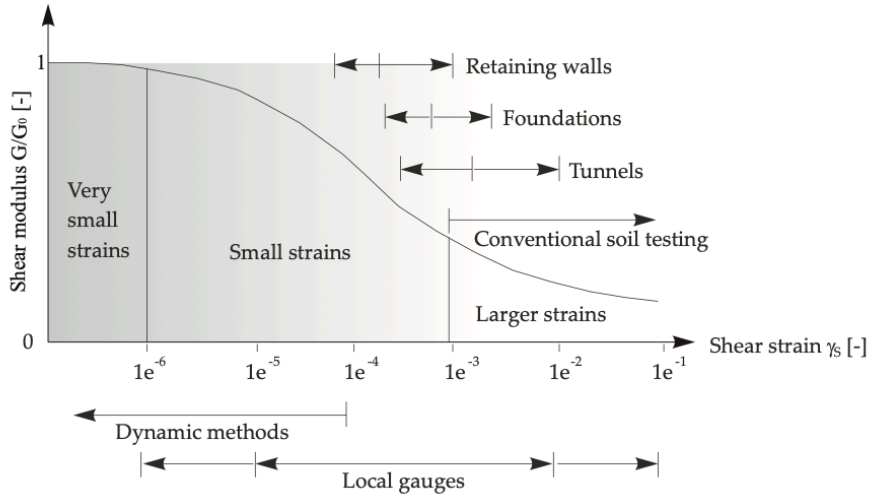

Figure 17: Small-strain stiffness in relation to conventional stiffness (Atkinson & Sallfors, 1991)

The small-strain stiffness has been an established phenomenon in soil dynamics for a long time but has only recently been considered to have an influence in the static analysis. (Clayton, 2011)

Dynamic methods have been used to define the stratification of soils and still are. The stiffness found from in-situ seismic methods yields significantly higher stiffness values and before 1980's this was thought only to be characteristic for the dynamic stiffness of soils. Stiffness tests were then made statically at small-strains, which revealed similar values of those found from the dynamic testing, and it became apparent that there is a clear relation between the magnitude of the strain and the stiffness of the soils. This relation has later been found to be non-linear, where the stiffness is decreasing at increasing strains due to a degradation of the soil skeleton. (Clayton, 2011)

The difference in the stiffness from static to dynamic loading has been thought to be related to the difference in loading properties such as inertia and strain rate, but as it is discovered that this influence is only minimal, dynamic stiffness is often assumed to be equal to small-strain stiffness. (PLAXIS, 2019)

As small-strain stiffness is still a relatively new phenomena, there is only little data available and methods for predicting the small-stiffness of materials are limited. (Alpan, 1970) found a relation between the static and the dynamic soil stiffness, which indicates the magnitude of the difference in stiffness. This relation is shown in Figure 18.

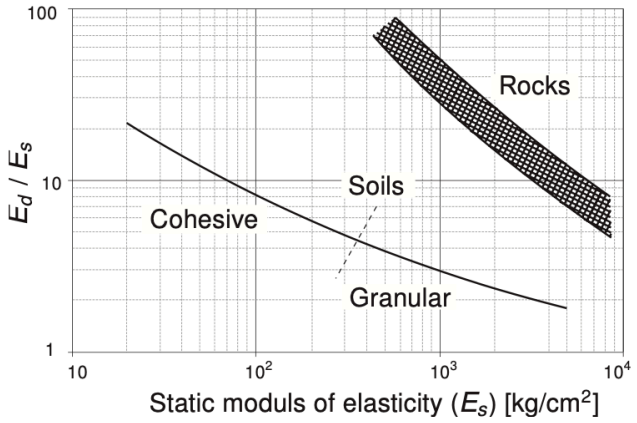

Figure 18: Relation between static and dynamic stiffness (Alpan, 1970)

As the static stiffness of the crushed concrete is assumed to be around $275 MPa$ $\left(\approx 2750 \frac{kg}{cm^2}\right)$, the dynamic stiffness (small-strain stiffness) should be around $275\ MPa \cdot 4.8 \approx 1300\ MPa$, using the relation in Figure 18.

3.5.1 Small-strain stiffness of crushed concrete

The availability of dynamic properties of crushed concrete is very limited and it is unsure whether the available estimation methods also apply to this type of material. One of the major differences from crushed concrete to e.g. sand and crushed stone is the hardening effect of crushed concrete. However, small-strain and dynamic properties of crushed concrete are very relevant for the use in infrastructure projects where the potential use is likely. Referring, especially, to research questions 2[9], 3[10] and 4[11], the study of the small-strain properties of crushed concrete and similar materials is needed. This section highlights some of the methods used for estimation of small-strain parameters and evaluate the usability for crushed concrete.

The increase in the demand of sustainable solutions, the continuously smaller availability of resources and the acknowledgement of the economic benefits of the reuse of crushed concrete has opened a curiosity towards using the material in new ways. He and Senetakis has over a period of several years studied the properties of crushed concrete in various ways, which has led to several publications about the parameters of crushed concrete. Some of the findings, methods and results found in (He, et al., 2018) and (He. & Senetakis, 2016) are used for achieving the hypothesis presented in this section. Along with methods from H. He,

[9] How can the dynamic parameters for crushed concrete and similar granular materials be estimated reliably?
[10] How can the small-strain parameters for crushed concrete and similar granular materials be estimated reliably?
[11] How does the substitution of the commonly used material with crushed concrete affect the vibrations induced by tramways?

K. Senetakis and M.R. Coop also methods by (Wichtmann & Triantafyllidis, 2009) and (Wojciech, et al., 2016) are used.

As seen in Table 9, Poisson's ratio ranges from 0.26-0.37 which is found for concrete samples with grain sizes ranging from 0.60-0.18 mm and 1.18-2.36 mm with a mean grainsize of 0.84 and 1.67 respectively, and coefficient of uniformity of 1.40 and 1.30 respectively (He. & Senetakis, 2016). Hence, the material is significantly more uniformly graded in contrary to the material studied in this thesis. Despite the difference, this range of Poisson's ratio is used as an indication for the studied material, and in the calculations of the estimated small strain modulus a Poisson's ratio of 0.3 is used.

In the paper published by (He, et al., 2018), several formulas for estimating the small strain stiffness are introduced, some of which have been used in the estimation by themselves during their study. The material studied by (He, et al., 2018) is unfortunately also different from the material studied in this thesis. (He. & Senetakis, 2016) have divided the material into 5 different gradings; 0.15-0.30, 0.30-0.60, 0.60-1.18, 1.18-2.36 and 2.36-4.75. In their study of the stiffness of recycled concrete aggregate they found that "*both the small-strain constrained modulus and small-strain Young's modulus of the RCA are quite sensitive to the particle mean grain size".* The small-strain Young's modulus was fitted by a power law formulation. During the fitting of the power law it was found that the results were very sensitive to the coefficient of uniformity. The small strain constant A_E decreased significantly when increasing the coefficient of uniformity. The power law which was used and fitted to the test results is presented as estimation method 1 (M1), with the constants according to the fit.

Estimation method 1 (M1) - (He, et al., 2018)

The small-strain Young's modulus

$$E_{max} = A_E \cdot \left(\frac{p'}{1kPa}\right)^{n_E} \cdot f(e) \qquad \textit{Eq. 6}$$

Where p' is the effective confining pressure or the effective vertical stress.
Small-strain constant (fitted)

$$A_E = 18{,}8 \cdot d_{50}^{0,23} \qquad \textit{Eq. 7}$$

Power coefficient (fitted)

$$n_E = 0.51 \cdot d_{50}^{-0,07} \qquad \textit{Eq. 8}$$

The void ratio function (used to eliminate density effects (He, et al., 2018))
$$f(e) = e^{-1,3} \qquad \textit{Eq. 9}$$

The sample material used in (He, et al., 2018) was tested at two different coefficients of uniformity $C_u \approx 1.4$ and $C_u \approx 2.8$, which are far from the coefficient of uniformity found

for the studied test material, which has $C_u \approx 28.2$ (see Table 9). In the light of the sensitivity to the coefficient of uniformity, the estimation made with $Eq.6$ is not expected to yield 100% reliable results, but still give an indication of the magnitude of the small-strain modulus for the crushed concrete. As this estimation formula is the only one which has been fitted to results obtained from crushed concrete, the predicted values obtained from this equation are expected to yield better results than the other methods. The results from estimation of the small-strain modulus estimated using $Eq.6$ can be seen in Figure 19.

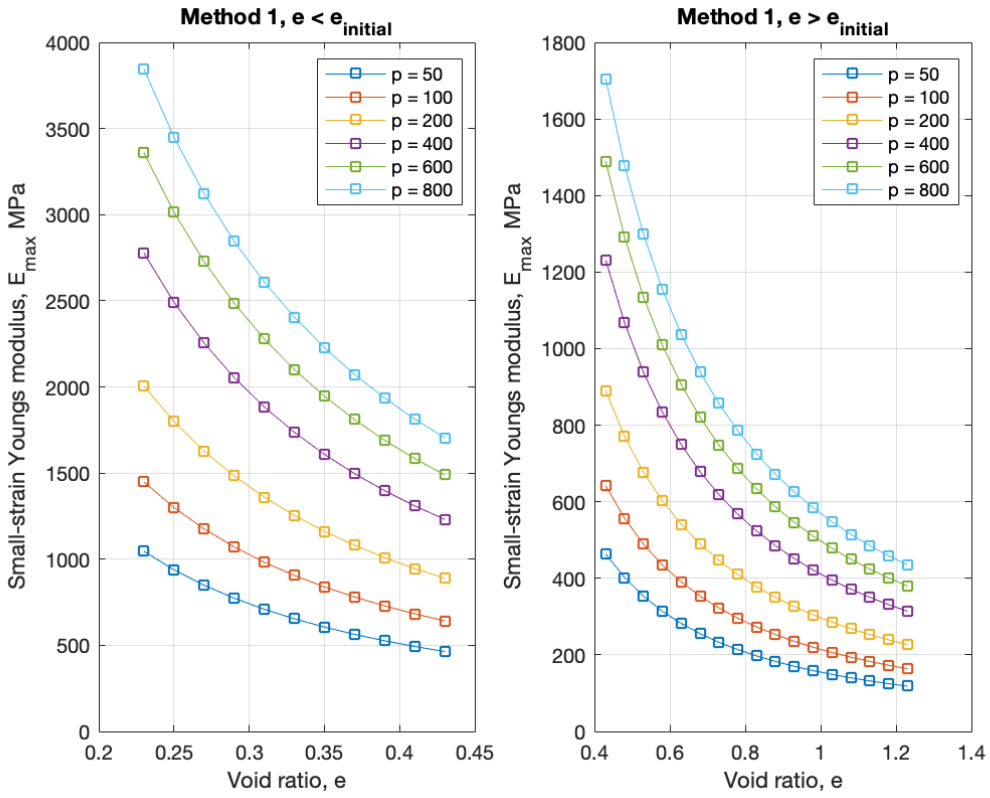

Figure 19: Method 1 small-strain Young's modulus

Around the void ratio for the compacted sample the small-strain Young's modulus ranges from around 460MPa to 1700MPa depending on the stress.

Another study has been made by (Payan, et al., 2017), who were studying the influence of the particle shape on the small-strain Young's modulus and Poisson's ratio for sands. Their study yielded an expression to estimate the small-strain modulus depending on the coefficient of uniformity and the particle shape. As no particle shape measurements of the sample material have been made, this parameter has been estimated according to (He, et al., 2018), to range from 0.4-0.6 where the smaller fractions had the larger value and larger fractions had the smaller value. As the relation between the particle size and the particle shape value is not a generally acknowledged relationship, the best estimation at this point is to estimate the value to be 0.5. The formula for estimation suggested by (Payan, et al., 2017) is seen below.

Estimation method 2 (M2) - (Payan, et al., 2017)

$$E_{max} = \left(245 \cdot C_u^{-0,09} \cdot \rho^{0.82}\right) \cdot e^{-1,32} \cdot \left(\frac{p'}{100kPa}\right)^{(C_u^{0,11}) \cdot (-0,44\rho + 0.66)} \qquad Eq.\ 10$$

Eq. 10 is based on results found for sands and the parameter of particle shape regularity is estimated based on material which has a significantly different grain size distribution than the studied material. The errors resulting from using this formula are expected to be large similarly to the findings in (He, et al., 2018), where the error was found to be around 50%. Nevertheless, the results seen in Figure 20, again give an indication of the small-strain stiffness of the crushed concrete.

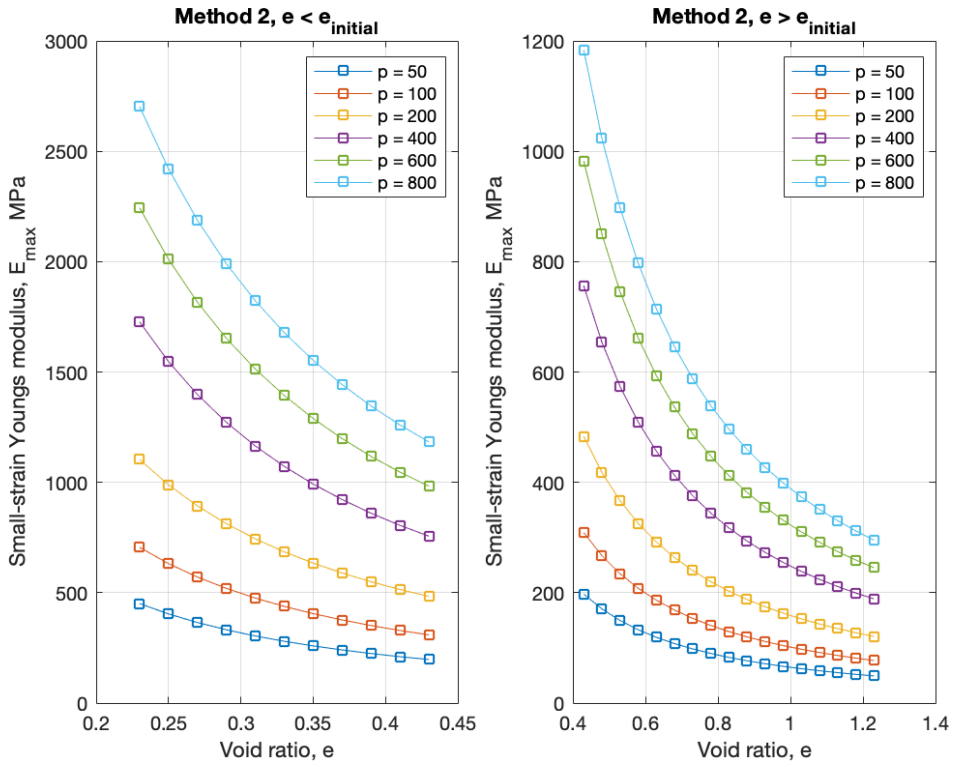

Figure 20: Method 2, small-strain Young's modulus

In (He, et al., 2018), the relation between the estimated modulus found by *Eq. 10* and the modulus obtained from tests were compared. Similarly, the results found by this simulation are compared to see any similarities between the obtained results. The comparison between method 1 and method 2 can be seen in Figure 22. The graphs show similar deviation as was found by (He, et al., 2018), where the difference between the moduli was around 50%. Interestingly it seems that the error is increasing logarithmically as the pressure is increasing, which makes it interesting to see how the difference between the moduli is when simulated at low pressures. The comparison made by (He, et al., 2018) can be seen from Figure 21.

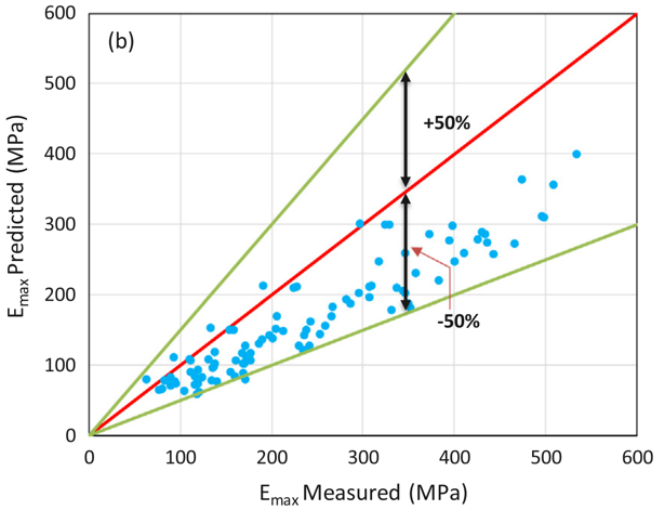

Figure 21: Comparison between estimated modulus and measures modulus by (He, et al., 2018)

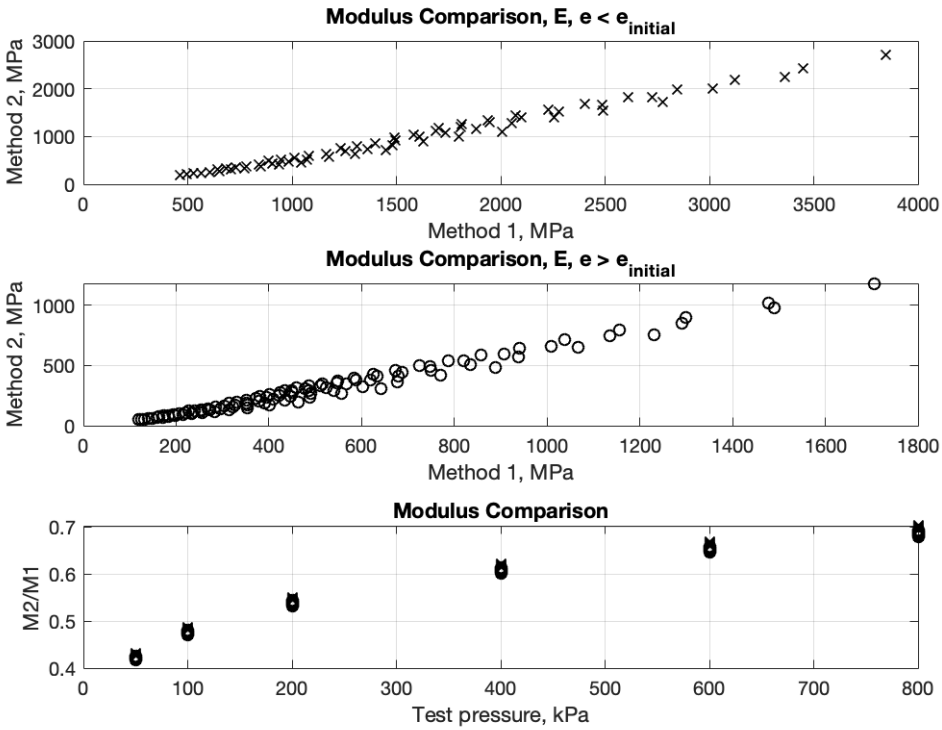

Figure 22: Comparison between estimated moduli M1 and M2

Doing the same simulations at smaller pressures should according to Figure 22 yield results with a smaller difference. The error at smaller pressures can be seen from Figure 23 and the logarithmic relation can be seen from Figure 24.

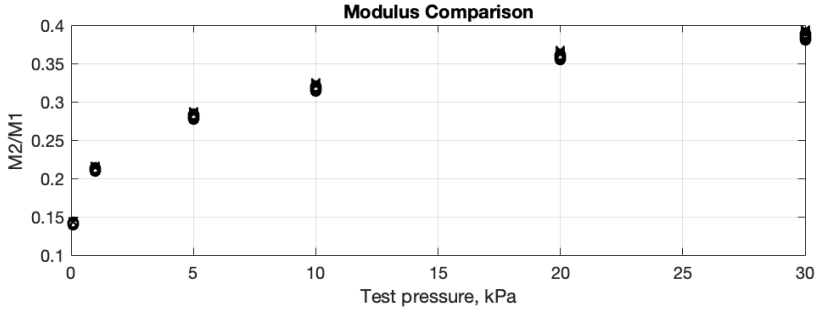

Figure 23: Difference between M1 and M2 at lower pressures

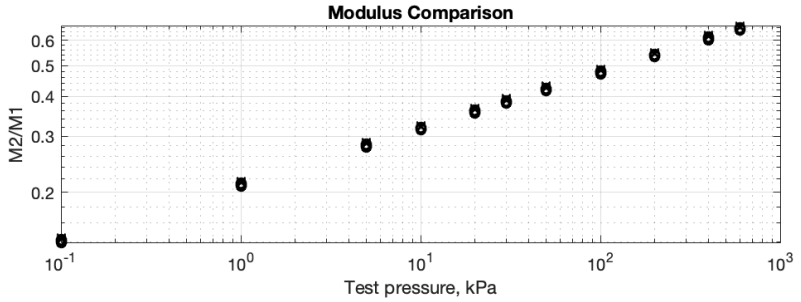

Figure 24: Logarithmic increase in error with the pressure of simulation

In (He, et al., 2018) a method to calculate the small strain stiffness is presented by using obtained results from e.g. bender element tests or resonant column tests. Having the Lamé's constants:

The first Lamé parameter.

$$\lambda = \frac{\nu \cdot E}{(1+\nu)\cdot(1-2\cdot\nu)} \qquad \textit{Eq. 11}$$

The second Lamé parameter, which is also the shear modulus:

$$\mu = G = \frac{E}{2\cdot(1+\nu)} \qquad \textit{Eq. 12}$$

The Lamé's constants can be used to make an estimation of the wave velocities:

$$V_p = \sqrt{\frac{\lambda+2\cdot\mu}{\rho_s}} \qquad \textit{Eq. 13}$$

$$V_s = \sqrt{\frac{\mu}{\rho_s}} \qquad \textit{Eq. 14}$$

Note that this estimation is purely based on an estimated Poisson's ratio, which has been estimated, and on a Young's modulus from literature review. Besides the estimation of the small-strain Young's modulus with the formulas for method 3, formulas can also be used to back-calculate the wave velocities which relate to the small-strain moduli found from the other estimation methods. The method 3 is found by the following formulas:

Estimation method 3 (M3) - (He, et al., 2018)

Small-strain constrained modulus:

$$M_{max} = \rho_s \cdot V_p^2 \qquad \textit{Eq. 15}$$

Poisson's ratio based on wave velocities in the sample:

$$\nu = \frac{0{,}5 \cdot V_p^2 - V_s^2}{V_p^2 - V_s^2} \qquad \textit{Eq. 16}$$

Small-strain Young's modulus:

$$E_{max} = \frac{M_{max} \cdot (1+\nu) \cdot (1-2\cdot\nu)}{(1-\nu)} \qquad \text{Eq. 17}$$

It is noticeable that the equations given for method 3 originate directly both from the Lamé equations and the ones for finding the wave velocities. As an example, studying V_p, it becomes evident that $Eq.13$ can be written the following way:

$$V_p = \sqrt{\frac{\lambda + 2\cdot\mu}{\rho_s}} \;\rightarrow\; V_p^2 = \frac{\lambda + 2\cdot\mu}{\rho_s} \;\rightarrow\; V_p^2 \cdot \rho_s = \lambda + 2\cdot\mu = M_{max}$$

Furthermore, by first expanding the commonly known relation between Lamé's parameters and Young's modulus, and then simplifying:

$$E = \mu \cdot \left(\frac{3\cdot\lambda + 2\cdot\mu}{\lambda + \mu}\right) = \frac{(\lambda + 2\cdot\mu)\cdot(1+\nu)\cdot(1-2\cdot\nu)}{(1-\nu)} = \frac{M_{max}\cdot(1+\nu)\cdot(1-2\cdot\nu)}{(1-\nu)}$$

This proves that the basis of method 3 is all connected, which also explains the reason behind the small-strain modulus found by Lamé's parameters, yielding the same modulus as the normal Young's modulus. Furthermore, this proves that using these formulas for back-calculating the wave velocities related to the moduli found using other sources yield the exact same curve as those found for method 3. The wave velocities found for method 3 can be seen in Figure 25.

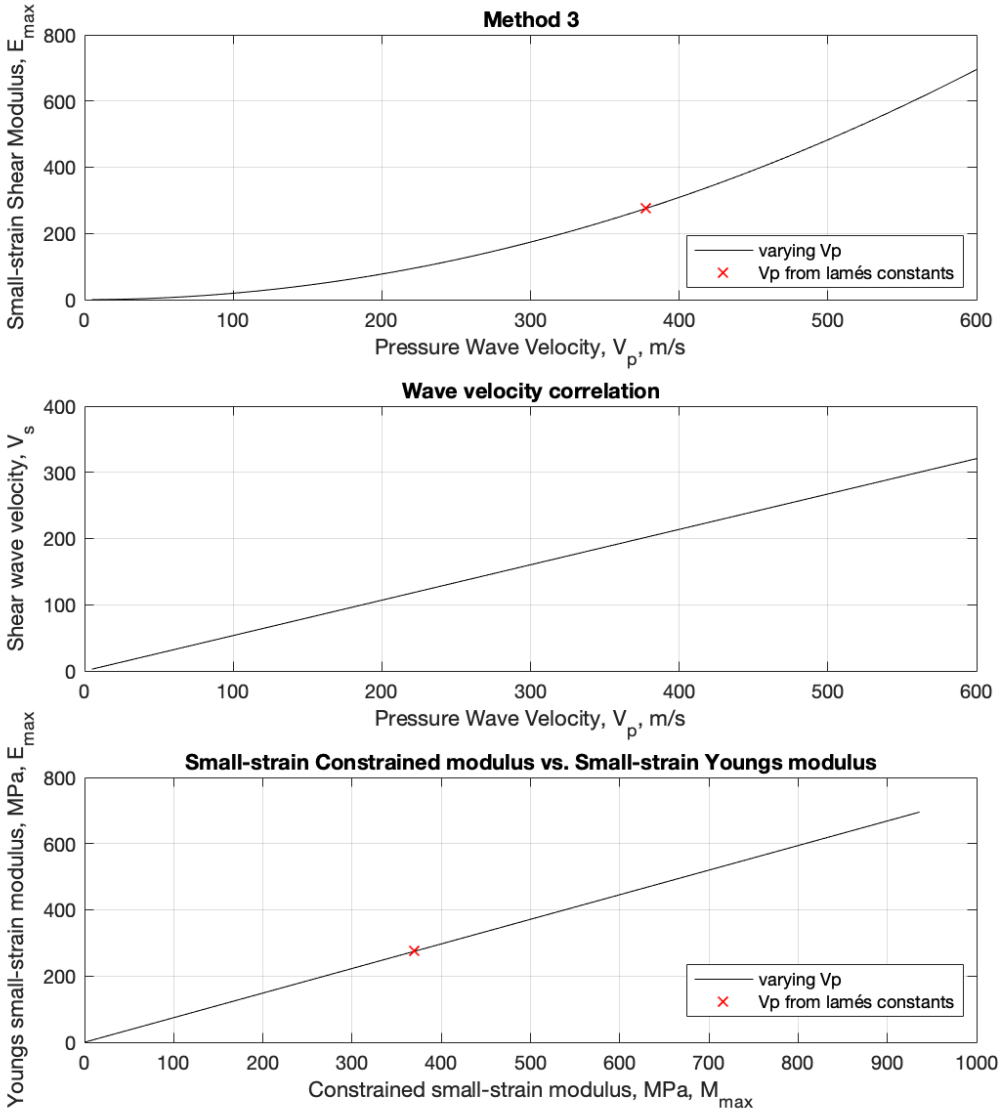

Figure 25: Method 3 and wave velocity estimation

That the small-strain modulus would have the same stiffness as the regular Young's modulus is not reliable.

The final method for estimating the small-strain stiffness used in this thesis is a method developed by and presented in (Wichtmann & Triantafyllidis, 2009). The paper presents a method for calculating the small-strain shear modulus for quartz sands. The formulas have been fitted to results obtained for sand and are therefore not directly representative for crushed concrete, but as crushed concrete also is a granular material it is assumed that the formulas, like the other methods, can give an indication of the small-strain stiffness of the crushed concrete material.

The expression has been fitted to results coming from both angular grains and results from round grains, which yielded different constants. The constants presented in Table 10 are recommended to be used.

Table 10: Unitless small-strain stiffness estimation constants

	Angular grains	Round grains
A	3.2	6.9
a	2.97	2.7
n	0.5	0.5

Formulas for calculating the coefficients have been suggested by (Wichtmann, et al., 2011). The formulas depend on parameters found from the grain size distribution curve and are based on data from numerous resonant column tests performed on sand. The constant calculations have been developed from sand material with C_u varying from 1.5 to 15.9, where are clear dependency on the coefficient of uniformity was seen as the constant *A* increases exponentially as C_u increases, which lead a very large difference in results when changing C_u. The coefficient of uniformity for the crushed concrete is 32.8, which is a bit more than twice the maximum value the formulas have been developed from, hence leading to unrealistic behaviour of G_{max} which is an order of 10^6 larger than the results using constants for angular grains. The formulas for *A, n* and *a* are not included in this thesis due to the large error, but more information can be found about these in (Wichtmann, et al., 2011).

As the calculation methods for the constants used for method 4 are unreliable, the moduli which will be representative for M4 are the moduli found using the constants defined for angular grains. This is based on the SEM study made by (He, et al., 2018). The results obtained from this modulus calculation are not expected to be representative for crushed concrete, but can be used for the comparison of moduli found for other materials. The coefficients are used in calculating the small-strain shear modulus using following formula.

Estimation method 4 (M4) - (Wichtmann & Triantafyllidis, 2009)
Small strain shear modulus:

$$G_{max} = A \cdot \frac{(a-e)^2}{1+e} \cdot p^n \qquad \textit{Eq. 18}$$

To compare this modulus with the Young's moduli it is necessary to convert the modulus to Young's modulus as well. This is done by isolating *E* in $Eq.12$.

The results obtained from calculating the small-strain shear modulus are found in Figure 26.

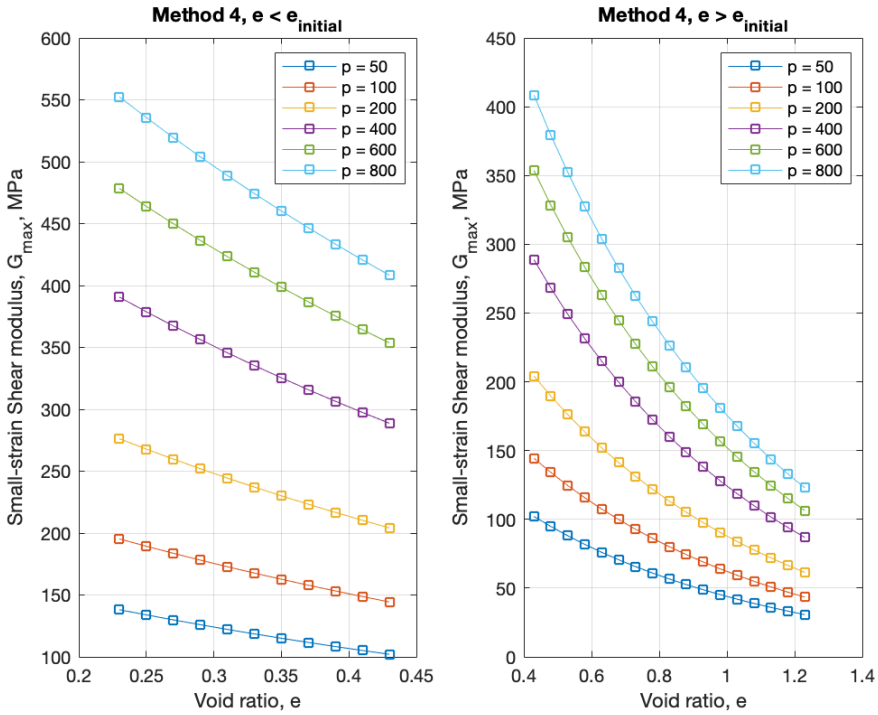

Figure 26: Method 4 (M4), small-strain shear modulus

3.6 Damping Parameters of Granular Soils

The damping properties of materials define the rate at which the speed of a wave is attenuated, hence the damping properties of soils define how far a wave will travel before it has been stopped. Usually soil is modelled as a viscous material ((Auersch, 2005), (Sheng, et al., 2003), (Jones, et al., 2004), (Lei, 2015), etc.), where the viscosity relates to the damping properties of the materials and is used in systems of differential equations. The damping found by the tests performed in this thesis relates to the small-strain damping and cannot directly be compared with the damping of materials at normal strain levels. According to (Menq, 2003), (Senetakis, et al., 2013) and (Senetakis, et al., 2012), the damping properties of materials are closely related to the magnitude of the strain, where the damping increases as the strain increases. Furthermore, (Menq, 2003) found the damping coefficient to be influenced by the mean grainsize and the coefficient of uniformity. However, this correlation was not consistently found for all materials by (Senetakis, et al., 2012). The damping properties of the crushed concrete is necessary for answering the research questions 4[12], 5[13] and 6[14], because it is assumed to have a significant influence on the wave propagation through soils.

(Darendeli, 2001) developed an expression for the damping coefficient assuming "Masing behaviour", which has later been used by (Menq, 2003), to develop an expression for estimating the damping of soils. The adjustment according to the Masing effect enables the

[12] How does the substitution of the commonly used material with crushed concrete affect the vibrations induced by tramways?
[13] How do the dynamic and small-strain parameters of the structural layers affect the ground induced vibrations caused by railway traffic?
[14] Which laboratory and in-situ methods can be used to predict and monitor the dynamic behaviour of crushed concrete waste in railway construction?

curve to follow a strain-damping relation which correlates closer to the actual behaviour at small and larger strains (Menq, 2003). These expressions have been used by (Senetakis, et al., 2012), to make an expression which relates the small-strain damping with the normal strain damping of materials. The calculation of the Masing adjusted damping is shown in $Eq.19$.

$$D_{Masing} = \frac{100}{\pi} \cdot \left[4 \cdot \frac{\gamma - \gamma_{ref} \cdot ln\left(\frac{\gamma+\gamma_{ref}}{\gamma_{ref}}\right)}{\frac{\gamma^2}{\gamma+\gamma_{ref}}} - 2 \right] \qquad Eq.\ 19$$

Where γ is the strain level at which the expression is evaluated and γ_{ref} is the strain level at which $\frac{G}{G_0} = 0.5$, which can be estimated according to (Menq, 2003):

$$\gamma_{ref} = A_\gamma \cdot \left(\frac{p'}{p_a}\right)^{n_\gamma} \qquad Eq.\ 20$$

Where constants can be estimated by $A_\gamma = 0.12 \cdot C_u^{-0.6}$ and $n_\gamma = 0.5 \cdot C_u^{-0.15}$.
The Masing damping is further used to find the damping correction factor denoted D_{adjust}:

$$D_{adjust} = c_1 \cdot D_{masing} + c_2 \cdot D_{masing}^2 + c_3 \cdot D_{masing}^3 \qquad Eq.\ 21$$

The factors, c_1, c_2 and c_3 are found according to (Menq, 2003):

$$c_1 = -1.1143 \cdot a^2 + 1.8618 \cdot a + 0.2523$$

$$c_2 = 0.0805 \cdot a^2 - 0.0710 \cdot a - 0.0095$$

$$c_3 = -0.0005 \cdot a^2 + 0.0002 \cdot a + 0.0003$$

Where

$$a = 0.86 + 0.1 \cdot \log\left(\frac{p'}{p_a}\right) \qquad Eq.\ 22$$

Once the adjustment factor is found it can be implemented in the expression giving the damping at larger strains developed by (Senetakis, et al., 2012):

$$D - D_{min} = b \cdot \left(\frac{G}{G_0}\right)^{0.1} \cdot D_{adjust} \qquad Eq.\ 23$$

The normalized shear modulus is estimated using the strain level, which is calculated by the factor depending on the coefficient of uniformity:

$$\frac{G}{G_0} = \frac{1}{1+\left(\frac{\gamma}{\gamma_{ref}}\right)^a} \qquad Eq.\ 24$$

Where b is a scaling coefficient that depend on the number of cycles, N.

$$b = 0.6329 - 0.0057 \cdot ln\ (N) \qquad Eq.\ 25$$

3.7 Hypothesis

In section 3.5 the small-strain stiffness has been estimated using several methods. The method used in method 1 is the only method which has previously been fitted to tests made on crushed concrete, which increases the reliability of this method. Figure 27 presents the comparison between the moduli obtained using different prediction methods.

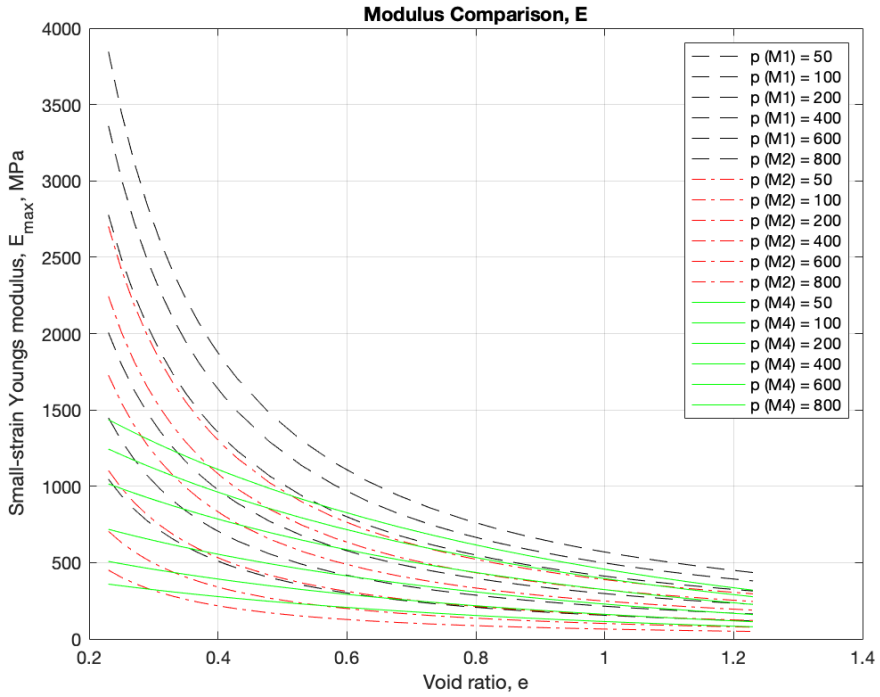

Figure 27: Comparison between methods for estimation of small-strain Young's modulus

As method 4 represents moduli found for angular grained sand according to (Wichtmann & Triantafyllidis, 2009), it is only showed for comparison with other materials.

The moduli obtained from M1 and M2 are following similar trends but are slightly different from each other. The differences seen in Figure 28 are not enormous, see Figure 29. Hence, the values of M1 and M2 are assumed to be representative for estimating the small-strain stiffness of the crushed concrete.

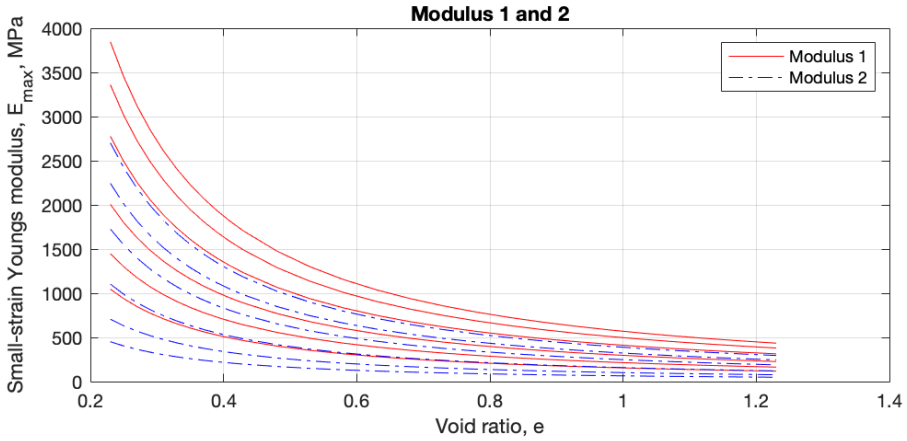

Figure 28: Estimated Small-strain Young's moduli at different stress levels

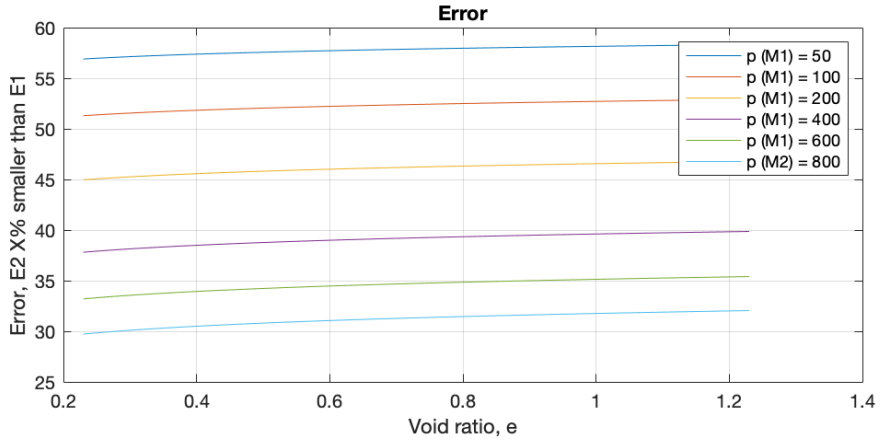

Figure 29: Difference between estimation methods

The initial void ratio estimated for the crushed concrete is based on laboratory results. Assuming that the crushed concrete would be compacted to the same level, hence having the same void ratio when used in construction yields a range of small-strain moduli depending on the stress in the crushed concrete. The small-strain moduli and corresponding shear wave velocities can be found from Figure 30.

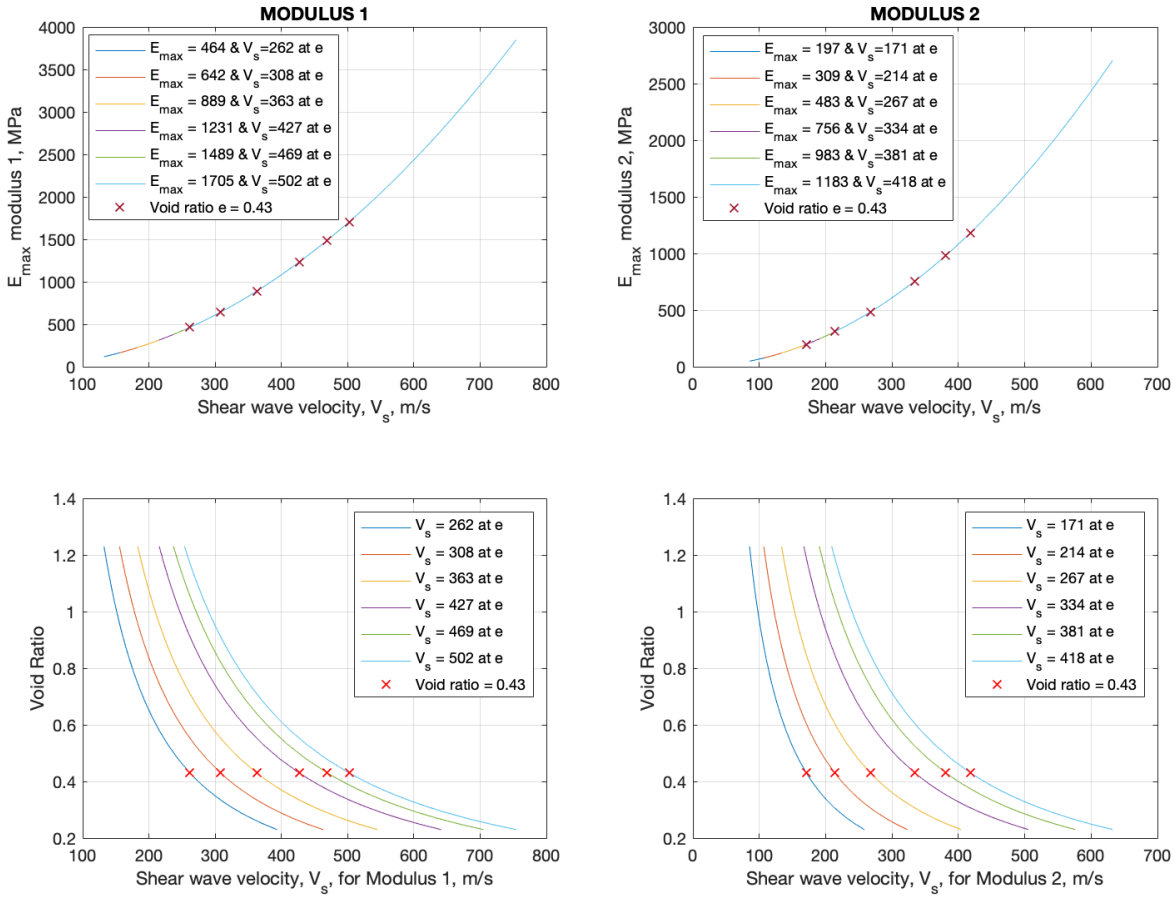

Figure 30: Estimated small-strain stiffness of crushed concrete and corresponding shear wave velocities

Assuming a general stress level ranging from 50 kPa to maximum 400 kPa, the magnitude and range of the small-strain stiffnesses correlates relatively well with the values for comparison seen in Table 5. For these stress levels and at void ratio $e = 0.43$, the range of the small-strain stiffness, considering method 1 and 2, is from $197MPa \rightarrow 1231\ MPa$ and the shear wave velocities ranging from $171\frac{m}{s} \rightarrow 427\frac{m}{s}$. The small-strain stiffness should be relatively higher than the regular static stiffness, Young's modulus, roughly by a factor of 4.8 higher according to (Alpan, 1970), see section 3.5. Thus, a small-strain stiffness of $1200\ MPa$ is used as an input parameter for initial modelling.

Compared to stiffnesses of materials which could be substituted by crushed concrete, the stiffness of the crushed concrete is sufficient. It is important to note that the estimation of the stiffness of the crushed concrete does not consider the hardening properties of the crushed concrete. The hardening properties of the crushed concrete are likely to increase the stiffness of the material.

Besides the small-strain stiffness, the wave velocities also converge towards similar results as found by others. And similarly, as with the stiffness, the wave velocities match the wave velocities of the crushed rock used in ballast layers and the material used in subgrade layers. As these are some of the most important parameters when studying the dynamics related to railways, the substitution with crushed concrete is not expected to have any negative effect on the wave propagation in the ground.

The hardening effect of the crushed concrete is expected to make the material behave more brittle than the traditionally used materials. As the traditionally used material is more uniform, does not have the hardening effect and carries the load only by friction, its long-term use will induce abrasion to the material rounding the edges, which will reduce the friction, hence the bearing capacity. Contrary, the crushed concrete is expected to carry the load not only by friction, but also by the effect of the hardening, and the abrasive effect due to the cyclic loading will probably be smaller.

For the crushed concrete, it is more likely that there will be cracks through the material as a result of repetitive loading. It is not yet clear which long-term failure mode would occur first nor which is most critical for the structure. Another scenario is if the weathering of the crushed concrete will, to some extent, wash out the fines and decrease the hardened bond in the material.

The damping properties found for the usual material used in railway construction varies very much, from 2% to 44%. Using the estimation methods presented in section 3.6, similar damping parameters are seen as those found from the literature study, see Figure 31.

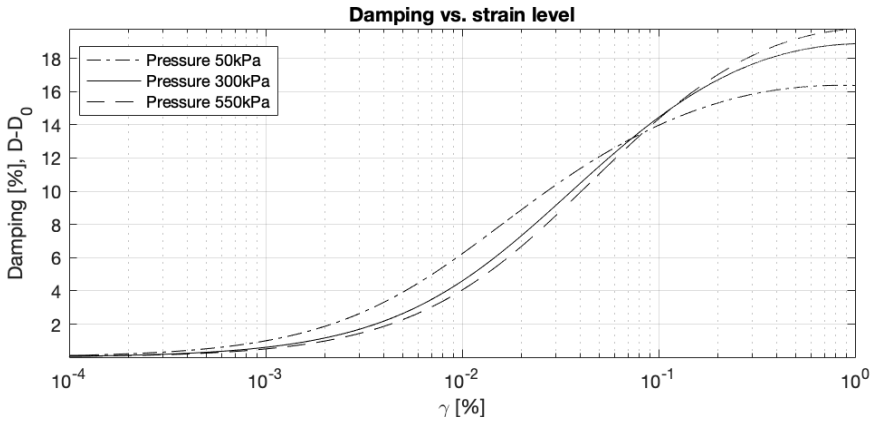

Figure 31: Estimated damping according to (Menq, 2003)

However, there is no data available, on material with similar properties, for confirming that these damping levels correspond to the reality, hence there is a need to get proper reliable damping properties for the material enabling reliable modelling of the response to the vibrations. If the damping of the material is too low, the transmission of vibrations to the stratum will be large and as it is challenging to predict and homogenize the dynamic properties of the existing ground at all places at the railway, this will increase the risk. Hence a high damping effect is expected and also wanted from the material used in the railway. As a result of the literature review, a damping effect of around 15-25% is expected for the crushed concrete. The effect might be even larger due to the hardening of the material.

For modelling purposes, the strain at which $\frac{G}{G_0} = 0.722$ is needed. This parameter is needed in the PLAXIS Hardening Soil Small model, which is the model which will be used for analysing the influence of the substitution of the materials. The theories by (Senetakis, et al., 2012), also suggest a method of predicting this strain level, see Figure 32.

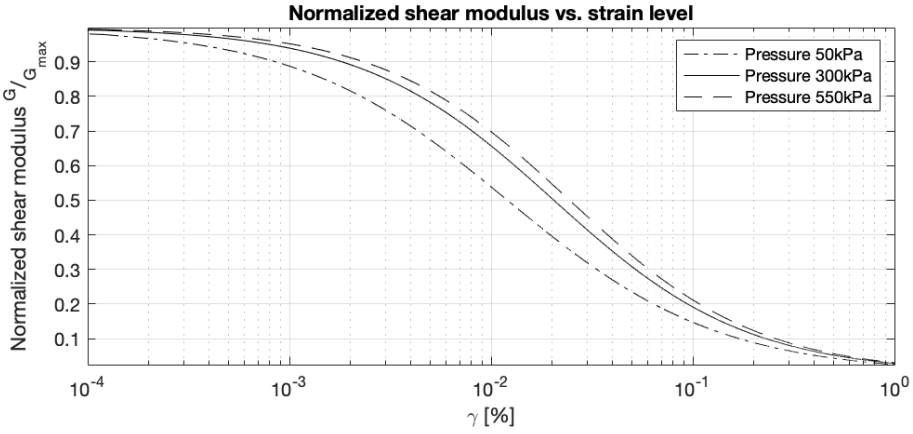

Figure 32: Normalized shear modulus related to strain level

In addition, another method is proposed by (PLAXIS, 2019), which yields a strain level at $\gamma \approx 0.00009\ [-]$. As a comparison the method used in Figure 32, which yields $\gamma \approx 0.00008\ [-]$ at the pressure of 30kPa and gives similar results for the other pressure levels.

4 Methodology

The aim of the methodology chapter is to describe the methods which are used to measure the small-strain and dynamic parameters of the crushed concrete. To answer research question 6[15], methods which are commonly used for the estimation of small-strain and dynamic parameters are highlighted.

Two widely accepted methods for measuring the small-strain and dynamic properties are the bender element test (BE) and the resonant column test (RC) or both of them in combination with each other. The estimation of properties using the bender element test is becoming increasingly popular and is assumed to be considerably accurate (Clayton, 2011) (e.g. $\pm 5\%$ for G_{max} and $\pm 2\%$ for V_s (Pennington, et al., 1997)). However, the interpretation of the results from bender element testing have been found to be difficult ((Clayton, 2011) (Lee & Santamarina, 2005)).

Using the resonant column test together with the bender element test does eliminate some of the errors which could be related to misinterpretation of results, hence the results carry a higher reliability. The bender element and resonant column test methods described in this chapter are furthermore used on the crushed concrete material described in section 3.4, and the results are used for comparison of the estimated parameters found in section 3.6.

Samples of crushed concrete have been prepared with a rotating condenser and the procedure for the sample creation is found in Appendix 3: ICT sample preparation. Two hardened samples have been prepared for resonant column and bender element test, and four samples have been prepared for one-dimensional compression test. The test results from the one-dimensional compression tests can been found from Appendix 4: One-dimensional compression test. The one-dimensional compression test was performed to determine the compressive strength of the sample, for comparison with previously tested BeM II and for determination of the static Young's modulus of the crushed concrete. Based on compressive strengths found by (Linden, et al., 2019), the compressive strength was estimated to be around a 1 MPa. The measured compressive strengths and the assumed can be seen from Appendix 4: One-dimensional compression test.

4.1 Bender Element Test

The typical bender element to be used in bender element testing is made of a couple of piezoceramic plates put together with a thin layer of metal in between. (Aris, et al., 2010) Piezoelectricity was discovered in the 1940's where Jacques and Pierre Curie found out that a ceramic material can be polarized resulting in a piezoelectric material. The piezoelectric material consists of crystals which are asymmetric. These properties enable a conversion from mechanical deformation to electric signals and vice versa, which is what can be benefitted from in the bender element testing. The bender elements electrical connection affects how large a signal is produced or rather how large deformation is produced. A parallel connection deforms twice as much as a serial connection. (Lee & Santamarina, 2005) In Figure 33 the bender element types and a general illustration of a bender element can be seen.

[15] Which laboratory and in-situ methods can be used to predict and monitor the dynamic behaviour of crushed concrete waste in railway construction?

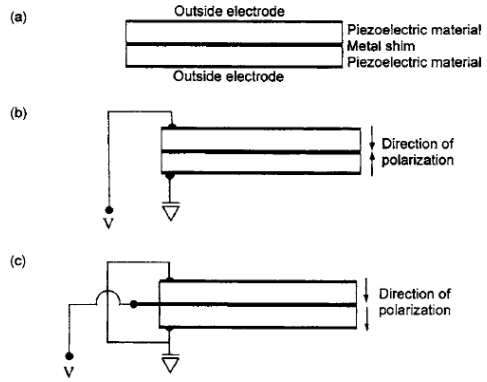

Figure 33: Bender elements, (a) schematic presentation of bender element, (b) series type, (c) Parallel type (Lee & Santamarina, 2005)

Because of the difference in deformation from the differently connected bender elements, it is recommended to install the parallel type of bender elements as the transmitter and a series connected type of bender element as the receiver element. (Lee & Santamarina, 2005)

The bender elements are used together with a triaxial apparatus, hence allowing testing at different deviatoric stresses. In this thesis the bender element test has only been performed in one direction, from tip to tip, in a setup as shown in Figure 34. The signal coming from the transmitter element will both produce P- and S-waves (Lee & Santamarina, 2005), which will be considered in the interpretation of the results.

4.1.1 Setup

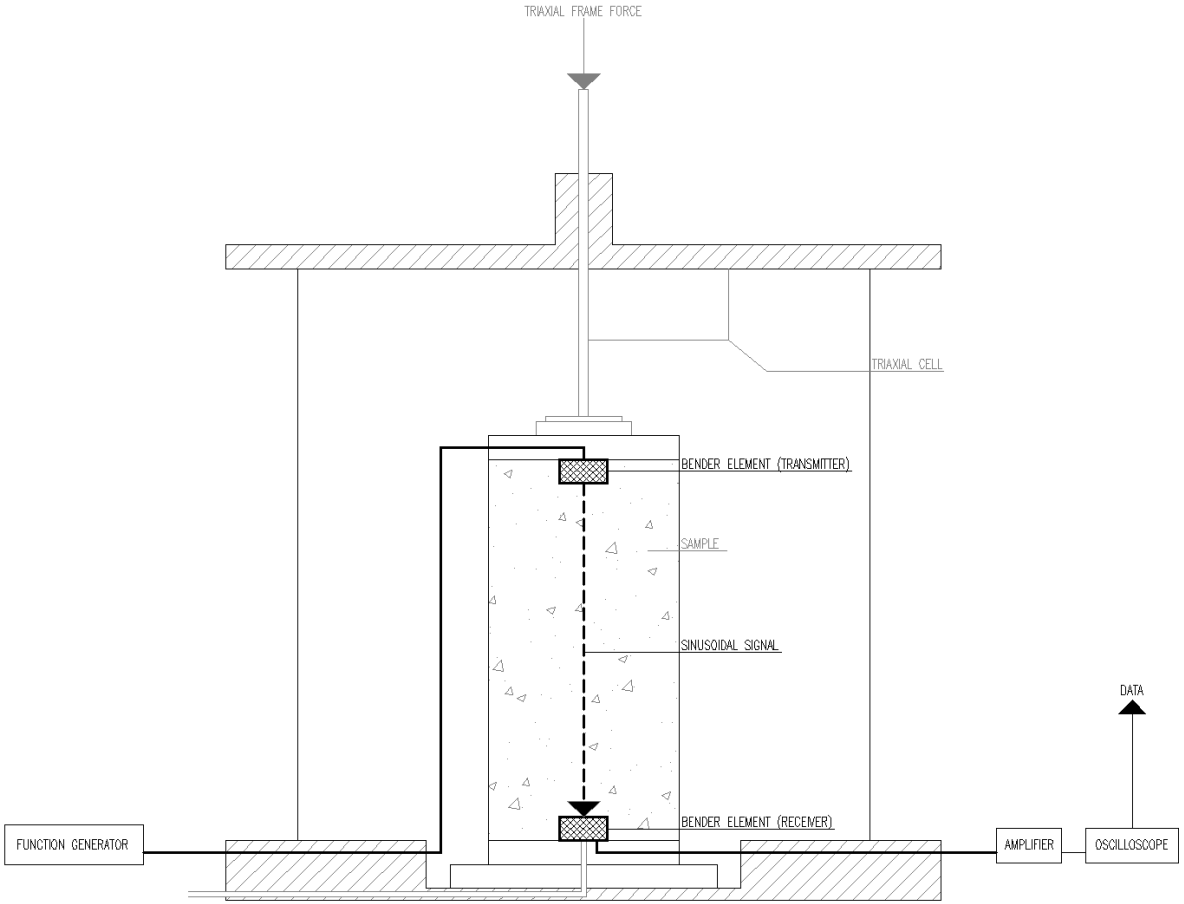

Figure 34: Bender element test setup

A function generator generates a predefined signal, which will be transmitted by the bender element at the top of the sample. As soon as the signal has gone through the sample to the receiver bender element, the shear deformations from the transmitter will result in small strain deformation of the receiver element. Due to the properties of the piezoceramic material it will produce an electrical signal, which is then amplified and sent to an oscilloscope. That way it is transformed into data which can be interpreted according to section 4.1.2. (Aris, et al., 2010)

4.1.2 Signal Interpretation Methods

There are several different data interpretation methods currently in use. Some of the more reliable and more widely accepted methods are the first arrival and peak-to-peak method. An illustration of the principle of these two methods can be seen in Figure 35: Signal interpretation methods. (He, et al., 2018)

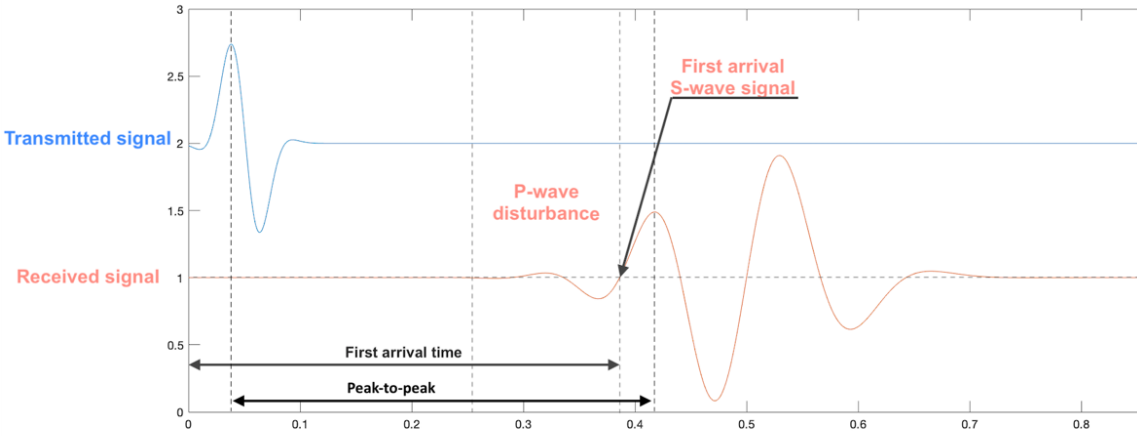

Figure 35: Signal interpretation methods (He, et al., 2018)

When the transmitter is sending out the predefined signal, it transmits both P- and S-waves, where the S-waves are the waves used in defining the shear wave velocity of the material. P-waves are a bit faster than the S-waves and thus arrive before the S-waves arrive. This is seen as a minor signal disturbance in the beginning of the received signal and can cause confusion regarding when the first arrival is occurring. This disturbance and the discrepancy regarding the guidelines for choosing the point of the first arrival are some of the main reasons for potential errors in the bender element test. (Yamashita, et al., 2009)Figure 36 shows the different options which have been considered or used as points of the first arrival.

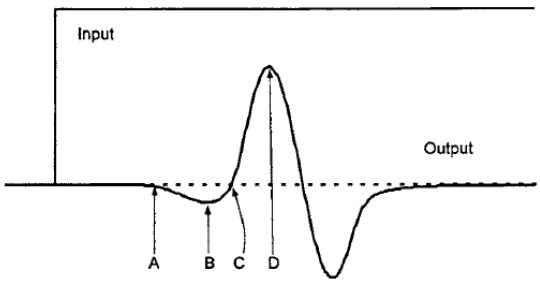

Figure 36: Typical options of arrival time (Lee & Santamarina, 2005)

Through testing it is found that the first arrival method, choosing the arrival point to be C, the point where a sinusoidal curve in the same direction as the initially transmitted curve starts, is giving the most reliable results. (Lee & Santamarina, 2005) However, it can be difficult to determine the location of this point due to disturbance in the signal. To avoid the disturbance in the signal the peak-to-peak method should be used. Using this method together with resonant column testing should give the most reliable results (Clayton, 2011).

4.2 Resonant Column Test

The resonant column test is another test method which can be used to obtain the maximum shear wave velocity, G_{max}, by accelerating the sample through electrodynamic exciters and receiving the signal in acceleration transducers. The signal, which is sent to and transmitted via the electrodynamic exciters comes from a function generator. The frequency is varied during the test until the sample's resonant frequency has been found. The resonant frequency can then be used in defining different parameters such as the secant modulus, G_{sec}, the maximum shear wave velocity etc.

The resonant column test can be executed with three different systems, where the connection properties are the main difference. A schematic presentation of these three systems in seen in Figure 37.

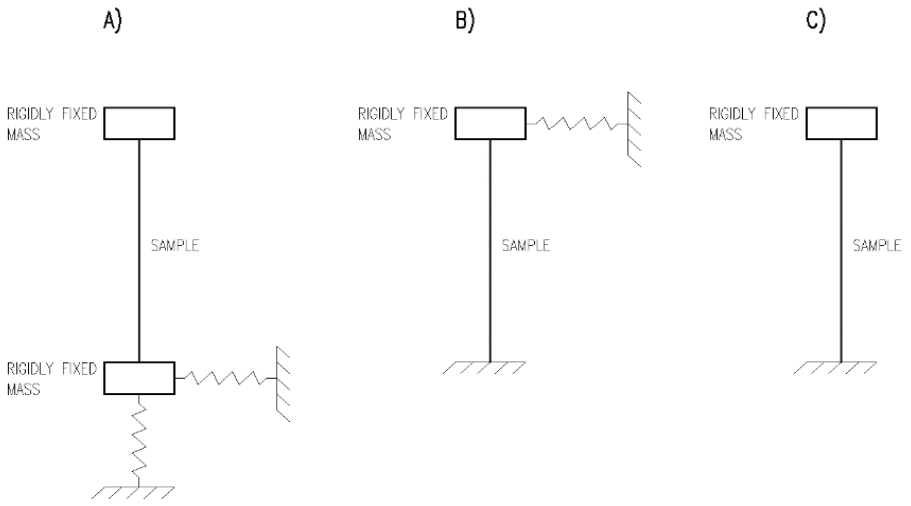

Figure 37: Resonant column types - free diagram

The different resonant column systems have different internal force diagrams, which affects the outcoming results. The resonant column system can be chosen so that it reflects the system for which the tests are made for to a greater extent. The resonant column force is normally applied as torsional force at the top of the specimen as illustrated in Figure 38. (Cascante, et al., 1998)

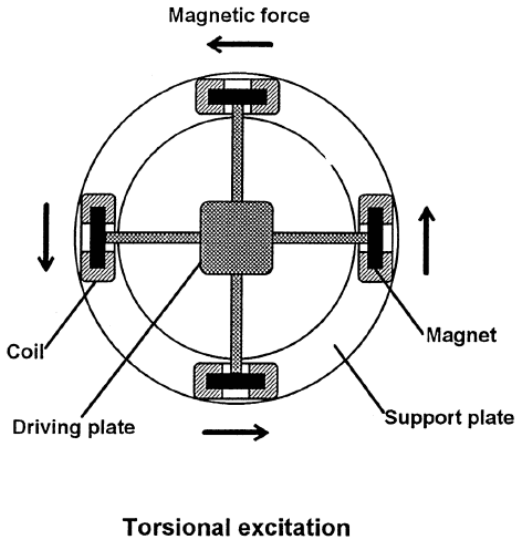

Figure 38: Torsional excitation in resonant column testing (Cascante, et al., 1998)

4.2.1 Setup

An example of a typical resonant column testing setup can be seen in Figure 39.

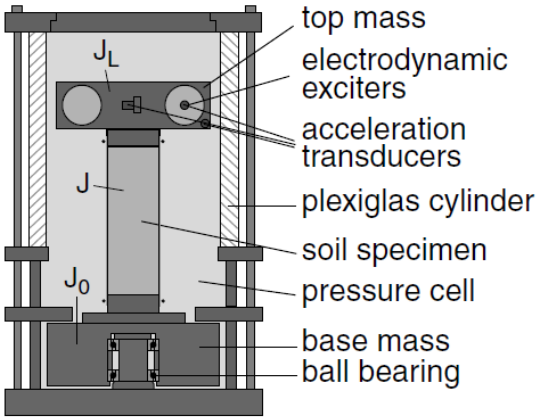

Figure 39: Resonant column setup (Wichtmann & Triantafyllidis, 2009)

The electrodynamic exciters produce a torsional excitation at the top of the sample. The frequency of this excitation will be modified while testing until the resonant frequency has been reached. The frequency will be received by the acceleration transducers and forwarded as data that can provide the damping, shear wave velocity etc. properties of the sample.

5 Results

Resonant column and bender element tests have been performed on two hardened crushed concrete samples. The method for preparation of samples is found from Appendix 3: ICT sample preparation. Besides the resonant column and bender element test, one-dimensional compression test has been performed for the purpose of comparing the strength of the crushed concrete with previously tested material and furthermore for classification purposes of the concrete. The test results from the resonant column and bender element test are presented in this section and compared with the estimated values in section 6 and 7.

5.1 Hardened Samples - Test Results

In this section the results from the tests on the hardened samples are presented. The samples were prepared by the author, Lasse Kudsk Rasmussen, at Aalto university where they also were stored during the hardening process. Subsequently, the samples were shipped to Bochum Universität in Germany, where the tests were executed. All test results related to bender element and resonant column testing, are from Bochum Universität. The sample properties are seen from Table 11.

Table 11: Sample properties, hardened samples

Specimen	$H_0\ [cm]$	$D_0\ [cm]$	$V_0\ [cm^3]$	$A_0\ [cm^2]$	$m\ [g]$	$\rho\ [g/cm^3]$
1	20.08	9.99	1573.40	78.34	3113	1.979
2	19.98	9.98	1562.82	78.21	3097	1.982

The test results are summarized in Table 12 and presented graphically in Figure 40 and Figure 41. For full test report see Appendix 5: Test report of hardened samples.

Table 12: Hardened test results, summary table

SPECIMEN 1 *RC; fix-free* *BE*

P	fr	V_s	G_{max}	D_{min}	Δt	V_s	G_{max}	ρ	ɣ
[kPa]	[Hz]	[m/s]	[Mpa]	[-]	[ms]	[m/s]	[Mpa]	[g/cm3]	[-]
50	73	381	287	2.93E-02	520	386	295	1,98	5.0E-07
300	111	577	666	1.84E-02	340	590	690	1,98	5.0E-07
550	125	654	851	1.67E-02	300	668	887	1,99	5.0E-07

SPECIMEN 2 *RC; fix-free* *BE*

P	fr	V_s	G_{max}	D_{min}	Δt	V_s	G_{max}	ρ	ɣ
[kPa]	[Hz]	[m/s]	[Mpa]	[-]	[ms]	[m/s]	[Mpa]	[g/cm3]	[-]
50	66	344	235	3.23E-02	520	384	293	1,98	5.0E-07
300	111	582	673	1.85E-02	350	571	646	1,99	5.0E-07
550	123	643	823	1.82E-02	300	665	880	1,99	5.0E-07

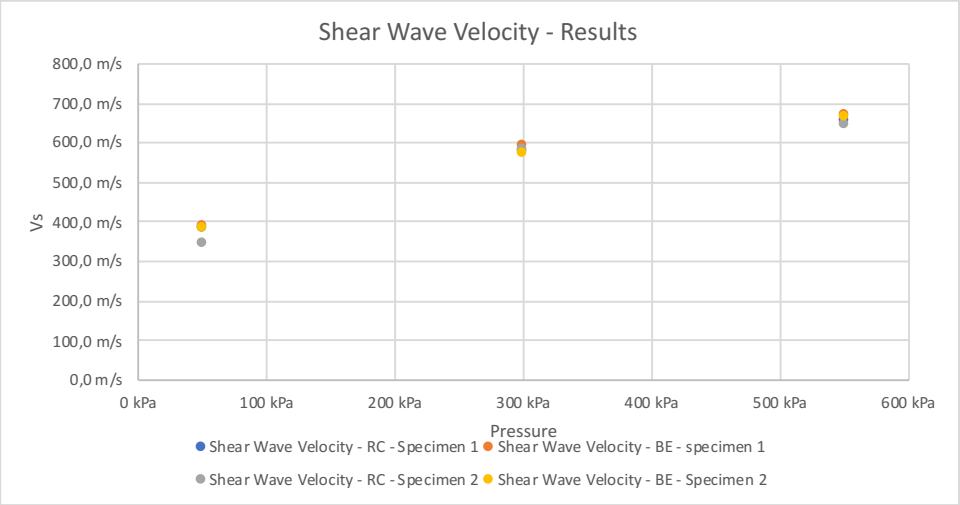

Figure 40: Wave velocities, hardened samples

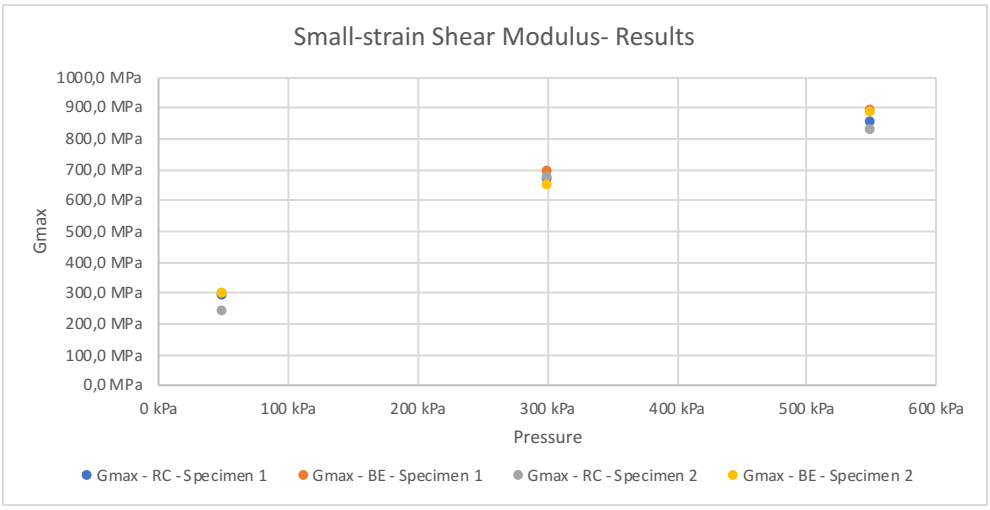

Figure 41: Small-strain shear modulus, hardened samples

6 Analysis

In the analysis the estimated parameters presented in the Hypothesis are compared to the parameters found from the bender element and resonant column testing. They are further compared in a Finite element analysis with the estimated crushed concrete values, subgrade parameters and ballast parameters. The aim is to achieve an indication of the effect of substituting the conventionally used materials with the crushed concrete and to see how the estimated values deviate from the experimentally defined values and how this deviation effects the wave propagation in the soils. The software which is used to produce the Finite element calculations is PLAXIS©.

6.1 Comparison Between Hypothesis and Results

The main parameters which are estimated for the crushed concrete are the damping properties, the small-strain stiffness and the wave velocities. As the estimated values are small-strain Young's moduli and the obtained results are small-strain shear moduli, the estimated values are transformed by the second Lamé parameter:

$$\mu = G_{max} = \frac{E_{max}}{2 \cdot (1 + \nu)}$$

The comparison of the estimated results and the obtained results is seen from Figure 42.

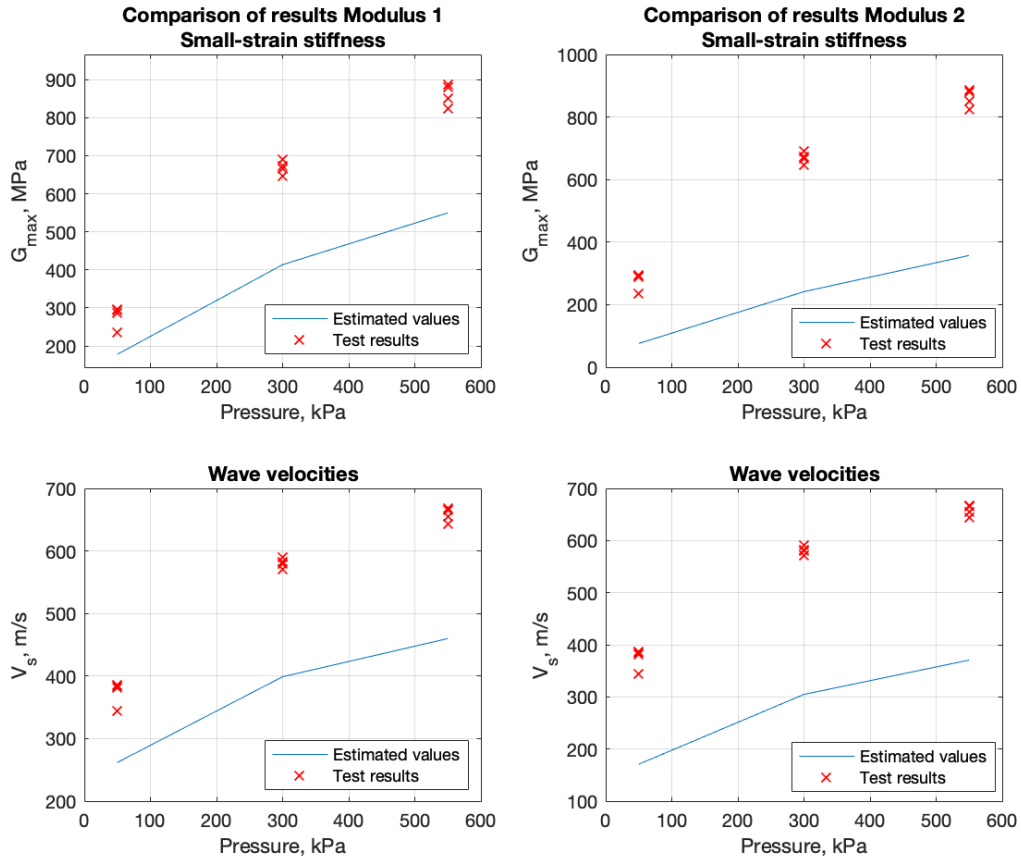

Figure 42:Comparison between estimated and measured results at assumed; $e = 0.43$ *and* $\rho_s = 2600 \frac{kg}{m^3}$

As the void ratio is dependent of the particle density ρ_s, which has been assumed based on results from (Vuorimies, 2002), this can potentially be a large source of error. Studying the results against the estimated values for method 1, a void ratio of $e = 0.31$ yields significantly better converging results for the small-strain stiffness. Decreasing the particle density simultaneously yields almost perfectly matching results, see Figure 43.

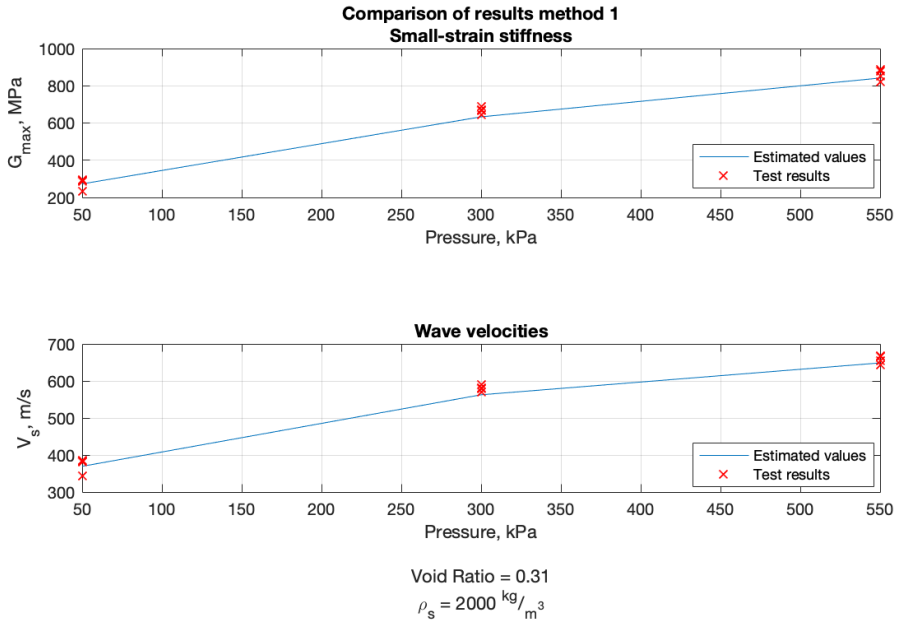

Figure 43: Converging results for estimation method 1

As the void ratio and the particle density have not been measured for the samples, this can be an explanation to the relatively large deviation of estimated and measured results. Due to the relatively high coefficient of uniformity and the higher fines content relative to (He, et al., 2018) and (He. & Senetakis, 2016), this difference in void ratio and particle density is possible. Furthermore, the expression in method 1 has been developed based on materials with significantly lower C_u and d_{50} values, and thus the constants in $Eq. 6-9$, might have to be changed to get a better fit for this material. However, studying the influence of the coefficients in A_E, n_E and $f(e)$, has not yielded a better fit than the one presented in Figure 43. By making the best fit, adjusting void ratio and particle density for both estimation method 1 and 2, it is possible to view the small-strain shear modulus – shear wave velocity relationship, see Figure 44.

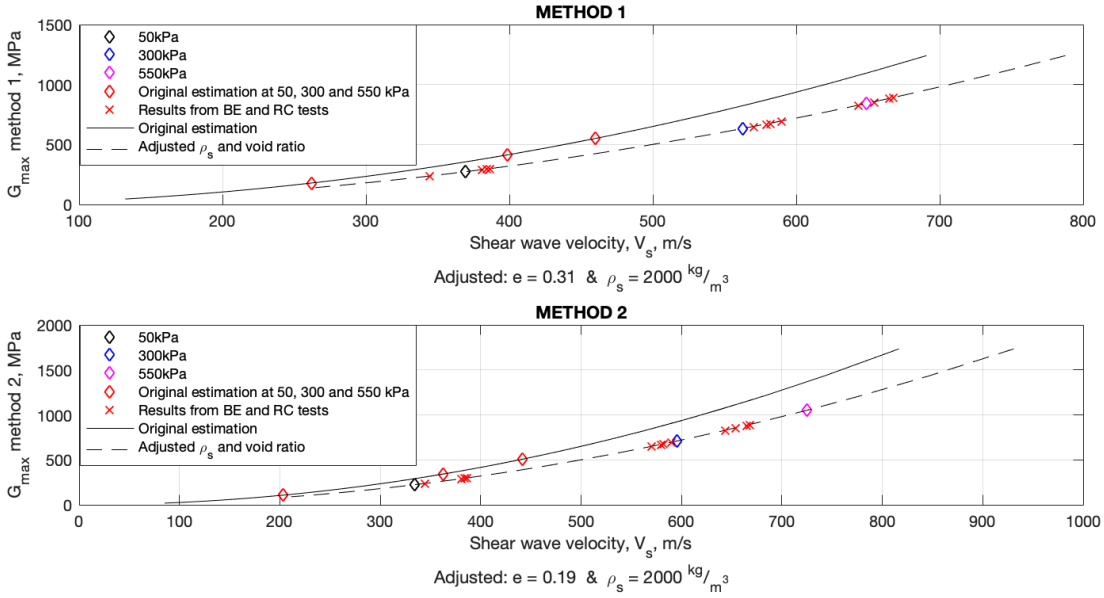

Figure 44: Best fit for method 1 and 2 by adjustment of void ratio and particle density

The void ratio at which the methods fit the best are different. For method 2 the void ratio has to be reduced so much that the method is believed not to be applicable for crushed concrete. The measured values are more than twice as large as those values estimated with method 2, hence for method 2 to be applicable, the constants would have to be significantly adjusted.

The damping coefficients are found for very small strains in the laboratory tests, and are found to correlate relatively well with the estimations made in section 3.6, see Figure 45.

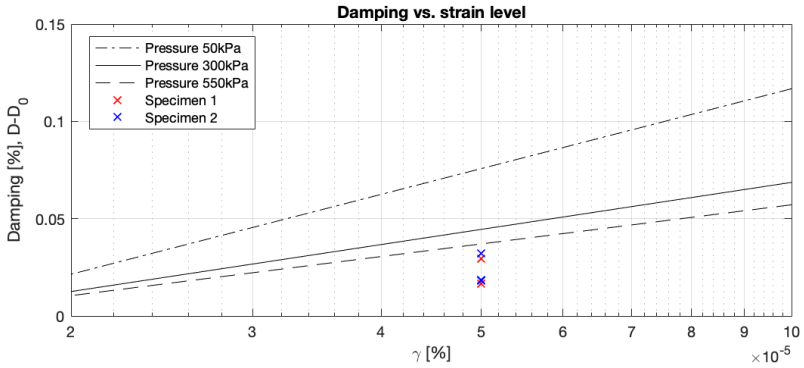

Figure 45: Predicted damping compared with measured damping

From the many coefficients which are used in the methods proposed by (Menq, 2003), it is apparent that the method is based on empirical data. From the small amount of data available for the crushed concrete it is not possible to propose any changes to the coefficients in the equations, this is also due to the large amount of empirically estimated coefficients. However, fitting the curve to the results by adjusting the parameters which rely on the material parameter C_u, yield a relatively good fit. Note that this fitting is made with a limited amount of results, and values are only estimated at strain levels beyond the measured values, see Figure 46. The adjustments were made to A_γ and n_γ:

$$A_\gamma = 0.15 \cdot C_u^{-0.6} \xrightarrow[adjusted\ to]{} A_\gamma = 0.3 \cdot C_u^{-0.6}$$
$$n_\gamma = 0.5 \cdot C_u^{-0.15} \xrightarrow[adjusted\ to]{} n_\gamma = 0.4 \cdot C_u^{-0.15}$$

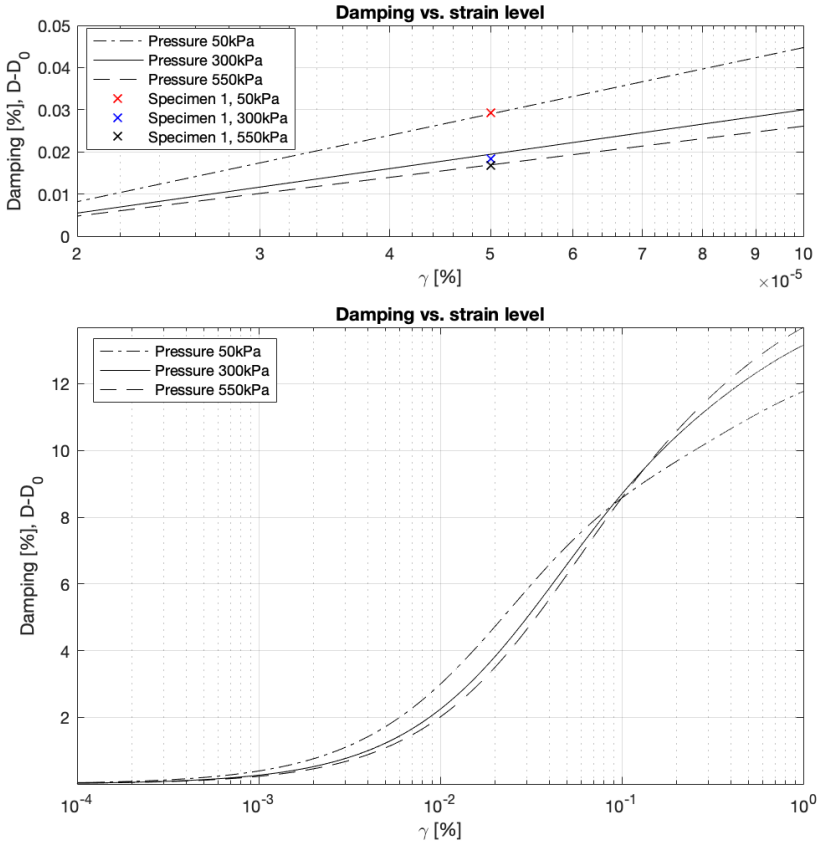

Figure 46: Fit at measured damping values and estimated behaviour at larger strains

The same adjustment of the parameters also gives a different curve for the normalized shear modulus, which affects the threshold strain $\nu_{0.7}$, at which $\frac{G}{G_0} = 0.722$. This factor is used in the finite element modelling with the Hardening Soil Small model. The new curve for $\frac{G}{G_0}$ is seen in Figure 47.

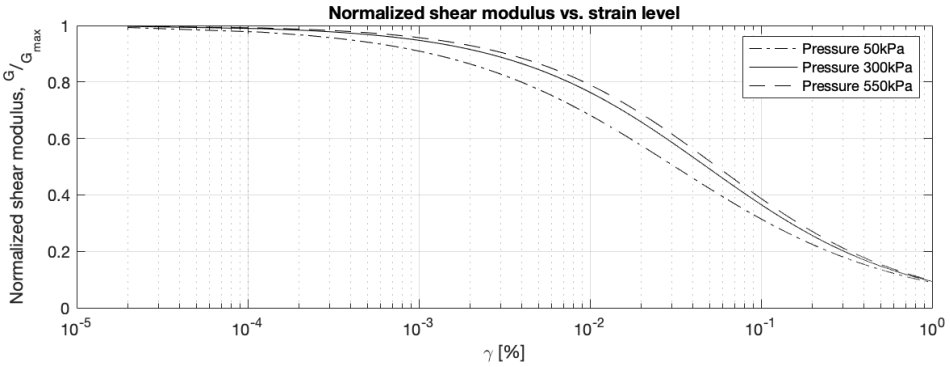

Figure 47: Adjusted Normalized shear modulus and strain relation

This yields a threshold value of $v_{0.7} = 0.00016$. Compared to the estimated value of 0.00009, this is slightly higher.

6.2 FEM analysis – PLAXIS

The suitability for using crushed concrete in railway structures are, with the research currently made, limited to be used as subgrade or base-course layers. As research is increasing there is a possibility that the crushed concrete can also be included in some of the more important structural layers. The dynamic impact related to changing the material from subgrade material to crushed concrete is studied in this section. Furthermore, a substitution with ballast material is studied.

For the substitution of subgrade material, the geometry in Figure 48 is studied. The wave propagation to point A and B is studied with different materials in cluster 2. Simulations are made with the material in cluster 2 both as subgrade material, ballast material, estimated crushed concrete parameters and crushed concrete parameters found from tests. The material properties for the subgrade, ballast and estimated crushed concrete, can be found from Appendix 2: Model parameters for ballast, subgrade. The material properties for the crushed concrete, based on tests, are found from Table 15. The modelling has been limited to only model five different frequencies, which are all in the range of ground-borne vibrations, $0 \rightarrow 100Hz$.

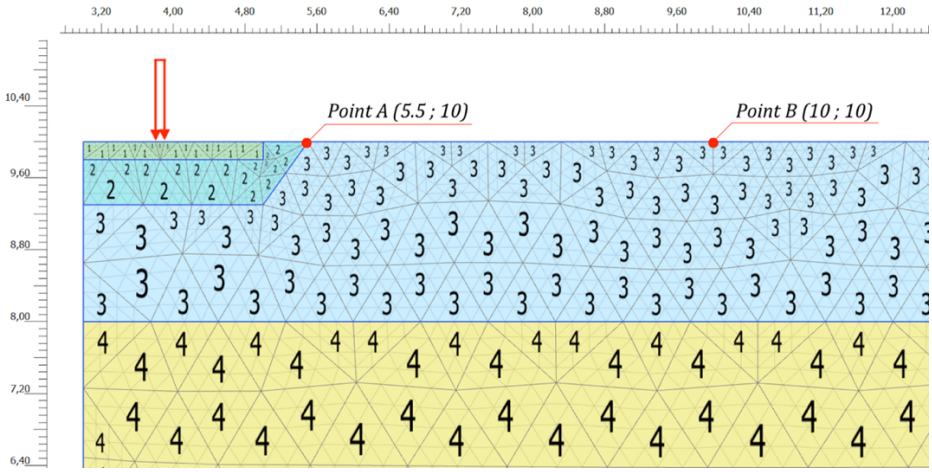

Figure 48: Modelling geometry and cluster numbers

The geometry shown in Figure 48 is not the whole geometry as the geometry continues in the y-direction to level 0 m and in the x-direction to 18 m. It is assumed symmetry around $x = 3\ m$, and the reliability of the boundary conditions used to model the symmetry have been tested by making initial calculations of the whole geometry. The axes x_{min} and y_{max} are assumed not to be viscous in the dynamic calculations and the axes x_{max} and y_{min} are assumed to be viscous. During all calculations x_{min} and x_{max} axes are assumed to be free in the y-direction and fixed in the x-direction. The top boundary is assumed to be free in all directions and y_{min} is modelled as fixed in x- and y-direction.

The following phases are being modelled:

Table 13: Model phases

Phase number	Phase name	Phase description
InitialPhase	Initial phase	Initial stress calculation
Phase 1	Excavation	Excavation to bottom of subgrade
Phase 2	Constr. 1,5	Constructing the structural layers including the concrete slab.
Phase 3	Activate 1,5	Activating a static load of 9 kN/m
Phase 4	1,5 Hz	Activating dynamic load multiplier defined with frequency of 1,5 Hz and amplitude of 10. (phase time 1.5s)
Phase 5	Stop 1,5 Hz	Stopping the dynamic multiplier. (phase time 0.5s)
Additional frequency spectra	Besides the above described phases, additional phases are modelled to see the response for different frequencies. Phases 2-5 are modelled for the following frequencies: 15 Hz, 30 Hz, 75 Hz & 100 Hz.	

The model parameters used for the subgrade and ballast can be found from Appendix 2: Model parameters for ballast, subgrade. The material around the railway structure (Cluster number 3 from Figure 48) is sand material, with small-strain parameters inspired by examples from (PLAXIS, 2019), and the material below is modelled as a stiff Mohr Coulomb material based on wave velocities found for stiff materials in the literature review.

The damping parameters are by default modelled in PLAXIS© as Rayleigh damping parameters, hence the Rayleigh damping coefficients change according to the modelled frequency spectrum. The change in coefficients are modelled by creating materials for each frequency step. The Rayleigh damping coefficients for the crushed concrete material are found to be:

Table 14: Rayleigh damping coefficients

	1,5Hz	15Hz	30Hz	75Hz	100Hz
Rayleigh α	0.377	6.032	13.71	36.4	47.62
Rayleigh β	0.01273	$1.019 \cdot 10^{-3}$	$0.463 \cdot 10^{-3}$	$0.1756 \cdot 10^{-3}$	$0.134 \cdot 10^{-3}$

Following Table 15, shows parameters for the crushed concrete, which are used in modelling the vibration propagation in crushed concrete:

Table 15: Model parameters, Crushed concrete

Property	Unit	Description	Value	Estimation method
Material model	-	Hardening Soil with Small-strain	HSS	-
γ_{unsat}	$\frac{kN}{m^3}$	Unsaturated unit weight	19	Lab data

γ_{sat}	$\frac{kN}{m^3}$	Saturated unit weight	22	Lab data
e_{init}	-	Initial void ratio	0.31	Lab data
α		Rayleigh damping coefficient	Vary depending frequency domain	Estimated based on Figure 46
β		Rayleigh damping coefficient	Vary depending frequency domain	Estimated based on Figure 46
E_{50}^{ref}	kPa	Secant stiffness (std. drained triaxial)	$3.5 \cdot 10^5$	$E_{50}^{ref} = \frac{E_{ur}^{ref}}{3}$
E_{oed}^{ref}	kPa	Tangent stiffness (Primary oedometer)	$2.8 \cdot 10^5$	$E_{oed}^{ref} = \frac{E_{50}^{ref}}{1.25}$
E_{ur}^{ref}	kPa	Unloading/reloading stiffness (drained triaxial)	$1.05 \cdot 10^6$	From Appendix 4: One-dimensional compression test
m	-	Power	0.5	(PLAXIS, 2019)
c'_{ref}	kPa	Cohesion	1	For model stability
φ_c	°	Angle of internal friction	40	(Anttila, 2020)
$\nu_{0.7}$	-	Threshold shear strain at which $G_s = 0.722 \cdot G_0$	0.00016	Figure 47
G_0^{ref}	kPa	Reference shear modulus at very small strains	$\approx 6.6 \cdot 10^5$	Table 12, at reference stress 300kPa

6.2.1 FEM analysis results

The Finite Element Analysis has been made on the geometry shown in Figure 48, where the material in cluster 2 has been modelled as ballast, subgrade and crushed concrete. The crushed concrete has been modelled with the estimated soil properties and with the soil properties found from laboratory tests.

Initially the vibration with the worst impact is determined as the stages presented in Table 13 were simulated. However, this limits the impact assessment to five different frequencies, which are all at the level of ground-borne vibrations, and varying from 1.5 Hz to 100 Hz. The worst vibration impact has for this study been determined as the vibrations which cause the largest excitation of the ground, at highest velocities and accelerations. In Figure 49, the vertical excitation from all five stages are presented, and from this figure there is a clear difference at 30 Hz, which is also the trend for the velocities and accelerations. The vibrations induced by 30 Hz oscillations give the highest displacements, velocities and accelerations during the forced vibrations and are damped the slowest after stopping the excitation

of the ground. 30Hz oscillations might have the highest impact due to the properties of the surrounding sand rather than the properties of the structural layer in cluster 2, see more in section 7. However, as the impact is largest at 30Hz, the further study is based on this frequency.

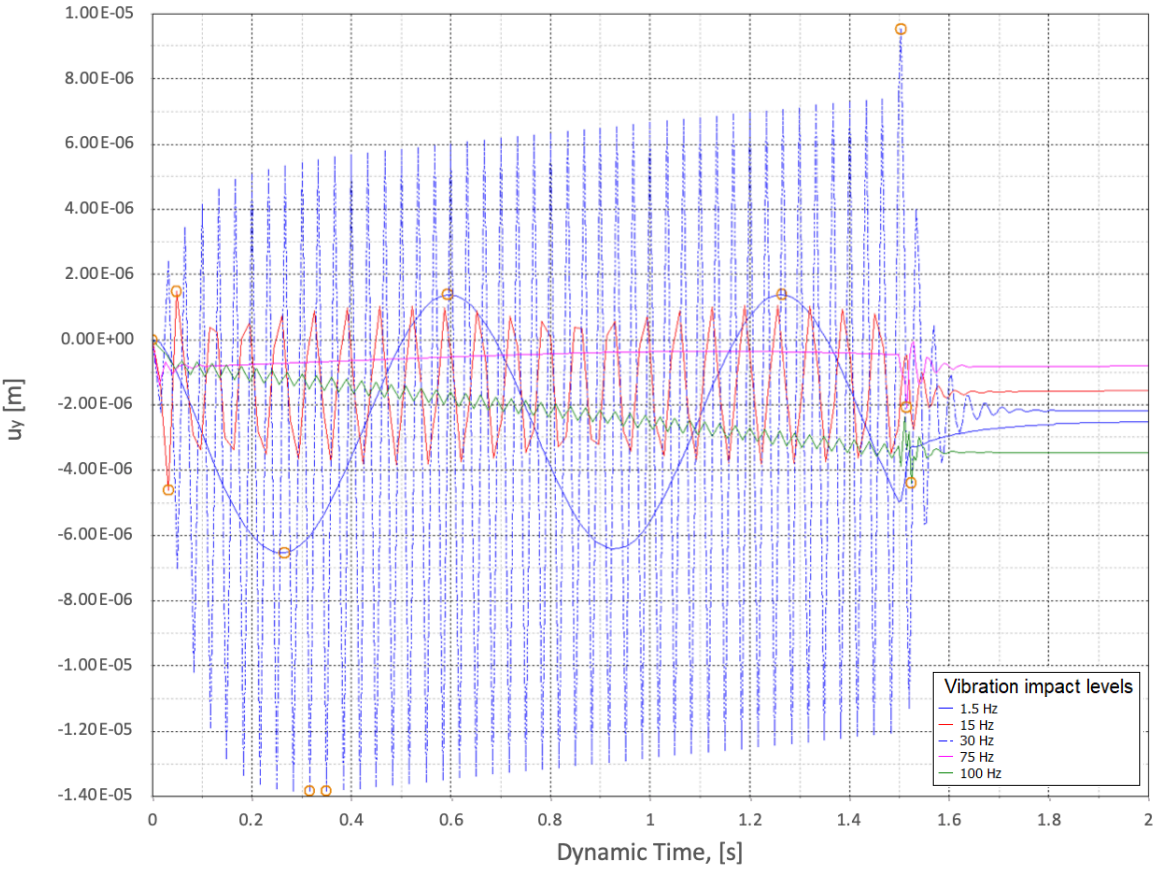

Figure 49: Vibration impact assessment

The analysis includes a study of the impact of the vibrations at Point A and Point B, where Point A is at the transition between the crushed concrete and the surrounding sand and Point B is in the sand. A comparison between the acceleration levels at Point A and Point B is presented in Figure 50, where it is seen that the damping parameters of the sand clearly affect the attenuation of the vibrations after stopping the forced vibration.

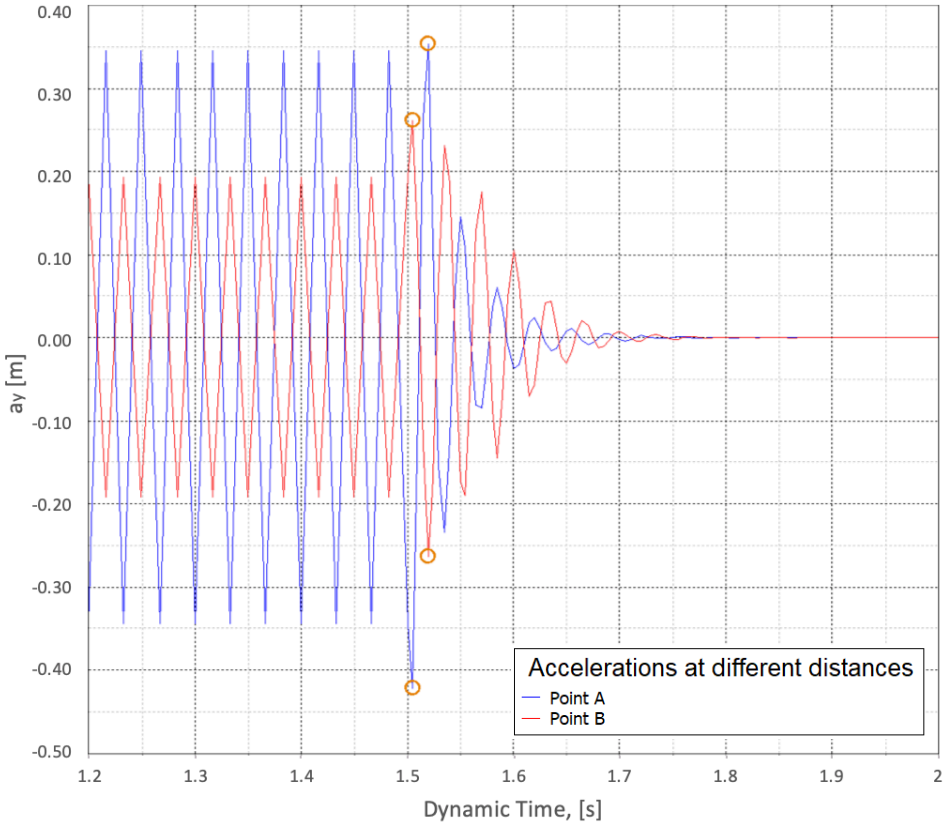

Figure 50: Vibration impact at Point A and Point B

Even though the acceleration levels during the forced vibrations are lower at point B, the accelerations increase to be larger than at Point A after stopping the forced vibrations. The same trend is seen for the velocity and displacement curves. This behaviour indicates that the oscillations are mostly affected by the sand properties at Point B, and hence for the study of the behaviour of the crushed concrete, the behaviour at Point A is more interesting. However, the dispersion of the vibrations is important to the surrounding structures, and with a proper railway design, a larger amount of vibrations will be attenuated before they are transmitted to the surrounding soil. Figure 51 illustrates how the vibrations for a 30 Hz oscillation can be dispersed. In this case the dispersion is highly dependent of the surrounding materials properties, but for another geometry of the railway this dispersion might be reduced.

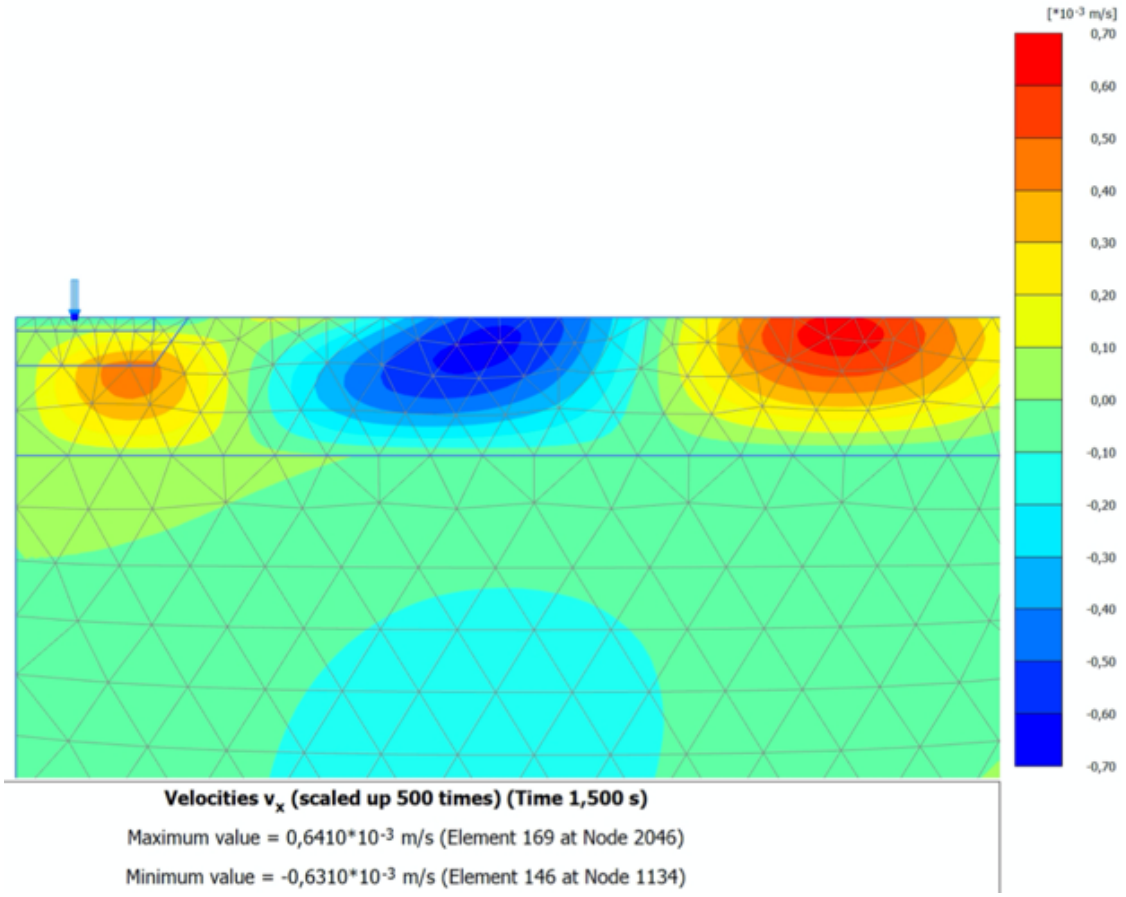

Figure 51: Dispersion of vibrations

Observing the vibration velocities at Point A, the results from different materials seem very similar. However, there is a small difference in peak velocities during the forced vibration and a stronger damping for the ballast material after stopping the vibrations.

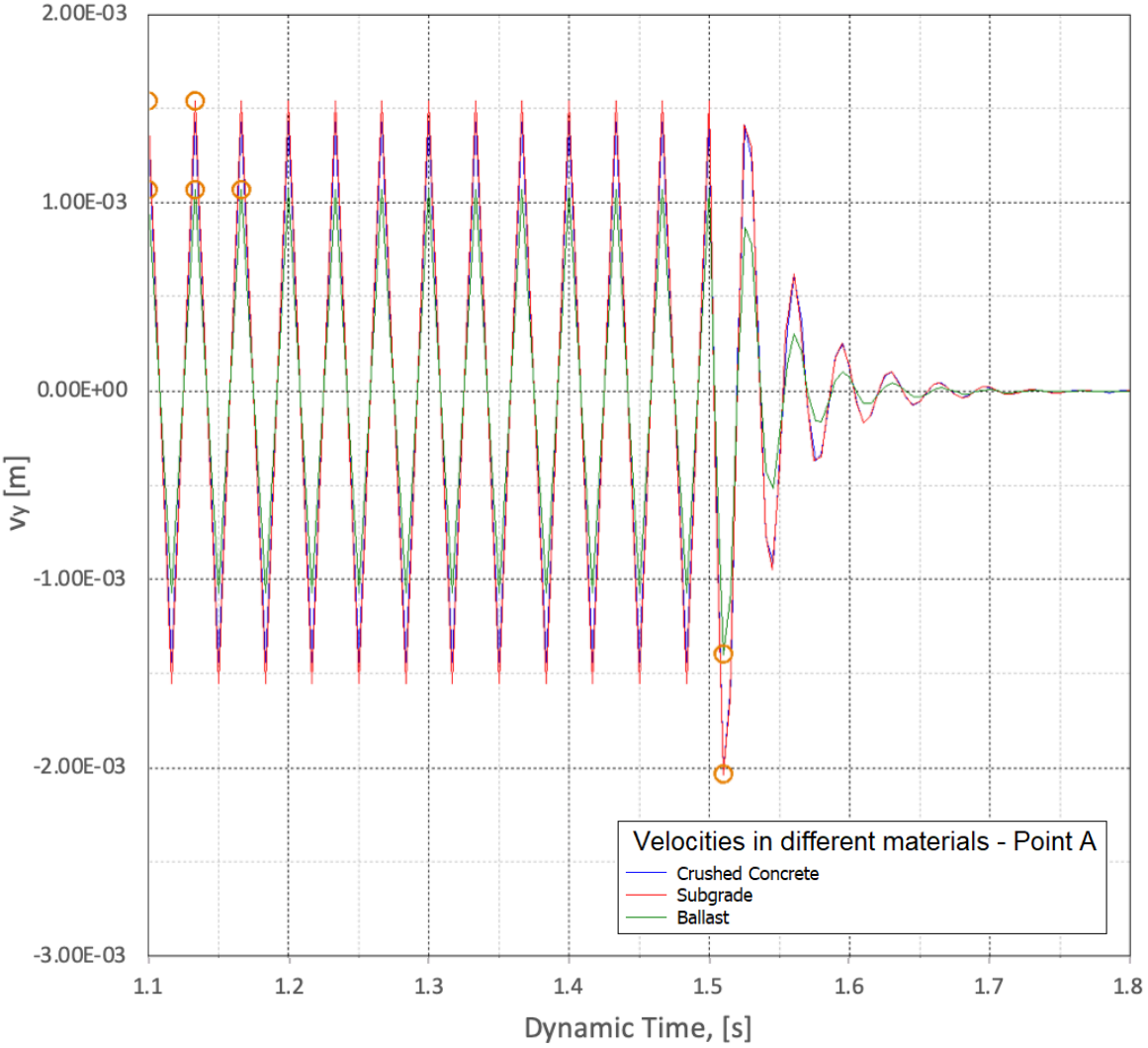

Figure 52: Velocities in different materials - Point A

The damping of the ballast material is estimated based on damping ratios used in other literature, see Table 5, and might be overestimated, see section 7. The estimated parameters for the crushed concrete, however, seem to give similar results as those defined from laboratory tests, see Figure 53. There is a difference in the attenuation of the vibration after stopping the forced vibration and a small difference in the peak velocities. The damping properties defined based on measured values have been estimated according to Figure 46, and the damping for the estimated values are estimated based on literature studies, and for both values there might be some error, which can affect the results, see more in section 6.2.1.1.

Furthermore, there is a difference in the stiffness of those materials, which in the Hardening Soil Small model affects the hysteric damping. The difference in stiffness affects the deformations due to excitation, which might also affect the velocities and the accelerations.

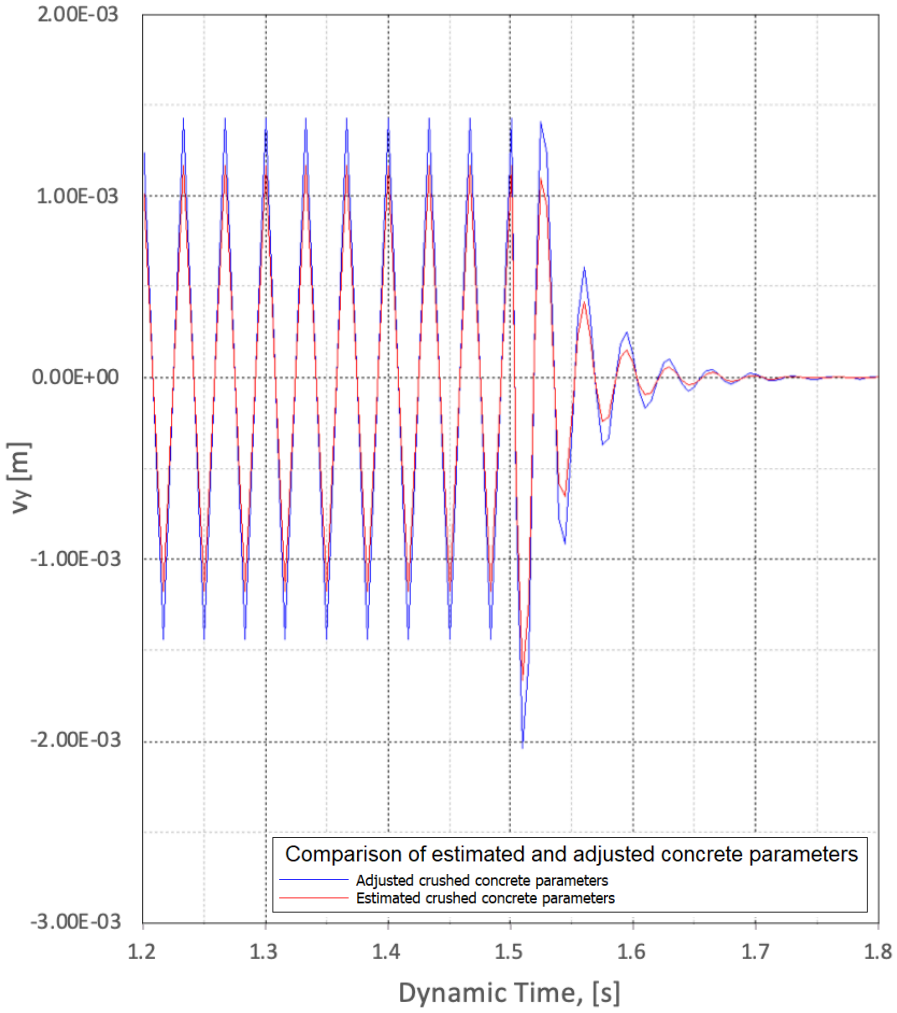

Figure 53: Comparison of estimated and measured crushed concrete parameters

To confirm the compliance with the assumed small-strain behaviour, the actual stiffness during simulation is studied. The stiffness is seen in Figure 54, where it is observed that it is highest around the crushed concrete, which is due to a higher small-strain stiffness than the surrounding material. In addition, the stiffness matches the input small-strain stiffness. This figure indicates that the strains are in fact small enough for the stiffness to be the small-strain stiffness. For further confirmation, the strain history is presented in Figure 55.

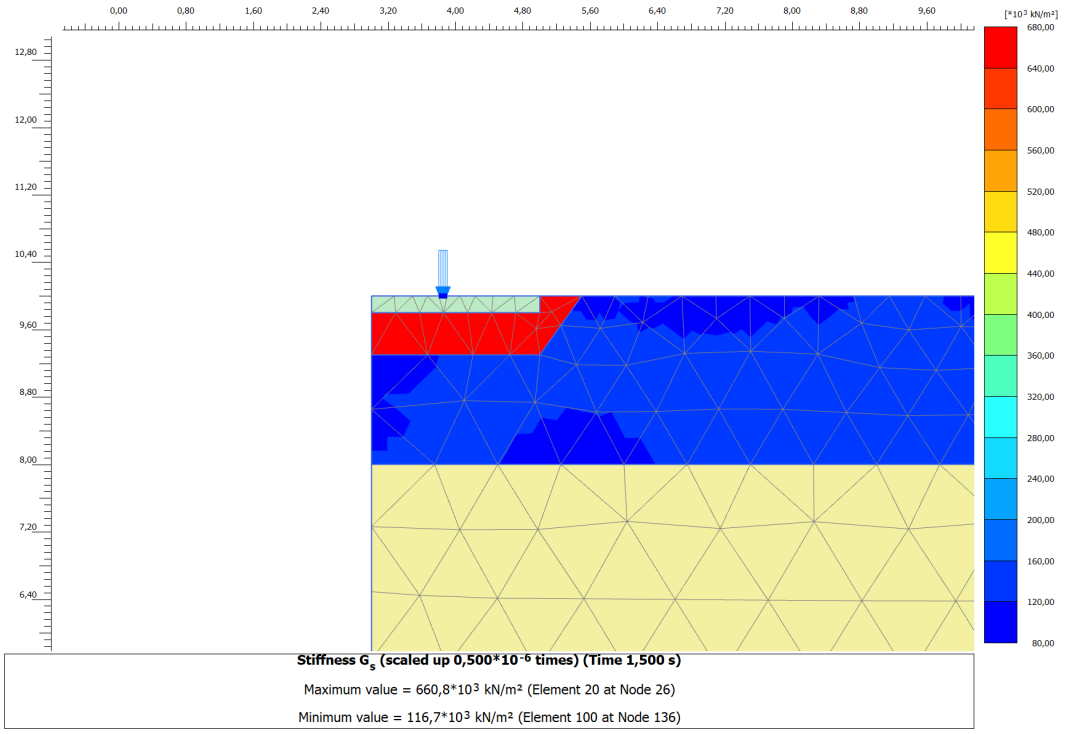

Figure 54: Material stiffness during FEM simulation

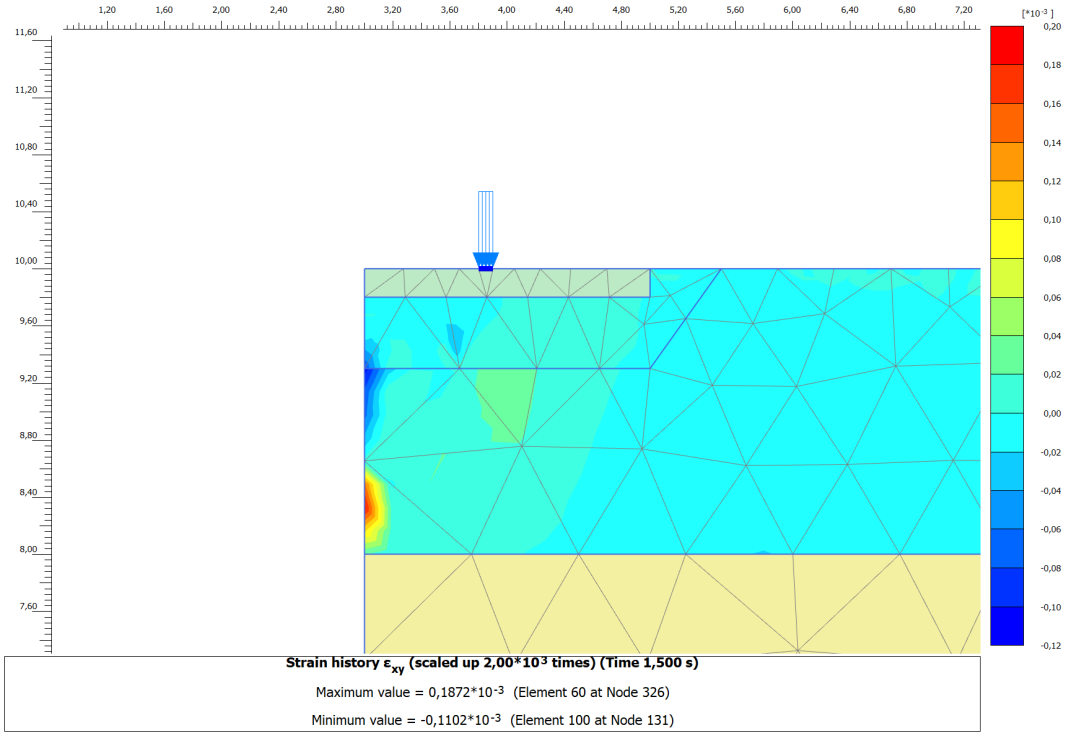

Figure 55: Strain history at 30Hz oscillations

The strain history shows strains, which are small, and hence the assumptions of small-strain behaviour is confirmed.

6.2.1.1 Sensitivity Study of Damping Parameters

There is a large uncertainty related to the damping parameters of the crushed concrete and it is not possible to define the Rayleigh damping parameters for a certain strain level. The Hardening Soil Small model has incorporated hysteretic damping which is related to a loss of energy internally in the soil structure itself. The hysteric damping is a strain dependent material damping, which is not significantly affected by the viscous damping, but is very sensitive to the small-strain input parameters. Using the hysteric damping, enable a more realistic soil behaviour due to the strain dependency. It is also possible to define viscous damping parameters as Rayleigh coefficients α and β. This type of damping is often defined for e.g. Mohr Coulomb model and is mainly sensitive to the input frequency versus the defined damping frequency range. The viscous damping parameters have to be changed according to the induced frequency, and relates more to the loss of energy due to liquid in the body. The hysteretic damping parameters are defined based on the state parameter $\nu_{0.7}$, which is the level at which $\frac{G_S}{G_0} = 0.722$. In addition, the hysteretic damping is strain dependent like the small-strain stiffness, and is activated in a state of cyclic loading such as in dynamic calculations. Still, the viscous damping might have a small effect on the attenuation of the vibrations; hence the sensitivity study. A simulation has been made for 30 Hz oscillations with changing viscous material damping; 0.5 %, 2 %, 5 %, 8 % and 12 %. Which are damping parameters in the range of the damping shown in Figure 46.

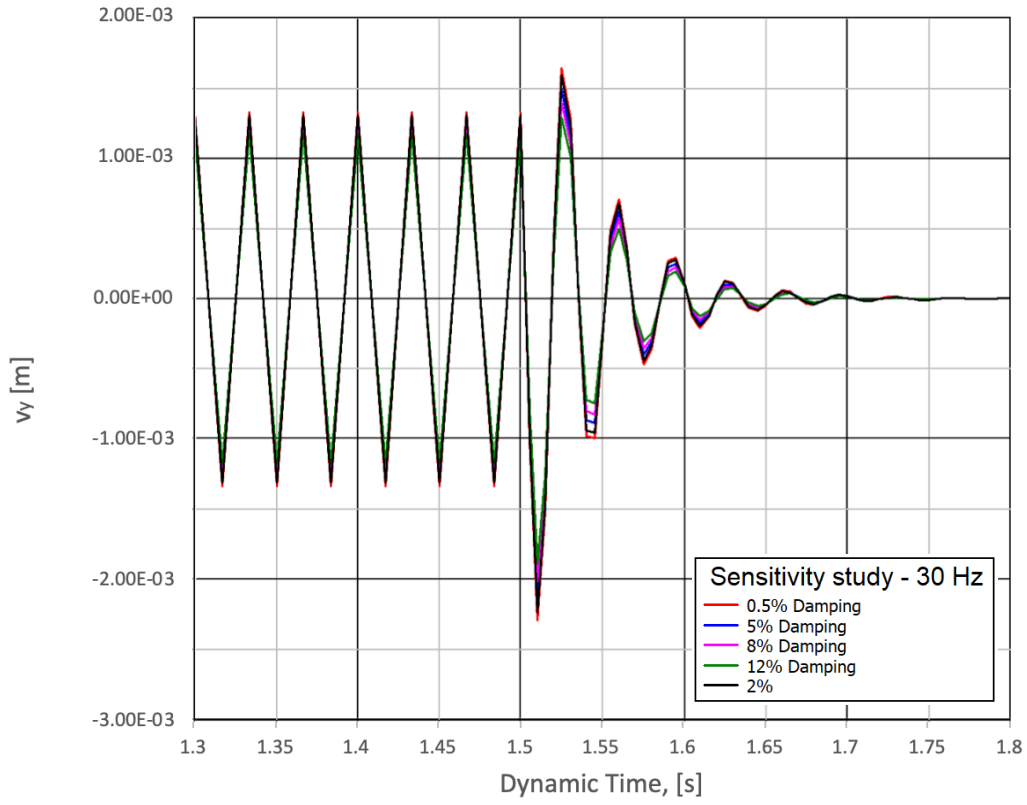

Figure 56: Sensitivity study on the damping parameters

The result of the simulation with different viscous damping parameters of the crushed concrete are presented in Figure 56, where it is clear to see that the Rayleigh damping parameters does not affect the results significantly. The hysteretic damping calculated in PLAXIS©, is calculated by assuming Masing behaviour similarly as in the calculation used in this thesis. Although the hysteretic damping gives more realistic damping properties for the material, the change in damping is relatively low at these high stiffnesses and is both dependent of the small-strain stiffness and the threshold strain $\nu_{0.7}$. To analyse the sensitivity of the hysteretic damping of the material, different threshold strain values has been simulated, which show no significant difference compared with the viscous damping, see Figure 57.

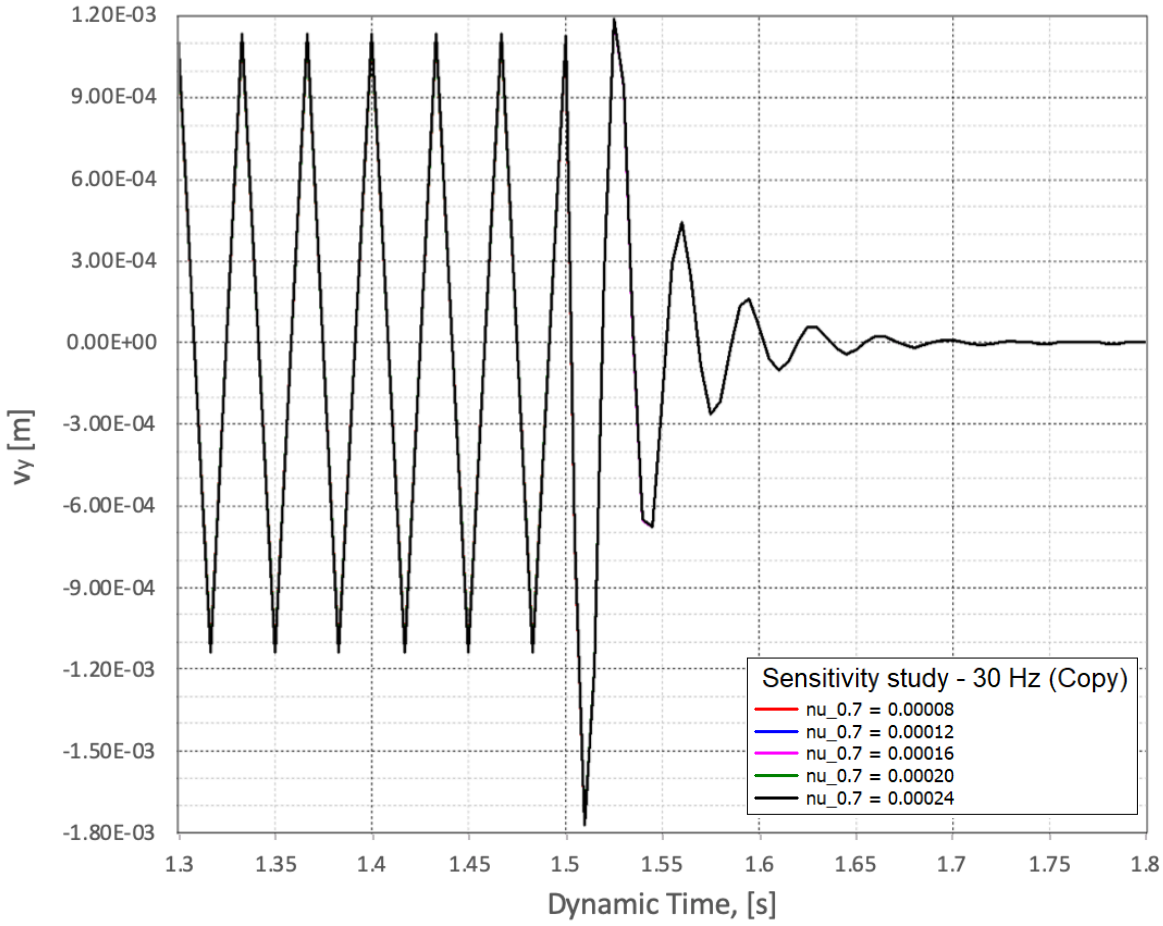

Figure 57: Sensitivity of hysteretic damping

However, during calculations the small-strain stiffness and threshold strain for the surrounding material is significant lower, which can be seen on the damping of the vibrations.

7 Critical Assessment of Results

The aim of the critical assessment is to analyse how well the obtained measured results correlate with the estimated values from the hypothesis. The critical assessment includes a revision of the assumptions made in the achievement of the hypothesis. As the hypothesis might differ from the obtained results, the revision of the assumptions might yield information which is useful for the future estimation of the dynamic parameters of crushed concrete. Furthermore, the finite element simulations are assessed in the critical assessment, with a focus on potential errors and deviations from the reality.

7.1 Errors Related to Estimation of New Parameters

The estimated small-strain stiffness parameters were obtained using equations which were previously fitted to match other materials properties. Most of the estimation methods were based on poorly graded sand material with relatively low mean grain size. As the crushed concrete, unlike those materials, is very well graded and has a relatively high mean grainsize, those models are not representative for crushed concrete, but has been included as they represent granular materials. In addition, the material models representing granular material were not fitted to materials with a relatively high fines content and a hardening effect, which are properties of the crushed concrete. However, the calculation of the small-strain stiffness properties using these models, lead to results which indicated the magnitude of the properties for the crushed concrete.

The estimation method which yielded the best fitting results was method 1 (He, et al., 2018), which has been fitted based on tests on crushed concrete. The crushed concrete which were tested for method 1 had a significantly lower coefficient of uniformity and mean grainsize than the material which has been tested in this thesis. Nevertheless, the material has had some similar properties, as it was also crushed concrete. In the Comparison Between Hypothesis and Results, an attempt is made to fit the existing model to the measured values by adjusting the void ratio and the particle density. This adjustment results in a close fit, but is made on a small number of tests; hence there are several other parameters which can be adjusted, which might yield the same results. The expression in method 1 contains several empirically obtained constants, which should be analysed on a larger number of tests.

Similarly, as with the moduli, the damping graph were adjusted to make a better fit to the results, by adjusting empirically obtained coefficients. In the estimation of the damping in section 3.6, the empirical methods by (Menq, 2003) were used, which include more than 10 empirically obtained coefficients, found from an extensive study on another material than crushed concrete. The coefficients related to the material property C_u were adjusted to get the better fit to the obtained results. This adjustment affects not only the damping curve but also the normalized shear modulus curve, which has a direct impact on $\nu_{0.7}$ which is used in the Hardening Soil Small model for simulation. In the Hardening Soil Small model, the $\nu_{0.7}$ has a direct impact on the hysteretic damping of the material; hence the if the adjustment of the damping factors is not exact, it will significantly affect the vibration simulations.

7.2 Errors Related to FEM Modelling

Geometry of structural layers

The finite element model was initially constructed as the full geometry and no symmetry around the left axis was considered. This initial modelling was good for the comparison of boundary parameters when taking advantage of the symmetry. The symmetry was exploited and the model made smaller due to the long processing time. The geometry of the railway structure is modelled as a simplification of the geometry of urban transit systems. It has been simplified to only one structural layer, with a concrete slab inserted to the crushed concrete. The simplification affects the damping of the system in such a way that the only attenuating layer in the structure is the crushed concrete layer, which is only 0.5m thick.

The crushed concrete layer is constructed under the surface of the ground to resemble the real geometry of urban transit systems. However, it seems that possibly, due to the small thickness of the layer and the relatively high stiffness, the vibrations are transmitted very directly to the surrounding soil. To discover how the influence of the thickness and position of the structural layers, the analysis should be extended to include several different and more realistic geometries. However, it is seen in the analysis that the stiffness of the layer does have some effect on the wave propagation and for the purpose of comparing the effect of different material properties, the geometry seems to have the desired effect. Furthermore, the inclination of the excavation to the crushed concrete layer could disturb the wave propagation in the x-direction. The effect of the inclination of this excavation should be tested, also for future urban transit systems. Due to the very high stiffness of the structural layers, the rigid movement of the structural layers in combination with the inclination, the dispersion to the surrounding ground might change depending on the inclination.

2D versus 3D

The purpose of the finite element model has been to compare the effect of using different materials in railway construction, and for this purpose the simplification of the model to 2D is sufficient. However, the soil properties of the surrounding soil have a great influence on the wave propagation and as the ground properties, in reality, are constantly changing with depth of the model, a 3D model would be ideal to model the exact behaviour of the ground. This would, however, require a more in-depth study of a specific site, the soil parameters of the site and monitoring of the actual vibrations for back-calculating and checking the simulation results. In this study the 2D model was used to save calculation time and increase the precision in each element, due to the higher mesh-density.

Mesh

In the initial calculations a mesh density of fine to very fine was used, but after the first calculations the model showed unstable behaviour and the mesh density had to be reduced to medium dense with higher densities at important locations of the model, such as in the crushed concrete layer. Ideally, a finer mesh would increase the precision of the model, but might require a further reduction in the model extents, which would decrease the precision. No mesh sensitivity study has been made for this thesis, but should be done to see the effect.

Material properties and Damping

As the Hardening Soil Small uses hysteretic damping as a function of the strain, defining viscous damping parameters has only little effect. However, this introduces an even higher

importance of defining the soil properties properly. There are some estimation methods given in (PLAXIS, 2019), for estimating $\nu_{0.7}$ and the small-strain stiffness, but for a more precise modelling and for the more important layers it is recommended to carefully determine these properties. Another option is to model the surrounding layers as Mohr Coulomb layers with parameters defined based on shear wave velocities and Poisson's ratio. This does not require as many parameters and the damping is only defined as the Rayleigh damping. This material model is not recommended for the more important layers, such as the structural layers in the railway structure. The Hardening Soil Small model enables a more realistic soil behaviour due to the strain dependent stiffness and damping.

The properties for the ballast and subgrade were estimated based on a literature review and their small-strain properties were estimated using the methods from (PLAXIS, 2019). This introduces a high amount of uncertainty to the comparison on the results. However, they have been estimated the same way, and the estimated parameters for the crushed concrete were also been compared and adjusted according to these methods. Thus, the results are of similar comparability and seem to yield results in the right magnitude.

8 Conclusion

The essential aim of this thesis was to determine dynamic parameters for crushed concrete and to study the influence of replacing conventionally used materials with crushed concrete in urban railway systems. The study includes a literature review, laboratory testing, simulations and numerical estimations. Different sources of vibrations and their corresponding frequency range has been determined. The thesis review clearly indicates that frequencies which are transmitted to the track structure are in a range of nearly 0 Hz to above 1000 Hz, whereof frequencies from +0 Hz to 100 Hz are defined as ground-borne vibrations. As the ground-borne vibrations have the largest impact on nearby structures they have been studied more extensively than frequencies above 100 Hz. There are many mitigation measures available for reducing vibrations, whereof several of them base on an improvement of the alignment and quality of the track structure. This underline the importance of the material quality in the track structure, and the knowledge of the materials' behaviour during dynamic loading. However, there is only limited information available on dynamic properties of both conventionally used materials and crushed concrete. The reviewed empirical models, however, are based on in-situ measurements from railways in France, Italy, Sweden, United Kingdom, etc., which all are built using conventional materials and through many years of use they have proved to work acceptably. Recycled crushed concrete, however, has not been commonly accepted as a building material for railways, hence, knowledge about the dynamic behaviour of crushed concrete is limited to a few laboratory studies. The studies, which have been made on small-strain properties of crushed concrete are limited to tests made on crushed concrete with a relatively small coefficient of uniformity and mean grain size, which is not representative for the material which potentially can be used in railway construction. Through this study of crushed concrete, BeM II, several estimation methods have been used to achieve approximations of the small-strain stiffness of crushed concrete. The methods give relatively different small-strain properties for the crushed concrete, likely due to characteristics of the materials the methods have been developed for. However, the method proposed by (He, et al., 2018), based on tests on crushed concrete, yielded results at a void ratio of $e = 0.43$ and particle density $\rho_s = 2600 \frac{kg}{m^3}$, which were around 30% lower than then results obtained from laboratory tests. Adjusting the void ratio and particle density to $e = 0.31$ and $\rho_s = 2000 \frac{kg}{m^3}$, give results matching those achieved by laboratory tests. However, the void ratio and particle density should be measured for a sample of the same material prepared the same way, to be more certain about this relationship. The aim of this thesis is to study dynamic properties of crushed concrete and to estimate the effect of replacing conventionally used materials with crushed concrete in railway construction. The study was conducted by studying and answering the research questions below.

Research questions and answers:

1) Which methods are currently used in empirical models for ground induced vibrations caused by railway traffic?

The vibrations from trains are subdivided into ground-borne vibrations and ground borne noise. The definition of these groups is found from section 3.1.1 and 3.1.4. The current empirical methods used in Finland for estimating the vibrations is based on measurements made in Sweden, Italy, France, United Kingdom, etc. The measurements have provided the

empirical knowledge for the reports made by (Harris Miller Hanson Inc, 2005) *and* (Hanson, et al., 2006)*, which describe the methods for estimating vibrations in USA. The methods are described in depth in section 3.1.5. The principle of the empirical model is to initially categorise the structure of interest and then determine the basic vibration level according to a baseline principle and the distance to the structure. The baseline vibration level is then adjusted according to correction factors which can be seen from* Appendix 1: Adjustment Factors for Generalized Predictions of Ground-Borne Vibration and Noise*.*

Several models have been made purely by differential equations ((Auersch, 2005), (Jones, et al., 2004), (Sheng, et al., 2003), (Lei, 2015), etc.)*, which has been obtained by analysing the track structure and the ground as a system of springs, where soils act as viscous materials. These methods are more advanced and not easy to start using unless you possess the needed knowledge about differential equations and dynamics. However, these methods provide a better understanding of the parts in the railway structure which affect the vibrations and the vibration dispersion the most.*

2) How can the dynamic parameters for crushed concrete and similar granular materials be estimated reliably?

There has not yet been developed equations for estimating dynamic properties of crushed concrete with a coefficient of uniformity similar to the BeM II material tested in this thesis. However, there are several estimation methods available, which are all presented in section 3.5 and 3.6. The methods are made for materials such as clay, sand, gravel, etc. (He, et al., 2018) *has tested crushed concrete and developed an estimation method which can give potentially reliable results, this method is the method referred to in section 3.5 as Method 1. The estimations of the dynamic properties for the crushed concrete is found from section 3.7 and the comparison which is seen in* Figure 53*, clearly indicate that the difference between the estimated properties are not far from the measured values. The potential of method 1, see section 3.5 for the use on BeM II, should be verified by further testing of the small-strain parameters and testing of the void ratio and particle density. By adjusting void ratio and particle density, a good fit between the measured and estimated values is obtained, see section 6.1.*

Furthermore, the damping properties of the materials can be estimated by methods from (Menq, 2003)*, see section 3.6. The estimated damping properties are larger than the damping found from laboratory tests, see* Figure 45*. Adjusting the coefficients related to* C_u *give a relatively good curve fit, see* Figure 46*. However, estimation of damping properties should be studied much more to determine the reliability of these estimation methods for crushed concrete. There are several coefficients which have been determined empirically by* (Menq, 2003) *and there is not at this stage 100 % confidence in the adjustment. Discussions on the reliability of this adjustments can be found from section 7.1.*

Dynamic properties have been found to be similar to the small-strain properties and these can be reliably estimated through bender element and resonant column testing. The testing procedures are explained in section 4. The precision has been found to be higher by testing both through bender elements and resonant column, due to the inaccuracy related to analysing output data from bender element testing.

3) How can the small-strain parameters for crushed concrete and similar granular materials be estimated reliably?

Some of the available methods for estimating small-strain parameters are described in section 3.5. The methods have been developed for materials such as sand and other granular materials. Small-strain parameters are sensitive to parameters related to grainsize distribution of the material, such as fines content, coefficient of uniformity and mean grainsize (He, et al., 2018)*. The most reliable estimation of small-strain parameters is by laboratory testing, doing resonant column and bender element test which are described in section 4. Methods exist for determination of small-strain parameters, which give results relatively close to those found by laboratory testing. The difference in the impact on the ground-borne vibrations was analysed through Finite Element simulations, see section 6.2, the resulting ground-borne vibration levels turn out to be very similar, see* Figure 53*. The estimation method by* (He, et al., 2018) *was also compared with the measured small-strain properties, see section 6.1, where it was found that a small adjustment of the initially assumed void ratio and particle density result in a very good data fit, see* Figure 44*. The estimation method developed by* (He, et al., 2018)*, is developed based on tests on crushed concrete with significantly smaller C_u and d_{50} values, but the method still give the best results, see section 3.7 and 6.*

4) How does the substitution of the commonly used material with crushed concrete affect the vibrations induced by tramways?

Substitution of the conventionally used materials, ballast and subgrade, to crushed concrete, seem to have a small effect on the vibrations, see Figure 52*. However, this is recommended to be studied further through more extensive finite element simulations and possibly testing, see discussions hereof in section 7.2. The largest difference between the crushed concrete and the conventionally use materials could be the hardening process of the crushed concrete, which possibly will affect the failure mechanism and the durability, see section 3.7. The hardening effect has not been studied significantly in this study, but an increase in strength has been found for increasing hardening time* (Linden, et al., 2019)*. If this effect will be negative or positive has not been studied.*

Furthermore, the properties of the conventionally used materials, ballast and subgrade, found from the literature review in section 3.3 are quite similar to those for the crushed concrete, see section 5.

The geometry of the track structure, used mitigation measures and surrounding soil seem to have large impact on the vibration propagation, hence constructing the track structure in a good quality, to improve the alignment and reduce uneven settlements has a large impact on the transmitted vibrations. Together with proper maintenance of rails, wheels and track structure this will effectively reduce the vibration level, by limiting the amount of transmitted vibrations.

5) How do the dynamic and small-strain parameters of the structural layers affect the ground induced vibrations caused by railway traffic?

Damping properties affect the attenuation of the vibrations, but will have less effect if the distance where they can dampen the vibrations is too small. From the perspective of differential equations, the damping directly affects the velocity and as the travel distance is larger, the velocity will also be much more reduced. The small-strain stiffness affects the damping properties as well and the stiffness has a large impact on resonance frequency and level of excitation of the ground. A higher stiffness result in a higher resonance frequency and hence vibration frequencies will be magnified less, see section 3.1.5.1.

The difference between the response from different materials can be seen from Figure 50*, where the vibrations are compared at the crushed concrete and at the surrounding sand. The surrounding sand has a significantly lower small-strain stiffness, which clearly affect the vibrations. The impact seen comparing the ballast and the crushed concrete is much smaller, see* Figure 52 *and discussions in section 6 and 7.*

However, the geometry of the railway track should be optimised to utilize the full potential of the structural materials. The effect of the geometry has not been studied in this thesis, but the simulations, section 6.2, and the theory of wave propagations, section 3.1, indicate that the geometry have an influence. This is due to the distance the waves travel in the structural layers, which affect how much the waves are damped before they are transmitted to the surrounding material, see discussions in section 7. The geometry also affects the angle of transmission, which impact the reflection and refraction of the waves, see section 3.1.3. The refraction and reflection through the material might have an effect on the surface waves.

6) Which laboratory and in-situ methods can be used to predict and monitor the dynamic behaviour of crushed concrete waste in railway construction?

The two most common methods for determining the dynamic properties of materials are bender element test and resonant column test, which give the most reliable results in a combination, see section 4. Determining dynamic properties of crushed concrete through bender element test and resonant column test, give parameters which can be used in finite element models, which can help understanding the vibration propagation in the materials, see section 6. Vibrations can be monitored in-situ by the use of geophones. This monitoring can be a useful tool for calibrating the finite element model and for monitoring that the vibration levels are inside an acceptable range.

9 Suggestions for Further Research

1. ***Void ratio and Particle Density of Crushed Concrete Material***
   - It is suggested that a few samples are made of the crushed concrete material to validate or invalidate the assumptions made in section 6.1.
2. ***In-situ monitoring***
   - It is suggested to monitor the vibrations at locations where the crushed concrete material will be used. The monitoring results can be used for back-calculations and refinement of a numerical model.
   - The in-situ monitoring at conventionally used materials and crushed concrete, enable a better evaluation of the effect of the substitution and can further help refining a numerical model.
3. ***Model variations***
   - A geometry analysis focused on the effect of the inclination of the excavation to the structural layers is suggested, to analyse how this inclination affect the dispersion of the vibrations.
   - An analysis of the effect of the position of the structural layers is recommended, to see how the confinement of the structural layers in the ground affect the vibration dispersion compared with a structure located on top of the ground.
     - Naturally a structure located on top of the ground is not relevant in urban areas due to traffic integration, but it can have an effect outside the densely populated areas.
   - An analysis of the effect of the thickness of the crushed concrete layer, is suggested to study how the damping and small-strain properties of the structural layers can be utilized best in the urban areas.
4. ***Extensive material testing at different strain levels***
   - For developing reliable small-strain estimation methods for crushed concrete material with higher C_u and d_{50} values than those in (He, et al., 2018), it is suggested to perform a larger number of tests, varying the strain levels to obtain a certain model fit for e.g. damping and normalized shear modulus curves.
   - A larger number of tests naturally increase the reliability of the results and enable a justifiable adjustment of the empirical constants used in established small-strain estimation models.

10 Tables

11 Figures

12 Bibliography

Alpan, I., 1970. The geotechnical properties of soils. *Earth Science Reviews*, February, pp. 5-49.

Anttila, S., 2020. *Betonimurskeen Geotekninen Soveltuvuus Meritäyttömateriaaliksi,* Turku: Turku Ammattikorkeakoulu.

Aris, M., Benahmed, N. & Bonelli, S., 2010. Experimental geomechanics: a laboratory study on the behaviour of granular material using bender elements. *European Journal of Environmental and Civil Engineering,* pp. 97-110.

Atkinson, J. & Sallfors, G., 1991. *Experimental determination of soil properties. In Proc..* s.l., ECSMFE, pp. 915-956.

Auersch, L., 2005. The excitation of ground vibration byrail traffic: theory of vehicle–track–soil interaction and measurements on high-speed lines. *Journal of Sound and Vibration,* pp. 103-132.

3Blue1Brown, 2018. *But what is the Fourier Transform? A visual introduction.* [Online] Available at: https://www.youtube.com/watch?v=spUNpyF58BY

Bjarnason, G. & Petursson, P., 2004. *Comparison of CEN and Nordic aggregate requirements,* s.l.: Nordisk Vejteknisk Forbund, NVF.

Bonnett, C. F., 1996. *Practical Railway Engineering.* London: Imperial College Press.

Burland, J. B., 1989. *"Small is beautiful" - Stiffness of soils at small strains.* London, Department of Civil Engineering, Emperial College.

Cascante, G., Santamarina, C. & Yassir, N., 1998. Flexural excitation in a standard torsional-resonant column device. *Canadian Geotechnical Journal,* pp. 478-490.

Clayton, C. R. I., 2011. Stiffness at small strain: Research and practice. *Géotechnique*, pp. 5-37.

Coulier, P. et al., 2015. *Stiff Wave Barriers for the Mitigation of Railway Induced Vibrations.* Berlin, Springer, pp. 539-546.

Dahlberg, T., 2006. Track Issues. In: *Handbook of Railway Vehicle Dynamics.* Boca Raton: CRC Press, Taylor & Francis Group, pp. 143-179.

Darendeli, B. M., 2001. *Develope of a new family of normalize modulus reduction and material damping curves,* s.l.: University of Texas at Austin.

Deloitte, et al., 2015. *European Comission.* [Online]
Available at:
https://ec.europa.eu/environment/waste/studies/deliverables/CDW_Finland_Factsheet_Final.pdf

Dettenborn, T., Forsman, J. & Korkiala-Tanttu, L., 2015. Crushed concrete in road structures - two decades of experience. *ICE - institution of Civil Engineers*, September.

Faure, B. et al., 2015. *Vibration Mitigation by Innovative Low Stiffness Rail Fastening Systems for Ballasted Track.* Berlin, Springer, pp. 627-634.

Finnish Ministry of Environment, 2017. *843/2017 Statsrådets förordning om återvinning av vissa avfall i markbyggnad.* [Online]
Available at: https://www.finlex.fi/sv/laki/alkup/2017/20170843

Forsman, J. & Dettenborn, T., 2019. *Betonimurske kaupunkien julkisessa maarakentamisessa,* Helsinki, Espoo, Tampere, turku, Vantaa: Ramboll Finland Oy.

Giancoli, D. C., 2016. Refraction: Snell's Law. In: *Physics principles with applications.* Harlow: Pearson Education Limited, pp. 657-658.

Hanson, C. E., Towers, D. A. & Meister, L. D., 2006. *Transit Noise and Vibration Impact Assessment,* Burlington: Harris Miller Miller & Hanson Inc.

Harris Miller Hanson Inc, 2005. *High-Speed Ground Transportation Noise and Vibration Impact Assessment,* Washington, D. C.: U. S. Department of Transportation, Federal Railroad Administration.
He., H. & Senetakis, K., 2016. A study of wave velocities and poisson ratio of recycled concrete aggregate. *Soils and Foundations,* pp. 593-607.
He, H., Senetakis, K. & Coop, M., 2018. Stiffness of a recycled composite aggregate. *Soil Dynamics and Earthquake Engineering,* pp. 185-194.
Hibbeler, R. C. & Beng Yap, K., 2013. Vibrations, Viscous damped forced vibration. In: *Mechanics for Engineers: Dynamics, SI Edition.* s.l.:Pearson.
Johansson, A. et al., 2008. Under sleeper pads--Influence on dynamic train--track interaction. *Wear,* pp. 1479-1487.
Jones, C. J. C., Sheng, X. & Petyt, M., 2000. Simulations of ground vibration from a moving harmonic load on a railway track. *Journal of Sound and Vibration*, pp. 739-751.
Jones, C., Sheng, X. & Thompson, D., 2004. A theoretical study on the influence of the track on train-induced ground vibration. *Journal of Sound and Vibration,* pp. 909-936.
Khan, S., 2013. *Refraction and Snell's Law.* [Online]
Available at: https://www.khanacademy.org/science/physics/geometric-optics/reflection-refraction/v/refraction-and-snell-s-law
Lee, J.-S. & Santamarina, J. C., 2005. Bender Elements: Performance and Signal Interpretation. *Journal of Geotechnical and Geoenvironmental Engineering,* pp. 1063-1070.
Lei, X., 2015. Analytic Method for Dynamic Analysis of the Track Structure. In: *High Speed Railway Track Dynamics.* Beijing: Science Press and Springer.
Li, D. & Selig, E. T., 1995. Evaluation of railway subgrade problems. *Transportation Research Record,* pp. 17-25.
Likitlersuang, S. et al., 2013. Small strain stiffness and stiffness degradation curve of Bangkok Clays. *Soils and Foundations*, August, pp. 498-509.
Linden, T. et al., 2019. *Utilization of crushed concrete aggregate in light rail construction.* Reykjavik, ECSMGE.
Lombaert, G., Degrande, G., Francois, S. & Thompson, D., 2015. *Ground-Borne Vibration due to Railway Traffic: A Review of Excitation Mechanisms, Prediction Methods and Mitigation Measures.* Uddevalla, Sweden, Springer, pp. 253-287.
Menq, F.-Y., 2003. *Dynamic Properties of Sandy and Gravelly Soils,* s.l.: The University of Texas at Austin.
Paul de Vos, S., 2017. *Railway induced vibration, State of the art report,* Paris: UIC, International Union of Railways.
Payan, M., Senetakis, K., Khoshghalb, A. & Khalili, N., 2017. Effect of gradation and particle shape on small-strain young's modulus and poisson's ratio of sands. *International Journal of Geomechanics*, 1 May, p. 17(5).
Pennington, D. S., Nash, D. F. T. & Lings, M. L., 1997. Anisotropy of G0 shear stiffness in Gault Clay. *Géotechnique*, pp. 391-398.
PLAXIS, 2019. *Plaxis 2D manuals.* [Online]
Available at: https://www.plaxis.com/support/manuals/plaxis-2d-manuals/
Senetakis, K., Anastasiadis, A. & Pitilakis, K., 2012. The Small-Strain Shear Modulus and Damping Ratio of Quartz and Volcanic Sands. *Geotechnical Testing Journal*.
Senetakis, K., Anastasiadis, A. & Pitilakis, K., 2013. Normalized shear modulus reduction and damping ratio curves of quartz sand and rhyolitic crushed rock. *Soils and Foundations*, pp. 879-893.

Sheng, X., Jones, C. & Thompson, D., 2003. A comparison of a theoretical model for quasi-statically and dynamically induced environmental vibration from trains with measurements. *Journal of Sound and Vibration*, p. 621–635.
Talja, A. & Saarinen, A., 2009. *Maaliikenteen aiheuttaman runkomelun arviointi,* Espoo: VTT.
Technical Committee ISO/TC 108, 2005. *ISO 14837-1: Mechanical vibration — Ground-borne noise and vibration arising from rail systems — Part 1: General guidance,* s.l.: the International Organization for Standardization.
Verbraken, H. et al., 2015. *The Prediction of Vibration Transfer for Railway Induced Ground Vibration.* Berlin, Springer, pp. 245-252.
Verdict Media Limited, 2020. *Projects by Region: Europe.* [Online]
Available at: https://www.railway-technology.com/projects/region/europe/
Vuchic, V. R., 2007. Rail Transit: Streetcars, Light Rail, Rapid Transit, and Regional Rail. In: *Urban Transit Systems and Technology.* Hoboken, New Jersey: John Wiley & Sons, Inc, pp. 297-443.
Vuorimies, N., 2002. *Betonimurskeen BeM 1 staattiset kolmiaksiaalikokeet,* Tampere: TTKK, Laboratory of Foundation and Earth Structures.
Wichtmann, T. et al., 2011. *Estimation of the small-strain stiffness of granular soils taking into account the grain size distribution curve.* Santiago, Chile, s.n.
Wichtmann, T. & Triantafyllidis, T., 2009. On the influence of the grain size distribution curve of quartz sand on the small strain shear modulus Gmax. *Journal of Geotechnical and Geoenvironmental Engineering, ASCE,* pp. 1404-1418.
Wojciech, S., Katarzyna, G., Sobol, E. & Szymanski, A., 2016. Dynamic Characterization of Cohesive Material Based on Wave Velocity Measurements. *applied sciences*, 15 January.
Yamashita, S. et al., 2009. Interpretation of International Parallel Test on the Measurement of Gmax Using Bender Elements. *Soils and Foundations,* pp. 631-650.
Zhang, X. et al., 2020. Measurements of the high frequency dynamic stiffness of railway ballast and subgrade. *Journal of Sound and Vibration.*

Appendix 1: Adjustment Factors for Generalized Predictions of Ground-Borne Vibration and Noise

Tables 15-18 for correction factors are based on data from the Federal Transit Administration report (Hanson, et al., 2006) and the Finnish version by (Talja & Saarinen, 2009).

Table 16: Factors affecting vibration source

Vehicle type		
Electric Multiple Unit (EMU)	$0\ dB$	Applies to commuter trains, long-distance trains, metros and trams (axle load 9-15 tonnes)
High speed train	$0\ dB$	Applies to Pendolino (axle load 13 tonnes)
Locomotive	$+11\ dB$	Applies to both passenger and freight train traffic. Applies to both electric and diesel locomotives (axle load 15-22.5 tonnes)
Rubber wheel traffic	$-6\ dB$	Applies to all road traffic
Speed related corrections		
$V_s = V_{ref} = 100\ kph$	$0\ dB$	Calculated by the following formula: $\Delta L_v = 20 \cdot \log_{10}\left(\frac{V_s}{V_{ref}}\right)$
$V_s = 80\ kph$	$-2\ dB$	
$V_s = 50\ kph$	$-6\ dB$	
$V_s = 200\ kph$	$+6\ dB$	
Vehicle parameters (not additive, apply greatest value only)		
Resilient wheels	$0\ dB$	Resilient wheels do not generally affect ground-borne vibration except at frequencies greater than about 80 Hz.*
Vehicle with stiff primary suspension	$+8\ dB$	Transit vehicles with stiff primary suspensions have been shown to create high vibration levels. Include this adjustment when the primary suspension has a vertical resonance frequency greater than 15 Hz.*
Worn wheels or wheels with flats	$+10\ dB$	Wheel flats or wheels that are unevenly worn can cause high vibration levels. This can be prevented with wheel truing and slip-slide detectors to prevent the wheels from sliding on the track. *
Track conditions (not additive, apply greatest value only)		
Track in good condition	$0\ dB$	Rails are smooth and there are no discontinuities on the track
Worn or corrugated track	$+10\ dB$	If both the wheels and the track is worn, the coefficient is only applied once. The effect of wear can be reduced by grinding the rails. Installing new rails will increase the vibrations until they are levelled.

Track discontinuities	$+10\ dB$	Wheel impacts at special points at the track (e.g. track gears and poor mechanical rail extensions) increase the vibrations. The increase will be less at greater distances from the track.
Rail joints	$+5\ dB$	A rail extension made with mechanical fasteners cause higher vibrations than a welded track.
Track treatments (not additive, apply greatest value only)		
No insulation	$0\ dB$	Rails with sleepers on top of $300-400mm$ crushed stone.
Rail insulation	$-5\ dB$	Soft rail-pads between rail and sleeper, usually dampens frequencies above 50Hz.
Sleeper insulation	$-10\ dB$	Under sleeper pads usually dampen frequencies above 40Hz.
Insulation of the crushed stone layer	$-10\ dB$	The effect of damping mats placed between the crushed stone layer and the hard base vary, but usually the effect is damping of frequencies above 30Hz.
Floating slab trackbed	$-15\ dB$	The reduction achieved with a floating trackbed is strongly dependent on the frequency characteristics of the vibrations. The floating slab can effectively attenuate audible vibrations.

Table 17: factors affecting vibration path

Track position		
Open track	$0\ dB$	The correction factor is affected by the structure itself, the way it was established and the increase of the length of the transmission path.
Ground tunnel	$-3\ dB$	
Rock tunnel	$-15\ dB$	
Elevated track	$-10\ dB$	
Type of building		
Rock founded building	$0\ dB$	Correction factors can be used when there is at least $3m$ from the foundation to the bedrock.
Wooden house, 1-2 floors	$-5\ dB$	
Concrete house, 1-2 floors	$-7\ dB$	
Apartment building	$-10\ dB$	

Table 18: Factors affecting vibration receiver

Floor-to-floor attenuation		
Floors, 1-5	$-2\frac{dB}{floor}$	This correction factor accounts for dispersion and attenuation of the vibration energy as it propagates through a building.
Upper floors (5-10)	$-1\frac{dB}{floor}$	
Amplification due to resonances of floors, walls, and ceilings	$-6\ dB$	The attenuation of the vibrations depend largely on the properties and construction solutions of the materials.

Table 19: Conversion to ground-borne noise

Peak frequency of ground vibration	**Correction factor**	**Comment**
Low frequency $< 30\ Hz$	$-50\ dB$	These correction factors are used to achieve the A-weighted sound level (dBA).
Typical frequency $30 \rightarrow 60\ Hz$	$-35\ dB$	
High frequency $> 60\ Hz$	$-20\ dB$	
Safety margin	$+6\ dB$	The estimation method is indicative and therefore values below the safety margin should not be used.

Appendix 2: Model parameters for ballast, subgrade & estimated crushed concrete

Table 20: Model parameters, ballast

Property	Unit	Description	Value	Estimation method
Material model	-	Hardening Soil with Small-strain	HSS	-
γ_{unsat}	$\frac{kN}{m^3}$	Unsaturated unit weight	20	(Faure, et al., 2015)
γ_{sat}	$\frac{kN}{m^3}$	Saturated unit weight	24	-
e_{init}	-	Initial void ratio	0.5	Default
α		Rayleigh damping coefficient	Vary depending on load frequency domain	Estimated based on damping ratio, $\zeta = 0.3$
β		Rayleigh damping coefficient	Vary depending on load frequency domain	Estimated based on damping ratio, $\zeta = 0.3$
E_{50}^{ref}	kPa	Secant stiffness (std. drained triaxial)	$3.15 \cdot 10^5$	Stiffness value used from (Jones, et al., 2004)
E_{oed}^{ref}	kPa	Tangent stiffness (Primary oedometer)	$2.52 \cdot 10^5$	$E_{oed}^{ref} = \frac{E_{50}^{ref}}{1.25}$
E_{ur}^{ref}	kPa	Unloading/reloading stiffness (drained triaxial)	$9.45 \cdot 10^5$	$E_{ur}^{ref} = 3 \cdot E_{50}^{ref}$
m	-	Power	0.5	(PLAXIS, 2019)
c'_{ref}	kPa	Cohesion	1	For model stability
φ_c	°	Angle of internal friction	45	-
$\nu_{0.7}$	-	Threshold shear strain at which $G_s = 0.722 \cdot G_0$	0.00009	Graph in (PLAXIS, 2019), section 7.5. Assumption: PI=0
G_0^{ref}	kPa	Reference shear modulus at very small strains	$\approx 6.6 \cdot 10^5$	$\frac{E_{max}}{2 \cdot (1 + \nu_{ur})}$

Table 21: Model parameters, Subgrade

Property	Unit	Description	Value	Estimation method
Material model	-	Hardening Soil with Small-strain	HSS	-
γ_{unsat}	$\frac{kN}{m^3}$	Unsaturated unit weight	18	(Lombaert, et al., 2015)
γ_{sat}	$\frac{kN}{m^3}$	Saturated unit weight	20	-
e_{init}	-	Initial void ratio	0.5	Default
α		Rayleigh damping coefficient	Vary depending on load frequency domain	Estimated based on damping ratio, $\zeta = 0.1$
β		Rayleigh damping coefficient	Vary depending on load frequency domain	Estimated based on damping ratio, $\zeta = 0.1$
E_{50}^{ref}	kPa	Secant stiffness (std. drained triaxial)	$6.0 \cdot 10^4$	Stiffness value used from (Jones, et al., 2000)
E_{oed}^{ref}	kPa	Tangent stiffness (Primary oedometer)	$4.8 \cdot 10^4$	$E_{oed}^{ref} = \frac{E_{50}^{ref}}{1.25}$
E_{ur}^{ref}	kPa	Unloading/reloading stiffness (drained triaxial)	$1.8 \cdot 10^5$	$E_{ur}^{ref} = 3 \cdot E_{50}^{ref}$
m	-	Power	0.5	(PLAXIS, 2019)
c'_{ref}	kPa	Cohesion	1	For model stability
φ_c	∘	Angle of internal friction	36	-
$\nu_{0.7}$	-	Threshold shear strain at which $G_s = 0.722 \cdot G_0$	0.00019	Graph in (PLAXIS, 2019), section 7.5. Assumption: PI=15
G_0^{ref}	kPa	Reference shear modulus at very small strains	$\approx 2.55 \cdot 10^5$	$\frac{E_{max}}{2 \cdot (1 + \nu_{ur})}$

Table 22: Estimated crushed concrete parameters.

Property	Unit	Description	Value	Estimation method
Material model	-	Hardening Soil with Small-strain	HSS	-
γ_{unsat}	$\frac{kN}{m^3}$	Unsaturated unit weight	19	Lab data
γ_{sat}	$\frac{kN}{m^3}$	Saturated unit weight	22	Lab data
e_{init}	-	Initial void ratio	0.43	Lab data
α		Rayleigh damping coefficient	Vary depending on load frequency domain	Estimated based on damping ratio, $\zeta = 0.2$
β		Rayleigh damping coefficient	Vary depending on load frequency domain	Estimated based on damping ratio, $\zeta = 0.2$
E_{50}^{ref}	kPa	Secant stiffness (std. drained triaxial)	$1.9 \cdot 10^5$	From tests, UCT and Triaxial
E_{oed}^{ref}	kPa	Tangent stiffness (Primary oedometer)	$1.52 \cdot 10^5$	$E_{oed}^{ref} = \frac{E_{50}^{ref}}{1.25}$
E_{ur}^{ref}	kPa	Unloading/reloading stiffness (drained triaxial)	$5.7 \cdot 10^5$	$E_{ur}^{ref} = 3 \cdot E_{50}^{ref}$
m	-	Power	0.5	(PLAXIS, 2019)
c'_{ref}	kPa	Cohesion	1	For model stability
φ_c	°	Angle of internal friction	40	(Anttila, 2020)
$\nu_{0.7}$	-	Threshold shear strain at which $G_s = 0.722 \cdot G_0$	0.00009	Graph in (PLAXIS, 2019), section 7.5. Assumption: PI=0
G_0^{ref}	kPa	Reference shear modulus at very small strains	$\approx 5.1 \cdot 10^5$	$\frac{E_{max}}{2 \cdot (1 + \nu_{ur})}$

	1,5Hz	15Hz	30Hz	75Hz	100Hz
Rayleigh α	0.9425	15.08	34.27	91.00	119.00
Rayleigh β	0.03183	$2.546 \cdot 10^{-3}$	$1.157 \cdot 10^{-3}$	$0.439 \cdot 10^{-3}$	$0.3351 \cdot 10^{-3}$

Appendix 3: ICT sample preparation

The samples tested in this thesis have been prepared by a rotating condenser (ICT machine).
The following guidelines have been followed doing the samples:

1. The BeM II material has been cut so that all material >16mm has been removed (the material on sieve #16 was removed).
2. The material has been divided in portions matching the estimated content on the rotating condenser by standard methods. (sample dividing device has been used to half the total sample volumes several times to obtain the wanted volume)
3. Water is mixed gently to dry material to obtain an approximate water content of 10.5%
4. Material is added to ICT cylinder in layers of approximately $3cm$ loose material and stamped with wooden stick ($d \approx 5cm$) 20 times.
5. Sample is compacted by a working pressure of 820kPa and with a limit of 160cycles.
6. Sample is gently packed in two plastic bags, which are then closed and placed in a room of ≈ 21°C.
7. Samples are hardening for minimum 28 days

Properties obtained during sample creation are presented in Table 23.

Table 23: Data obtained in the sample creation process - summarized

Water density 1000kg/m3
particle density 2600kg/m3 (assumed)
Width 100.00mm

Sample numbers	Water	Mass, WD	Mass, DD	Wet density	Dry density	Height	Volume	Vol. particles	Vol. water
	Kg	Kg	Kg	Kg/m^3	Kg/m^3	mm	m^3	m^3	m^3
4_U	0.33	3.13	2.80	2042.00	1827.04	194.9	0.00153	0.00108	0.00033
3_U	0.33	3.12	2.79	2028.00	1814.61	195.8	0.00154	0.00107	0.00033
2_U	0.33	3.15	2.82	2033.00	1819.28	197.2	0.00155	0.00108	0.00033
1_U	0.33	3.15	2.82	2025.00	1811.77	197.9	0.00155	0.00108	0.00033
01	0.33	3.16	2.82	2034.00	1820.04	197.6	0.00155	0.00109	0.00033
02	0.33	3.13	2.80	2030.00	1816.10	196.6	0.00154	0.00108	0.00033
03	0.33	3.12	2.79	2018.00	1805.65	196.6	0.00154	0.00107	0.00033
04_2	0.34	3.23	2.89	2001.00	1790.76	205.5	0.00161	0.00111	0.00034
05	0.34	3.19	2.86	2023.00	1810.49	200.8	0.00158	0.00110	0.00034
Average	0.33	3.15	2.82	2026.00	1812.86	198.10	0.00156	0.00108	0.00033

Void ratio, calculated = 0.43

Appendix 4: One-dimensional compression test

One-dimensional compression test (Uniaxial compression test), has been performed according to PANK 9003 with a loading speed of $0.3\,\frac{MPa}{s}$.
The samples (1-U…4-U) have been prepared using a rotating condenser with settings of 820 kPa working pressure and 160 cycles. The sample size has been $100 \cdot 200\ mm$ $(D \cdot H)$, and after preparation they have been curing for at least 28 days.
As an expansion to the usual one-dimensional compression test, the test has been performed in the following stages:

1st loading up to 30 % of estimated uniaxial compression strength
2nd loading up to 60 % of estimated uniaxial compression strength
3rd loading up to failure

The results from the one-dimensional compression test is seen from Figure 58 and the moduli calculated from the tests are presented in Table 24.

Table 24: Determination of E50

1-U	Max [kPa]	50%	Initial	E, [kPa]
Stress	719	360	25	1082499
Corresponding strain, %:	0.448	0.0416	0.0106	
2-U	Max [kPa]	50%	Initial	E, [kPa]
Stress	758	379	26	1310888
Corresponding strain, %:	0.492	0.0446	0.0176	
3-U	Max [kPa]	50%	Initial	E, [kPa]
Stress	766	383	25	1111062
Corresponding strain, %:	0.567	0.0505	0.0182	
4-U	Max [kPa]	50%	Initial	E, [kPa]
Stress	770	385	25	769531
Corresponding strain, %:	0.527	0.0534	0.0066	
Average E				1068495kPa 1069MPa

The estimated maximum compressive strength was 1 MPa due to observations made by (Linden, et al., 2019).

The results are around 25% lower, which can be due to the lower maximum grainsize, C_u value and/or d_{50}.

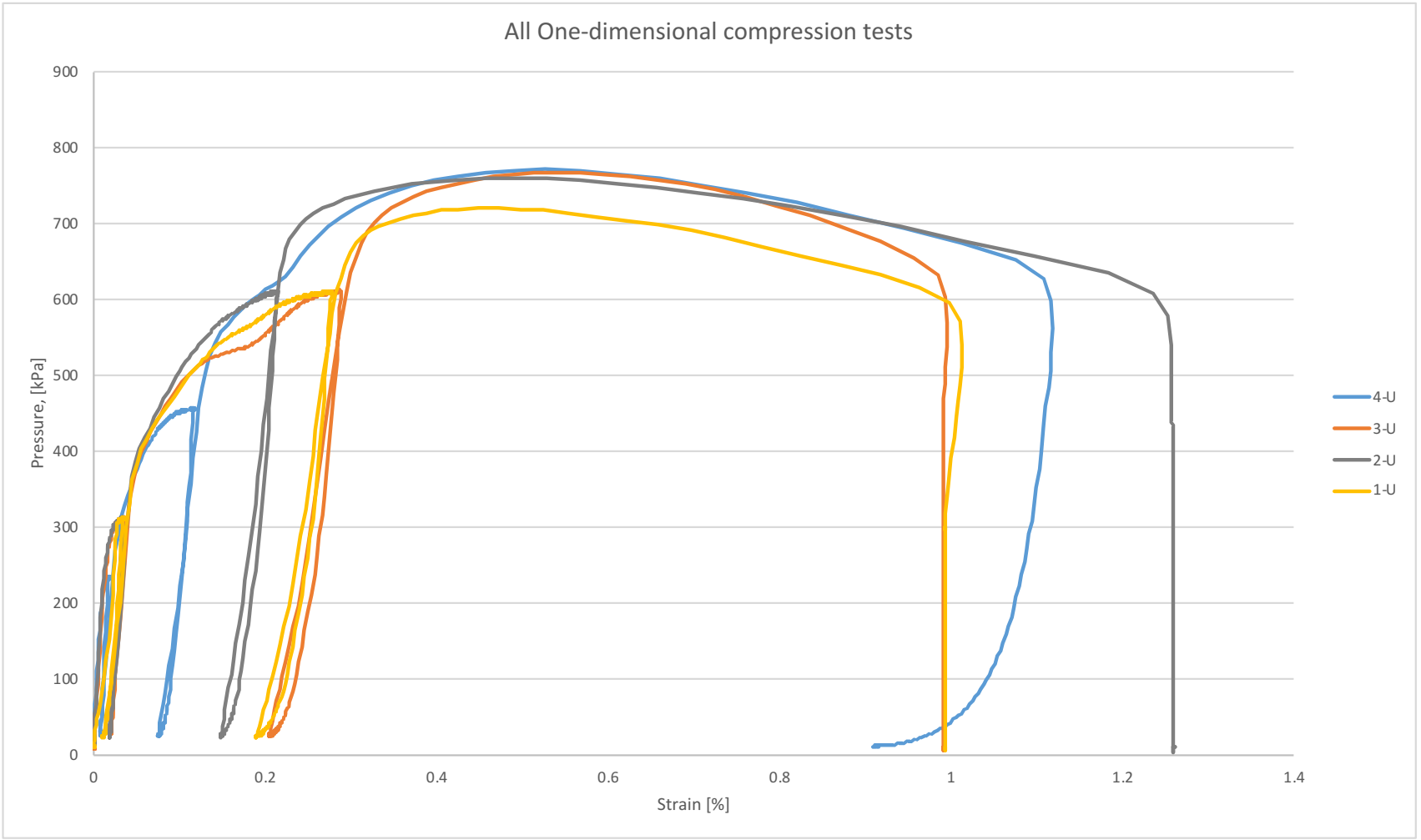

Figure 58: One-dimensional compression test

Appendix 5: Test report of hardened samples

The test report presented in this appendix is produced by the test personnel from the geotechnical laboratory at Bochum Universität, Bochum.

a) b)

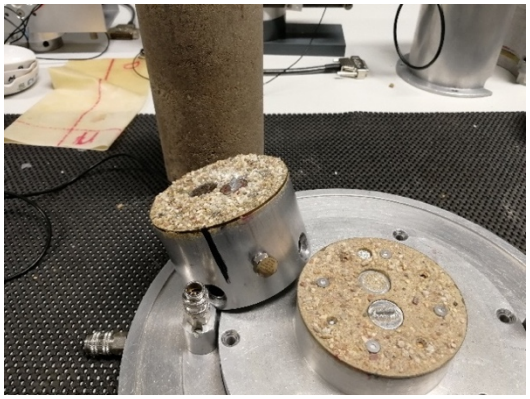

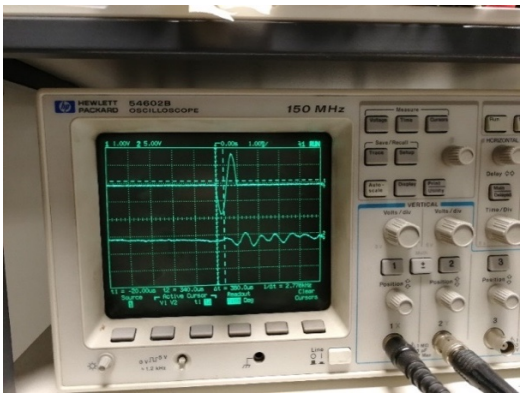

c) d)

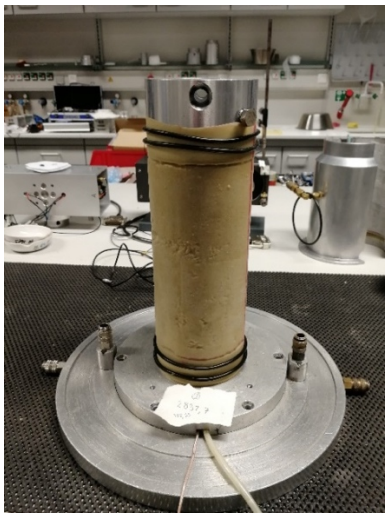

Figure 1: a) Bender elements for measuring wave velocity and stiffness using them; b) Specimen and RC device to measure resonant frequency, stiffness and damping ratio

Table 25: Geometry of specimens 1 and 2 for RC and BE experiments

Specimen	H_0 [cm]	D_0 [cm]	V_0 [cm^3]	A_0 [cm^2]	m [g]	ρ [g/cm^3]
1 (Hardened)	20,08	9,99	1573,40	78,34	3113	1,979
2 (Hardened)	19,98	9,98	1562,82	78,21	3097	1,982

Table 26: summary of results from RC and BE experiments on specimens 1 and 2

Specimen-1	RC (fix-free)				BE				
P [kPa]	fr [Hz]	vs [m/s]	Gmax [Mpa]	D_{min} [-]	Δt [ms]	vs [m/s]	Gmax [Mpa]	ρ g/cm^3	γ [-]
50,00	72,60	381,15	287,43	2,93E-02	520,00	386,22	295,12	1,98	5,00E-07
300,00	110,50	579,46	665,97	1,84E-02	340,00	590,01	690,44	1,98	5,00E-07
550,00	124,91	654,26	851,17	1,67E-02	300,00	667,90	887,01	1,99	5,00E-07
Specimen-2	RC (fix-free)				BE				
P [kPa]	fr [Hz]	vs [m/s]	Gmax [Mpa]	D_{min} [-]	Δt [ms]	Vs [m/s]	Gmax [Mpa]	ρ g/cm^3	γ [-]
50,00	65,71	344,24	234,83	3,23E-02	520,00	384,29	292,66	1,98	5,00E-07
300,00	111,21	582,09	672,81	1,85E-02	350,00	570,45	646,18	1,99	5,00E-07
550,00	123,01	643,39	823,10	1,82E-02	300,00	665,05	879,45	1,99	5,00E-07

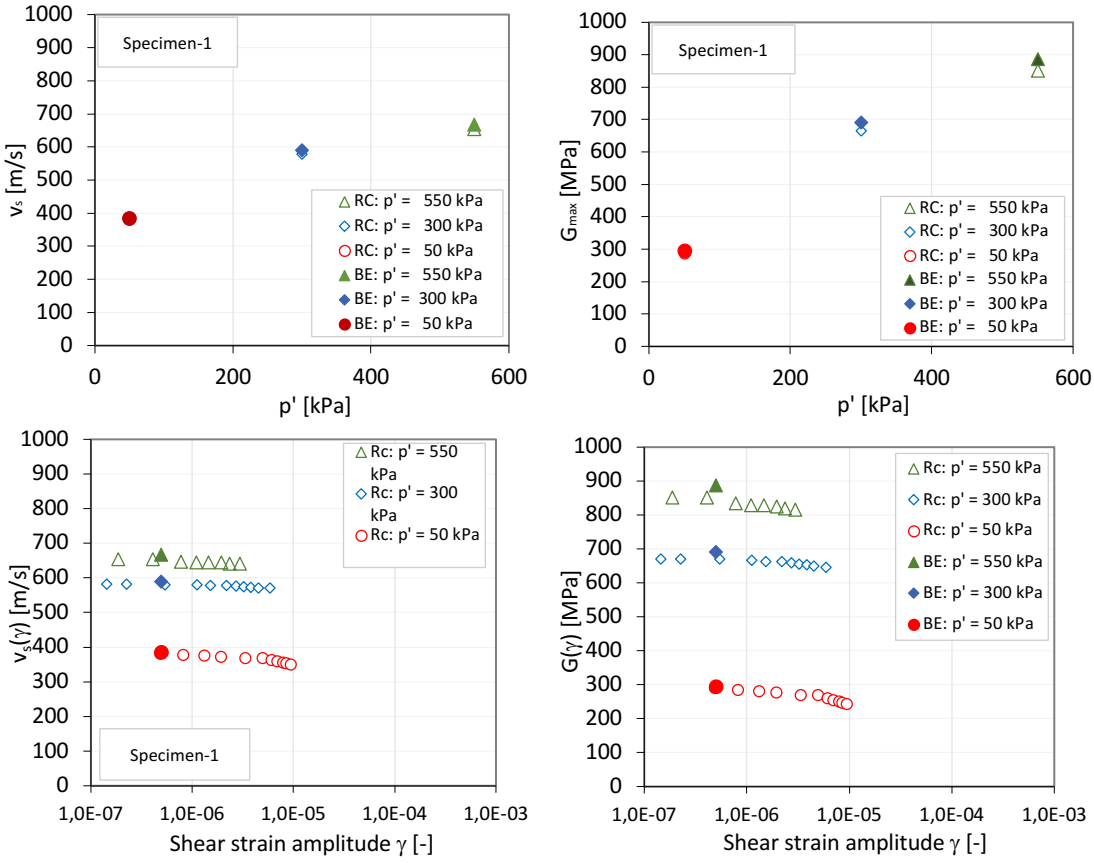

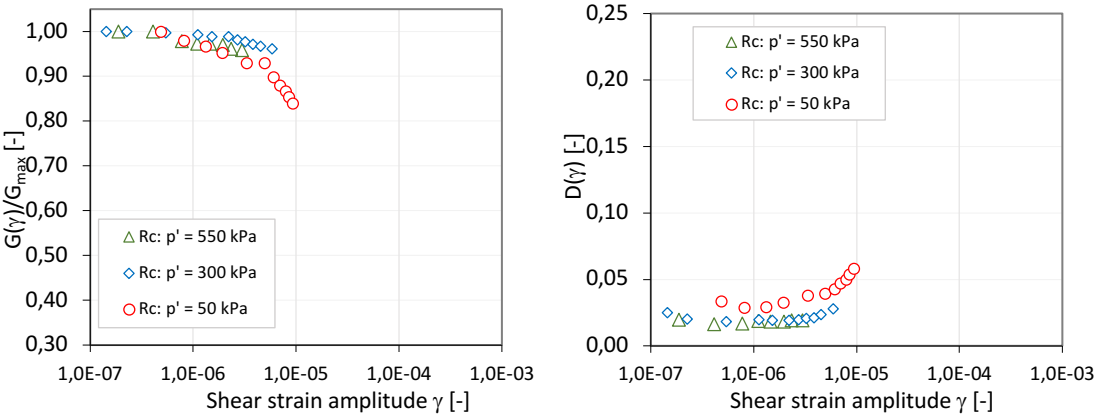

Figure 59: RC and BE results for Specimen 1

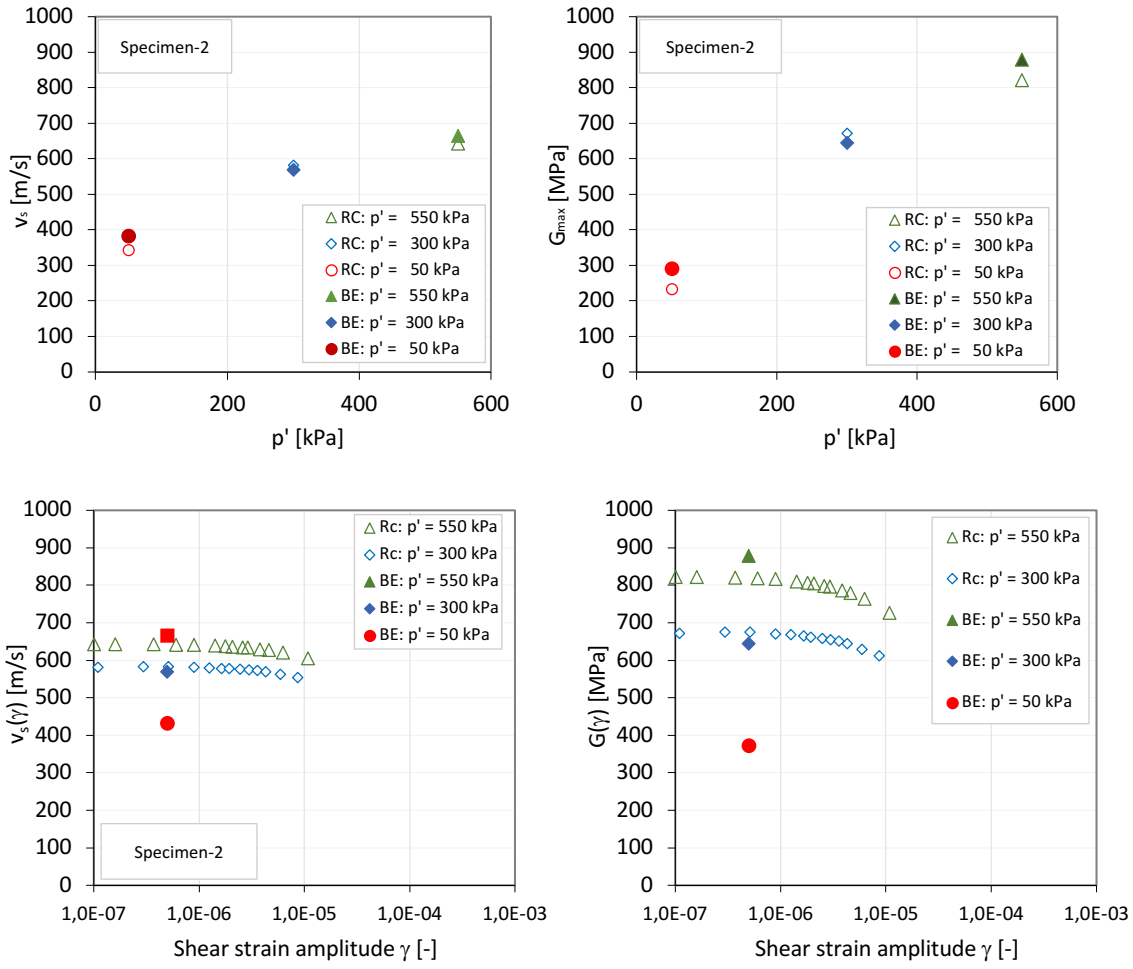

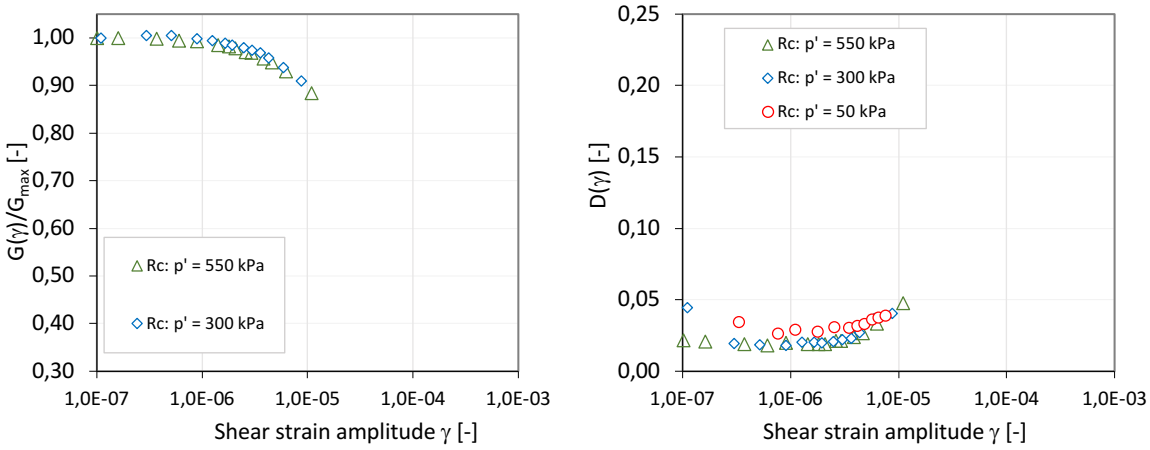

Figure 60: RC and BE results for Specimen 2